Two Transport Processes in a Single Protein: Molecular Mechanisms Underlying Glutamate Transporter Function

von der Naturwissenschaftlichen Fakultät der
Gottfried Wilhelm Leibniz Universität Hannover
zur Erlangung des Grades
Doktor der Naturwissenschaften
Dr. rer. nat.
genehmigte Dissertation
von

Magister en Ciencias Biológicas Delany Torres Salazar

geboren am 3. Dezember 1975 in Santa Clara, Kuba

2008

Referent: Prof. Dr. Christoph Fahlke

Korreferent: Prof. Dr. Anaclet Ngezahayo

Tag der Promotion: 25 Januar 2008

Contents

1. Abstract …………………………………………………………………………….. 7

1.1 Kurzdarstellung ………………………………………………………………… 8

2. Introduction ……………………………………………………………………. 9
  2.1. Membrane transport………………………………………………………………… 9
  2.2. Transporters and Channels………………………………………………………. 10
    2.2.1 Glutamate transporters have ligand-gated channel properties……………… 10
  2.3 Glutamate as Neurotransmitter…………………………………………………… 11
  2.4 Glutamate transporters family……………………………………………………. 14
    2.4.1 GLAST (EAAT1) and GLT1 (EAAT2) are glial glutamate transporters…………………………………………………………………….. 15
    2.4.2 EAAC1 (EAAT3) is homogeneously distributed throughout the CNS……. 17
    2.4.3 EAAT4 is predominantly expressed in cerebellar perysynapses and control synaptic excitability………………………………………………………………. 17
    2.4.4 EAAT5 is a retina-specific transporter…………...………………………… 19

3. Discussion……………………………………………………………………………. 21
  3.1 A trimeric quaternary structure is evolutionary conserved in glutamate transporters……………………………………………………………………………… 21
  3.2 EAAT4-associated anion channels participate in neuronal excitability………….. 23
  3.3 Individual subunits interact activating the EAAT4-associated anion channel…… 24
  3.4 EAATs exhibit isoform specific gating properties……………………………….. 27

4. Conclusions…………………………………………………………………………... 31

5. References……………………………………………………………………………. 33

List of Included Publications ..…………………………………………………….. 41

6. A trimeric quaternary structure is conserved in bacterial and human glutamate transporters…………………………………………………………………………….. 43

6.1 Abstract……………………………………………………………………………… 44

6.2 Introduction…………………………………………………………………………. 45

6.3 Experimental Procedure…………………………………………………………….. 46

6.3.1 Expression of His_6-tagged polypeptides in *Xenopus* oocytes and in mammalian cells…………………………………………………………………….. 46

6.3.2 Electrophysiological examination of injected *Xenopus* oocytes and stably transfected mammalian cells………………………………………………….. 47

6.3.3 Purification of [^{35}S]methionine-labeled protein form *Xenopus* oocytes and mammalian cells…………………………………………………………………….. 48

6.3.4 Chemical cross-linking…………………………………………………... 48

6.3.5 SDS-PAGE and BN-PAGE analysis…………………………………….. 49

6.3.6 Expression, purification, and reconstitution of ecgltP……………………… 49

6.4 Results………………………………………………………………………………. 51

6.4.1 His-tagged hEAAT2 transporters exhibit unaltered functional properties…. 51

6.4.2 SDS-PAGE analysis and glycosylation of glutamate transporters heterologously expressed in *Xenopus* oocytes…………………………………… 51

6.4.3 hEAAT2 transporters migrate as trimers in blue native PAGE gels……….. 54

6.4.4 ecgltP transporters migrate as trimers in blue native PAGE gels…………... 58

6.4.5 Cross-linking of hEAAT2 or ecgltP generates covalently bound dimers and trimers…………………………………………………………………………….. 62

6.4.6 Purification and characterization of ecgltP…………………………………. 64

6.5 Discussion…………………………………………………………………………… 67

6.6 References…………………………………………………………………………... 71

7. A dynamic switch between inhibitory and excitatory currents in a neuronal glutamate transporter………………………………………………………………………. 75

7.1 Abstract……………………………………………………………………………… 76

7.2 Introduction…………………………………………………………………………. 77

7.3 Methods……………………………………………………………………………... 78

7.3.1 Expression of EAAT4 and Whole-Cell Recording………………………… 78

7.3.2 Data Analysis…………………………………………………………….. 79

7.4 Results………………………………………………………………………………. 81

7.4.1 A novel gating process of EAAT4 anion channel………………………….. 81
7.4.2 Slow gating increases cation permeability of EAAT4 anion channels…….. 86
7.4.3 Slow gating alters the open probability of EAAT4 anion channels depending on the current direction……………………………………………….. 90
7.5 Discussion………………………………………………………………………… 94
7.6 References……………………………………………………………………... 97
7.7 Supporting Text………………………………………………………………... 99
7.7.1 Time-Dependent Changes of the Intracellular Anion Composition……….. 99
7.7.2 Trains of Phasic Depolarizations Cause Slow Activation………………….. 100
7.7.3 The Observed Current Variance Is EAAT4 Channel-Associated Noise…… 100
7.7.4 Approximation of EAAT4 Current Amplitudes and Resulting Voltage Changes in Spines of Purkinje Cell Dendrites…………………………………… 105
7.8 Supporting text References……………………………………………………….. 108

8. Inter-subunit interactions in EAAT4 glutamate transporters…………………… 109
8.1 Abstract…………………………………………………………………………… 110
8.2 Introduction………………………………………………………………………. 111
8.3 Materials and Methods…………………………………………………………… 113
8.3.1 Expression of EAAT4 in mammalian cells………………………………… 113
8.3.2 Electrophysiology……………………………………………………………... 113
8.3.3 Data Analysis………………………………………………………………. 114
8.3.4 Expression in *Xenopus* oocytes and radiotracer flux experiments……….…. 116
8.4 Results……………………………………………………………………………. 117
8.4.1 Transporter substrates increase the amplitudes and change the voltage dependence of EAAT4 anion currents…………………………………………… 117
8.4.2 Concentration dependence of external Na^+ and glutamate…………………. 119
8.4.3 Point mutations affecting glutamate and Na^+ binding and anion channel gating……………………………………………………………………………... 125
8.4.4 Mixed heterotrimers of WT and mutant EAAT4 with altered substrate selectivity………………………………………………………………………. 136
8.5 Discussion………………………………………………………………………… 139
8.6 References……………………………………………………………………... 145

9. Neuronal glutamate transporters vary in substrate transport rate, but not in unitary anion channel conductance……………………………………………………... 149
9.1 Abstract……………………………………………………………………… 150
9.2 Introduction…………………………………………………………………. 151
9.3 Experimental Procedures……………………………………………………. 152

9.3.1 Heterologous expression and functional characterization of EAAT3 and EAAT4………………………………………………………………………… 152
9.3.2 Electrophysiology……………………………………………………... 152
9.3.3 Data analysis………………………………………………………….. 153
9.3.4 Noise analysis…………………………………………………………. 154
9.4 Results………………………………………………………………………. 157
9.4.1 Voltage-dependent gating of EAAT3- and EAAT4-associated anion currents………………………………………………………………………… 157
9.4.2 Permeation properties of EAAT3 and EAAT4 anion channels…………….. 160
9.4.3 EAAT4 glutamate transport rates are significantly smaller than those of EAAT3………………………………………………………………………… 166
9.4.4 Glutamate dependence of EAAT3 and EAAT4 anion currents……………. 169
9.5 Discussion…………………………………………………………………… 173
9.6 References…………………………………………………………………... 178
9.7 Supplemental Information…………………………………………………... 180

Acknowledgments………………………………………………………………… 181

Curriculum Vitae……………………………………………………………….... 183

List of Figures and Tables

Figure 2.1 Glutamate recycling………………………………………………………... 13

Figure 2.2 Phylogenic tree of some members of the glutamate transporter family…………………………………………………………………. 16

Figure 3.1 Crystal structure of a bacterial glutamate transporter homologe from *Pyrococcus horikoshii*………………………………………………… 23

Figure 3.2 Schematic models for the glutamate translocation and chloride permeation pathways in glutamate transporters ………………………… 26

Figure 6.1 Basic functional and biochemical characterization of glutamate transporters expressed in *Xenopus* oocytes……………………………… 52

Figure 6.2 Oligomeric state of EAAT2 transporters in *Xenopus* oocytes and mammalian cells determined by BN-PAGE…………………………….. 55

Figure 6.3 Oligomeric state of ecgltP transporters in *Xenopus* oocytes determined by BN-PAGE………………………………..…………………… 59

Figure 6.4 Cross-linking of digitonin-solubilized purified glutamate transporters…………………………………………………………… 63

Figure 6.5 Biochemical and functional characterization of recombinant ecgltP produced in *E.coli* ……..……………………………………..……..... 65

Figure 7.1 A novel gating transition in EAAT4 anion channels during prolonged membrane depolarizations…..…………………………………….……….. 82

Figure 7.2 Enhanced EAAT4 inward currents are not due to anion accumulation……..……………………………………………………… 84

Figure 7.3 Activation of the slow gate is associated with increasing cation permeabilities of EAAT4 channels……………………………………… 87

Figure 7.4 Activation of the slow gate increases the open probability of the EAAT4 anion channels………………………………..….…………………. 91

Figure 7.5 Slow gating-induced alterations of the reversal potentials are much larger than those predicted for anion accumulation …………………….. 101

Figure 7.6 Whole-cell currents in EAAT4-expressing cells represent glutamate transporter-associated anion currents……………………………………. 102

Figure 7.7 Slow activation during repetitive short depolarisations ………………… 104

Figure 7.8 Noise analysis in shaker potassium channels …………………………… 106

Figure 8.1 Activation of EAAT4 anion channels by transporter substrates………… 118
Figure 8.2 Sodium dependence of EAAT4 anion currents…………….…………. 120
Figure 8.3 Glutamate dependence of EAAT4 anion currents and glutamate uptake………………………………………………………………. 122
Figure 8.4 Sodium and glutamate interact in activating EAAT4 anion channels... 126
Figure 8.5 Effects of two point mutations close to the putative glutamate binding site on coupled and uncoupled transport………………………………… 128
Figure 8.6 G464S and Q467S modify the intersubunit cooperativity in the EAAT4 anion channel activation……..…………………………….………………. 131
Figure 8.7 G464S and Q467S modify gating of EAAT4 anion channels…............. 134
Figure 8.8 Mixed heterotrimers consisting of WT and R501C EAAT4 exhibit functional properties that are intermediate to WT and R501C homotrimers…..………………………………………………………… 138
Figure 8.9 R501C changes the substrate sensitivity of EAAT4……….…….......... 148
Figure 9.1 Voltage– and substrate-dependence of EAAT3- and EAAT4-associated anion currents in cells dialyzed with SCN$^-$- based solutions…...……….. 158
Figure 9.2 Voltage and substrate-dependence of EAAT3- and EAAT4-associated anion currents in cells dialyzed with Cl$^-$- based solutions………………. 161
Figure 9.3 Unitary current amplitudes and absolute open probabilities of EAAT3 and EAAT4 anion channels………………………………………….. 164
Figure 9.4 Relative unitary glutamate transport rates of EAAT3 and EAAT4…….. 167
Figure 9.5 EAAT3 and EAAT4 differ in the glutamate dependence of associated anion currents………………………………………………………. 170
Figure 9.6 Anion permeability ratios of EAAT3- and EAAT4-associated anion channels………………………………………………..………… 180
Table 8.1 Gating properties for EAAT4 wild type and mutants in the absence and presence of glutamate for two anion conditions..................................... 132
Table 9.1 Boltzmann parameters of the activation curves of EAAT3- and EAAT4-associated anion channels in the absence and presence of 500 µM L-glutamate for two different anion distributions…..……………… 180

1. Abstract

Glutamate is the major excitatory neurotransmitter in the mammalian central nervous system. Excitatory amino acid transporters (EAATs) play a crucial role in the termination of synaptic transmission and in extracellular glutamate homeostasis, recapturing the glutamate from the synaptic cleft into the neuronal and glial cells. Despite their function as a secondary-active glutamate transport they also function as anion-selective ion channels. A functional transporter is assembled as an oligomer consisting of three identical subunits. While it is generally established that each monomer transports glutamate independently from the neighbouring subunits, the structural basis of the anion conduction pathway is still unclear. Using heterologous expression of EAATs in mammalian and amphibian cells, we studied the substrate- and voltage-dependent gating and the substrate-dependent activation of the EAAT-associated anion channels, as well as the oligomeric assembly of these proteins. Our results demonstrate: 1) that human and prokaryotic glutamate transporters expressed in heterologous systems are assembled as trimers composed of three identical subunits, indicating that the trimeric quaternary structure is evolutionarily conserved and represents the unique native and functional state of glutamate transporters, 2) that EAAT-associated anion conductance could modify the excitability of the cells were they are expressed, providing them with an unprecedented mechanism for adaptation, 3) that gating of the EAAT-associated channels is controlled by isoform specific intersubunit interactions, 4) and that EAAT3 and EAAT4 differ in unitary glutamate transport rates and voltage- and substrate-dependence of anion channel opening, while ion conduction properties are very similar.

Key words: glutamate transporters, anion channels, excitability

1.2 Kurzdarstellung

Glutamat ist der wichtigste exzitatorische Neurotransmitter im zentralen Nervensystem der Säugetiere. Glutamattransporter der Klasse EAAT („excitatory amino acid transporter“) spielen eine entscheidende Rolle in der Beendigung der glutamatergen synaptischen Transmission und in der extrazellulären Glutamathomöostase, indem sie Glutamat aus dem synaptischen Spalt in prä- und postsynaptische Neuronen sowie umliegende Gliazellen transportieren. Neben ihrer Eigenschaft als natrium-abhängige, sekundär aktive Transporter besitzen alle EAAT-Isoformen eine Anionenkanalfunktion. Glutamattransporter bilden funktionelle Homotrimere, in denen jede monomere Untereinheit eigenständig Glutamat transportieren kann. Die strukturelle Basis für den Anionentransportweg ist jedoch noch unklar. Mittels heterologer Expression verschiedener EAAT-Isoformen in Säugetier- und Amphibienzellen konnten wir die Substrat- und Spannungsabhängigkeit des Schaltverhaltens und der Aktivierung der EAAT-assoziierten Anionenkanäle sowie deren oligomere Zusammensetzung untersuchen. Es zeigte sich, dass 1.) humane wie auch prokaryotische Glutamattransporter Oligomere mit drei identischen Untereinheiten bilden, und dass damit die trimere Quarternärstruktur evolutionär konserviert erscheint und den einzigen nativen und funktionellen Zustand von Glutamattransportern darstellt; dass 2.) die EAAT-assoziierte Anionenleitfähigkeit die elektrische Erregbarkeit von Zellen beeinflussen kann, in denen die EAATs exprimiert werden, und ihnen so einen ungewöhnlichen Adaptionsmechanismus verleiht; dass 3.) das Schaltverhalten der EAAT-assoziierten Ionenkanäle von isoformspezifischen Interaktionen zwischen den Untereinheiten bestimmt wird und dass 4.) EAAT3 und EAAT4 sich zwar in ihrer Glutamattransportrate und der Spannungs- und Substratabhängigkeit des Schaltverhaltens ihrer Anionenkanäle, nicht aber in deren Einzelkanaleigenschaften wesentlich unterscheiden.

Schlagwörter: Glutamattransporter, Anionenkanäle, Erregbarkeit

2. Introduction

2.1 Membrane Transport

All living cells are isolated from the environment by a membrane which is mainly constituted by a lipid bilayer and commonly called cellular membrane or plasma membrane. This frontier has several important functions such as: maintaining the cellular organization, transmitting external signals and controlling the substance exchange between the cell and the extracellular medium. Exchange across the plasma membrane is accomplished by different transport mechanisms. The transport of macromolecules such as polysaccharides and proteins is mediated by endo and exocytosis transport processes. On the other hand, micromolecules transport is more diverse and complicated. Small and uncharged molecules like water, O_2 and CO_2, cross the membrane freely and this process is known as simple diffusion. Ions such as K^+, Cl^- and Ca^{2+}, and small hydrophilic molecules such as glucose and amino acids are not able to cross the membrane freely; therefore, they need a carrier that facilitates its pass across the plasma membrane (i.e. ion channels and transporters).

Active transport mechanisms mediate the pumping of molecules or ions through the membrane against their electrochemical gradient. When this mechanism is directly coupled to the binding and hydrolysis of ATP, is called primary active transport. The most studied ATPase-coupled ion pumps is the Na^+/K^+-ATPase, which actively transport Na^+ ions from the cytoplasm to the extracellular fluid, with the counter transport of K^+. Secondary active transporters perform the movement of one ion on its electrochemical gradient coupled to the movement of one or more molecules against its electrochemical gradient using the gradient of the first generated by primary active transport (e.i Na^+/Glucose cotransporter). A third transport process which is classified as passive transport because do not need energy, is carried by proteins that allow the transported substrate to cross the plasma membrane in the direction of its electrochemical gradient. These proteins have a gate that open and close stochastically in response to certain stimuli, they are known as ion channels. All these transport proteins are crucial for every living organism; they are responsible for diverse physiological functions that range from bacterial nutrition to human thinking.

2.2 Transporters and Channels

Ion transport proteins are categorized as being either channels or transporters. Transporters function involves three main processes: 1) a selective binding of the transported ion, 2) conformational changes in the transporter protein due to this binding and 3) the coupling of these conformational changes to the physical movement of the transported ions across the lipid bilayer. On the other hand, ion channels have one or several binding sites accessible from both sides of the plasma membrane at the same time, facilitating the physical translocation of ions when the channel is in the open state. Another remarkable difference is that for coupled transport, substrates and ions go through the membrane in a fixed stoichiometry, in contrast to ion channels which carry an arbitrary number of ions depending on the channel open time (Hille, 1970).

2.2.1 Glutamate transporters have ligand-gated channel properties

Transporters and ion channels have traditionally been thought as being structurally and functionally different. Neurotransmitter transport is a process in which substrates are carried against its electrochemical gradient across the membrane, whereas ion channels are considered to be pores that allow the dissipation of pre-existing electrochemical gradients (Danbolt, 2001). Years ago, many electrophysiological studies performed on excitatory amino acid carriers were predicated on the assumption that the currents observed during transport reflect substrate and co- and counter-transported ions translocation. The simultaneous measurements of ionic currents and transport of radiolabeled substrate molecules by cloned carriers expressed in heterologous systems, demonstrated the existence of robust uncoupled substrate-activated fluxes in three different excitatory amino acid transporters (EAAT) subtypes (Wadiche et al., 1995). The same year, the same group cloned an EAAT isoform with even more pronounced properties of ligand-gated chloride channels (Fairman et al., 1995).

In the last ten years, several neurotransmitter transporters, including GABA (Mager et al., 1996), norepinephrine (Galli et al., 1996), serotonin (Galli et al., 1997), proline (Galli et al., 1999) and dopamine transporters (Ingram and Amara, 2000;Ingram et al., 2002), have been described to be able to act as both a transporter and an ion channel. The finding of glutamate transporters, as well as a number of other neurotransmitter transporters operating as chloride channels, has blurred the distinction between transporters and channels. The principal objective of this work was to elucidate the structure-function relationship of these two different processes that are apparently carried by the same EAAT protein and study in more detail the gating properties of the EAAT-associated anion channels.

2.3 Glutamate as Neurotransmitter

Glutamate is the major excitatory neurotransmitter in the mammalian central nervous system (CNS) and is probably involved in most aspects of normal brain function as cognition, memory and learning (Danbolt, 2001). Glutamate also plays major roles in many processes during the CNS development including neuronal migration (Komuro and Rakic, 1993;Rossi and Slater, 1993), outgrowth of neuronal processes (Pearce et al., 1987) as well as GABAergic activity (van den Pol et al., 1998). It is also important for synapse elimination (Rabacchi et al., 1992) as well as for long term potentiation and functional synapse induction in the developing nervous system (Durand et al., 1996).

Synaptic release of glutamate activates a wide range of ionotropic and metabotropic receptors to mediate a complex array of functions. The glutamate concentration in the synaptic cleft is tightly controlled by members of the EAATs family (Danbolt, 2001;Amara and Fontana, 2002;Kanner, 1996;Billups et al., 1996). EAATs play a crucial role terminating the synaptic transmission and maintaining the extracellular glutamate concentration below neurotoxic levels (Kanner and Schuldiner, 1987;Nicholls and Attwell, 1990;Zerangue and Kavanaugh, 1996;Rothstein et al., 1996). The failure in the function of the EAATs will provoke elevations in the extracellular glutamate concentration, causing excessive stimulation of the glutamate receptors that, if prolonged, will result in an excitotoxicity process and cell death (Rossi et al., 2000). Considering the large amounts of glutamate in the brain and the importance of controlling the extracellular glutamate concentrations after release, the CNS needs powerful protective machinery that prevents extracellular glutamate accumulation. Because there is no (or at least negligible) extracellular conversion of glutamate (Danbolt, 2001), as there is for instance for acetylcholine, brain tissue needs a very high glutamate uptake activity to protect itself against glutamate toxicity. Studies that demonstrate the close relation of the excitotoxicity process with various neurodegenerative disorders such as amyotrophic lateral sclerosis (Howland et al., 2002) and Alzheimer disease (Scott et al., 2002), have accentuated the importance of the neuroprotective mechanisms.

Glutamate transporters are located in the presynaptic, postsynaptic and astroglial cells and they rapidly remove glutamate from the synaptic cleft and the perisynaptic area (Fig. 2.1). Glutamate taken up by pre-and post-synaptic cells may be used for metabolic purposes (protein synthesis, energy metabolism), in pre-synaptic cells it also may be reused as a transmitter (Danbolt, 2001). Glutamate taken up by astrocytes can be converted to glutamine by an ATP-dependent process; glutamine is subsequently released from the glial cells by means of a glutamine transporter and taken up by neurons by means of other glutamine

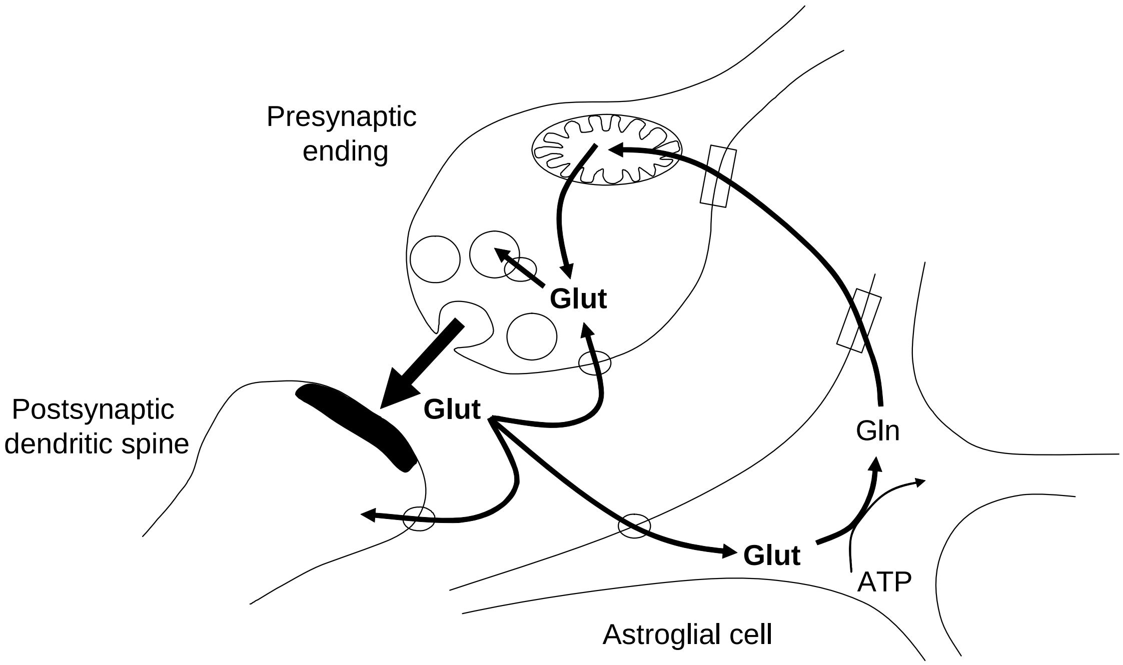
Presynaptic ending
Glut
Postsynaptic dendritic spine
Glut
Gln
Glut
ATP
Astroglial cell

Figure 2.1 Glutamate recycling. Representation of how the synaptic released glutamate is recaptured into the neuronal and glial cells. (Glut) represents glutamate, (Gln) represents glutamine, (circles) represent the glutamate transporters and rectangle represents glutamine transporters. Modified from Danbolt, 2001.

transporter. Neurons convert glutamine back to glutamate which is then transported in to the synaptic vesicles by vesicular glutamate transporters (Fig. 2.1)(Danbolt, 2001). Although the significance of this way, known as the glutamate-glutamine cycle, is still controversial, it has been proposed to be a major pathway by which transmitter glutamate is recycled (Broer and Brookes, 2001).

2.4 Glutamate transporters family

Five human EAAT isoforms have been cloned: EAAT1, 2 and 3 from human motor cortex (Arriza et al., 1994); EAAT4 from human cerebellum (Fairman et al., 1995) and EAAT5 from human retina (Arriza et al., 1997). Although the human isoforms are termed as EAAT, some of them have homologues in other species that were actually previously cloned and are termed: GLAST (Glutamate Aspartate Trasnsporter, rat equivalent of EAAT1) (Storck et al., 1992); GLT1 (Glutamate Transporter 1, rat equivalent of EAAT2) (Pines et al., 1992) and EAAC1 (Excitatory Amino Acid Carrier 1, rabbit equivalent of EAAT3) (Kanai and Hediger, 1992). The five eukaryotic isoforms are members of a family of integral membrane transport proteins that include two eukaryotic neutral amino acid transporters and a large number of prokaryotic amino acid and dicarboxilic acid transporters (Slotboom et al., 1999;Danbolt, 2001).

The five cloned glutamate transporter subtypes share 50-60% amino acid sequence identity with each other, 30-40% identity with the neutral amino acid transporters (Arriza et al., 1993) and around 20-30% identity with bacterial glutamate transporters (Tolner et al., 1992). Between mammals, the five isoforms are about 90% identical to the equivalent proteins of another species (Danbolt, 2001). Although these transporters have similar predicted structures, they exhibit distinct functional properties like variations of a common transport mechanism (Arriza et al., 1994;Melzer et al., 2003;Mim et al., 2005). Figure 2.2 shows the phylogenetic tree of some members of this family.

2.4.1 GLAST (EAAT1) and GLT1 (EAAT2) are glial glutamate transporters

GLAST is expressed in different regions throughout the CNS and in some peripheral organs and tissues, such as the placenta (Matthews et al., 1998) and bone (Mason and Huggett, 2002). It is also the major glutamate transporter in the cerebellum (Lehre and Danbolt, 1998), the inner ear (Furness and Lehre, 1997), and in the retina (Rauen et al., 1996). GLT1 is the most abundant glutamate transporter in all regions of the mammalian central nervous system except in those regions where GLAST is the major transporter (Danbolt, 2001).

Neuronal expression of GLAST has not been detected in the nervous system in vivo; however, a possible expression of GLAST mRNA in granule cells of the mouse hippocampus has been described (Sutherland et al., 1996) and it has also been reported that is transiently expressed in embryonic hippocampal neurons (Plachez et al., 2000). Although GLT1 proteins have been observed to be expressed in retinal neurons (Rauen and Kanner, 1994;Rauen et al., 1999) and some splice variants have been found in nerve terminals and related with synaptic activity (Chen et al., 2002;Chen et al., 2004), no other evidences for neuronal GLT1 localization have been reported. So far GLT1 has mainly been detected in astrocytes, in the normal adult rat brain and spinal cord (Danbolt et al., 1992;Levy et al., 1993;Zschocke et al., 2005) as well as in the adult human brain (Milton et al., 1997;Matute et al., 2005). Therefore, GLAST and GLT1 are known as the glial glutamate transporters. They provide the majority of the functional glutamate transport and they are essential for maintaining a low extracellular glutamate concentration and for preventing chronic glutamate neurotoxicity (Rothstein et al., 1996). GLT1 is responsible for the majority of the glutamate uptake in the mammalian brain

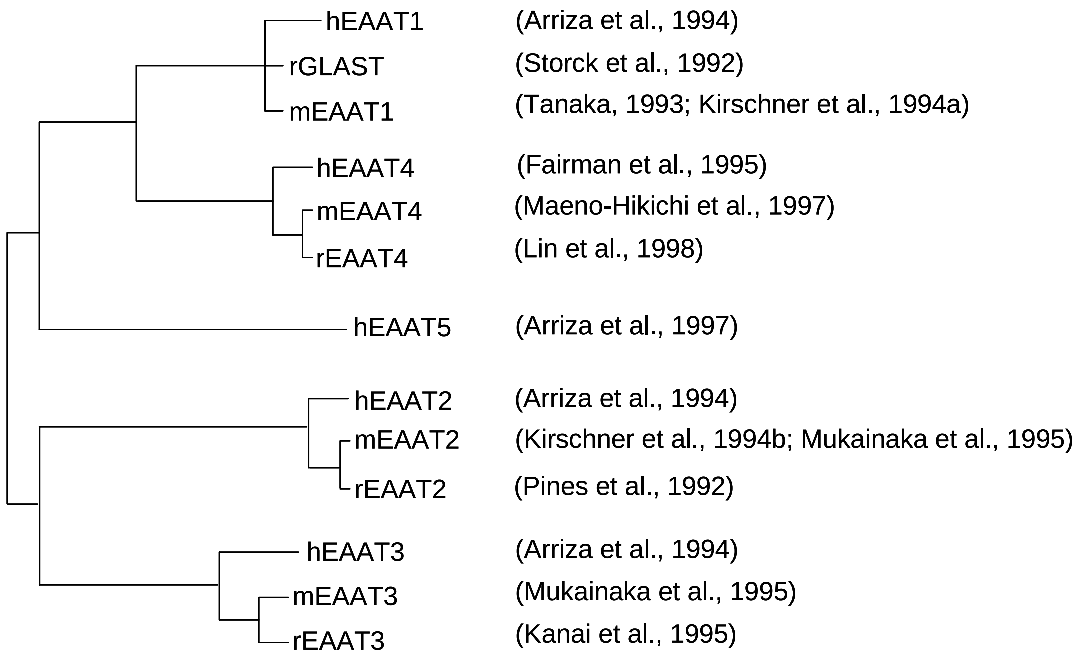
hEAAT1
(Arriza et al., 1994)
rGLAST
(Storck et al., 1992)
mEAAT1
(Tanaka, 1993; Kirschner et al., 1994a)
hEAAT4
(Fairman et al., 1995)
mEAAT4
(Maeno-Hikichi et al., 1997)
rEAAT4
(Lin et al., 1998)
hEAAT5
(Arriza et al., 1997)
hEAAT2
(Arriza et al., 1994)
mEAAT2
(Kirschner et al., 1994b; Mukainaka et al., 1995)
rEAAT2
(Pines et al., 1992)
hEAAT3
(Arriza et al., 1994)
mEAAT3
(Mukainaka et al., 1995)
rEAAT3
(Kanai et al., 1995)

Figure 2.2 Phylogenic tree of some members of the glutamate transporter family.

(Rothstein et al., 1996), so much that in a mice deficient in this protein, glutamate levels rise enough to cause epilepsy and cell death (Tanaka et al., 1997b).

2.4.2 EAAC1 (EAAT3) is homogeneously distributed throughout the CNS

The EAAT3 glutamate transporter presents a rather homogeneous distribution throughout the CNS, although it is predominantly expressed in neurons of various brain areas, particularly in hippocampus, cerebellum, olfactory bulb, striatum and thalamus (Berger and Hediger, 1998;Kanai et al., 1995;Rothstein et al., 1994). In addition, this isoform has been found in the apical membrane of the proximal tubules in the kidney (Shayakul et al., 1997). In a study by Peghini *et al.,* EAAC1-knockout mice did not develop remarkable neurological symptoms and neurodegeneration during a period of more than 12 month, except that homozygous mutants displayed a significantly reduced spontaneous locomotor activity. These knockout mice develop dicarboxylic aminoaciduria, confirming the role of EAAC1 in the reabsorption of glutamate from the renal proximal tubules (Peghini et al., 1997).

A particular characteristic of this isoform has been confirmed by immunocytochemical analysis in neurons. The protein was detected in both, the membrane and the cytosolic compartment, being mainly cytoplasmatic and only in about 20% present at the plasma membrane (Conti et al., 1998;Yang and Kilberg, 2002). This contrasts with the cellular distribution of glial transporters (Chaudhry et al., 1995) and EAAT4 (Dehnes et al., 1998), which appear to be primarily located at the membrane.

2.4.3 EAAT4 is predominantly expressed in cerebellar perysynapses and control synaptic excitability

EAAT4 is predominantly expressed in the cerebellum (Yamada et al., 1996;Furuta et al., 1997;Inage et al., 1998;Dehnes et al., 1998), specifically in the Purkinje cells. However, it has also been observed in other regions such as the forebrain (Dehnes et al., 1998), cortex (Massie et al., 2001) and retina (Ward et al., 2004). At the subcellular level, EAAT4 is generally located in the plasma membranes of the Purkinje cells soma and dendrites including spines (Yamada et al., 1996). Tanaka *et al.* did not detect EAAT4 expression in any of the synaptic regions of the Purkinje cells (Tanaka et al., 1997a) and therefore classified them as extra-synaptic transporters. A later study, using electron microscopy, found the majority of the EAAT4 immunoreactivity in the Purkinje cells plasma membrane and that the highest levels are extra-synaptically (Dehnes et al., 1998). However, Dehnes and colleagues were able to detect low, but significant concentration levels of EAAT4 in the synaptic membrane. Using RT-PCR and immunocytochemistry, EAAT4 have been recently localized also in astrocytes within the retina (Ward et al., 2004), whose functional significance they left as an open question.

EAAT4 exhibit a predominant anion conductance (Fairman et al., 1995;Wadiche et al., 1995;Melzer et al., 2003), and glial transporters are responsible for the majority of glutamate uptake in the brain (Bergles et al., 1999;Auger and Attwell, 2000;Danbolt, 2001), suggesting a role of EAAT4 controlling neuronal excitability by means of the anion channel. EAAT4 might be responsible of a “less important” glutamate clearance, transporting glutamate which has diffuse from the synaptic cleft to the extrasynaptic space, preventing glutamate spillover to adjacent synapses (Tanaka et al., 1997a;Takayasu et al., 2005).

In agreement with this apparently weak participation of EAAT4 in glutamate clearance, the contribution of EAAT4 to the glutamate uptake have been estimated to be only around 17% by taking the kainate receptor-mediated component of the synaptic current into consideration (Brasnjo and Otis, 2004). In addition, Huang *et al.* report the Purkinje cells, were EAAT4 is predominantly expressed, removing less than the 10% of the glutamate released by the climbing fibers (Huang et al., 2004). After all, although the relevance of the uncoupled anion conductance of EAAT4 is not fully understood, seems to be that EAAT4 was designed for something else than to capture glutamate. Some reports have suggested that the chloride conductance may act clamping the cell at negatives voltage values (Billups et al., 1996;Eliasof and Jahr, 1996), preventing the depolarization produced by the two positive charges moving in to the cell per glutamate cycle, which would reduce the driving force of the glutamate transport and consequently reduce the transport rate. We here report a novel voltage- and glutamate-dependent gating process mediated by EAAT4 which favors the idea of the chloride conductance of this isoform playing an important role in neuronal excitability. This process changes the selectivity of individual channels, permitting EAAT4 anion channels to conduct excitatory currents under certain conditions and inhibitory under others (see chapter 7).

2.4.4 EAAT5 is a retina-specific transporter

Very little is known about EAAT5 glutamate transporters. This isoform appears to be a retina-specific glutamate transporter (Arriza et al., 1997;Eliasof et al., 1998a;Eliasof et al., 1998b). It is present in both, cone and rod photoreceptors as well as in amacrine, ganglions (Fyk-Kolodziej et al., 2004) bipolar and Müller cells (Eliasof et al., 1998b). The glutamate-elicited current in EAAT5 is carried largely by chloride ions (Arriza et al., 1997). Therefore, as well as EAAT4, EAAT5 is thought to function mainly providing positive feedback rather than in removing glutamate, and furthermore through its hyperpolarizing action it may increase the uptake capacity of the other isoforms (Rauen, 2000;Veruki et al., 2006).

3. Discussion

3.1 A trimeric quaternary structure is evolutionary conserved in glutamate transporters

Glutamate transporters are known to be multimers. Haugeto *et al.* have demonstrate by double labeling post-embedding electron microscopy immunocytochemistry, SDS-PAGE and cross-linking analysis, that the two glial glutamate transporters, GLT1 and GLAST, as well as the neuronal EAAC1, form oligomeric complexes (Haugeto et al., 1996). However, the authors were not able to determine the subunit stoichiometry from their experiments. In 2000, Eskandari *et al.* proposeed a pentameric assembly based on results obtained with freeze-fracture electron microscopy (Eskandari et al., 2000). Nevertheless, freeze-fracture electron microscopy is only suitable to determine the subunit stoichiometry of membrane proteins with known transmembrane topology (Eskandari et al., 1998), a property that was not established at that time. Later on, a trimeric assembly was reported for two prokaryotic glutamate transporters (Yernool et al., 2003), opening the question whether oligomeric assembly could be different in eukaryotic and prokaryotic glutamate transporters.

We here demonstrated this is not the case and that EAATs exhibit an evolutionary conserved trimeric subunit stoichiometry (see chapter 6). Heterologously expressing a bacterial and a human glutamate transporter in *Xenopus* oocytes and mammalian cells and using Blue Native-PAGE and chemical cross-linking analysis, we show a trimeric quaternary structure for bacterial and human glutamate transporters. The expression of the human EAAT2 in an inducible cell line allowed the demonstration that this protein exclusively exists in a trimeric state independently of the expression level and that ionic currents elicited by EAAT2 glutamate translocation are correlated with the amount of trimeric protein (Fig 6.2D). Purified ecGltP reconstituted in lipid vesicles were fully functional in the trimeric state (Fig 6.5C and D), corroborating that the trimer is the functional conformational state of glutamate transporters. The trimeric quaternary structure have been corroborated by the crystal structure of a bacterial glutamate transporter homologue from *Pyrococcus horikoshii* (Fig. 3.1) (Yernool et al., 2004).

3.2 EAAT4-associated anion channels participate in neuronal excitability

During the last decades many evidences have been reported for EAATs sustaining two different transport processes. A secondary active transport mechanism in which one glutamate molecule is co-transported with 3 Na^+ and one proton into the cell and counter-transported with one K^+ ("coupled transport")(Levy et al., 1998;Zerangue and Kavanaugh, 1996), and a pore mediated anion conductance ("uncoupled transport")(Fairman et al., 1995;Larsson et al., 1996;Melzer et al., 2003;Wadiche et al., 1995). However, the molecular basis for these diverse transport functions, as well as the physiological relevance of the associated-anion conductance is still not well understood.

As discussed above, EAAT-associated anion currents have been suggested to play an important role in controlling the electric signal of certain excitable cells (Picaud et al., 1995;Larsson et al., 1996;Sonders and Amara, 1996;Rauen, 2000;Veruki et al., 2006). Using the patch clamp technique and heterologously expressing the rat isoform of EAAT4 in mammalian cells, we report a novel glutamate- and voltage-dependent gating process that changes the selectivity of EAAT4-associated channels from ideally anion-selective to partially cation-permeable (see chapter 7). This process permits a dynamic switch between inhibitory and excitatory currents mediated by EAAT4-associated anion channels. Prolonged depolarizations produce a slow activation process, which represents an accumulation of EAAT4 anion channels in a state favoring cation influx and anion efflux, allowing a switch between inhibitory currents in resting cells and excitatory currents in electrically active cells. This transporter-mediated conductance could modify the excitability of Purkinje neurons, providing them with an unprecedented mechanism for adaptation.

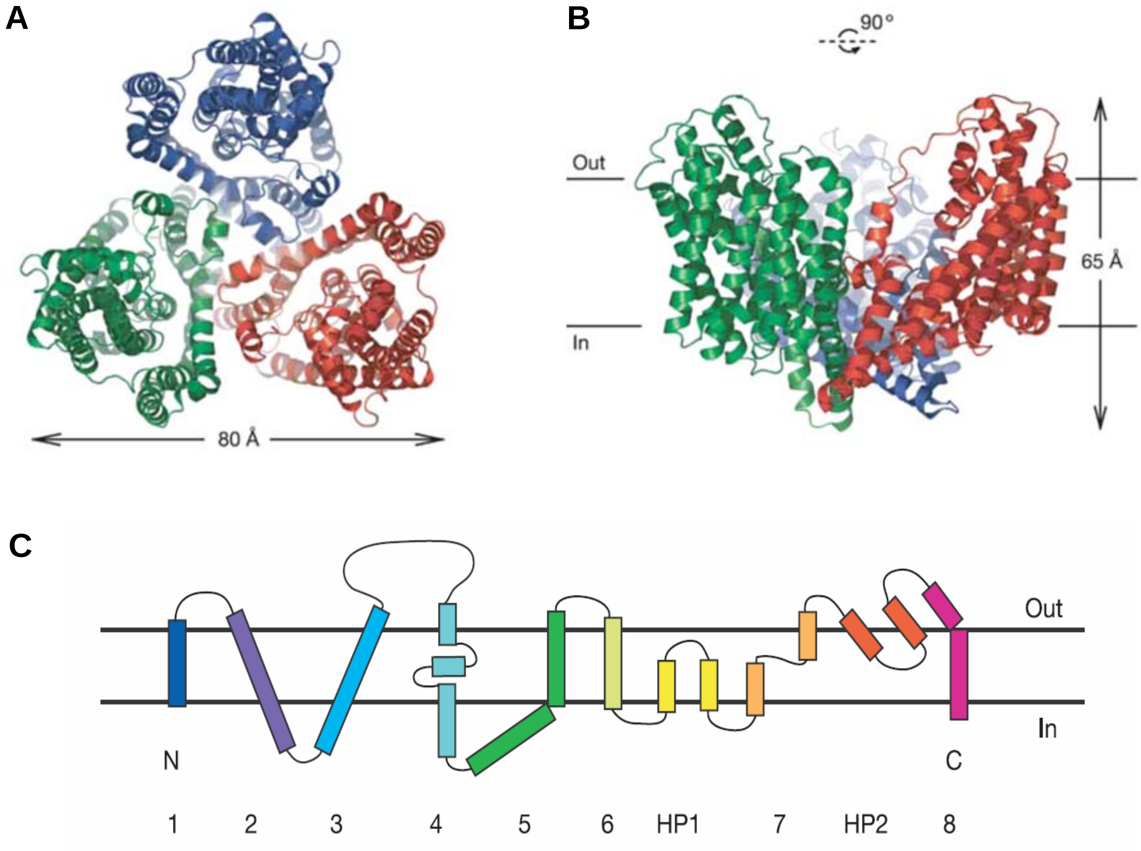

Figure 3.1. Crystal structure of a bacterial glutamate transporter homologe from *Pyrococcus horikoshii.* (A) Ribbon representation of the trimeric protein, in which the protomers are red, blue and green, viewed from the extracellular side of the membrane. (B) View of the trimer parallel to the membrane. (C) Schematic representation of $\mathrm{Glt}_{\mathrm{ph}}$ transmembrane topology. From Yernool *et al* 2004.

3.3 Individual subunits interact activating the EAAT4-associated anion channel

The crystal structure of a bacterial glutamate transporter homologue provided detailed insights into the architecture of the transporter and likely conformational changes underlying glutamate transport (Yernool et al., 2004), corroborate the trimeric quaternary structure of this proteins and finally clarify their transmembrane topology (Fig. 3.1)(Yernool et al., 2004). However, the molecular basis of the EAAT-associated anion channels function is not well understood today. EAAT glutamate transporters assemble as homotrimeric complexes (Haugeto et al., 1996;Yernool et al., 2003;Yernool et al., 2004;Koch and Larsson, 2005), and trimerization of monomers occurs after synthesis of the individual subunits resulting in stable trimers as the sole native and functional oligomeric state (see chapter 6). It is of general agreement that the trimeric structure is able to mediate both carrier- as well as pore-mediated transport processes. However, there are still many open questions. For example, how two very different processes are carried by the same oligomeric protein? How is this dual function structurally performed and how one influences on the other?

While each subunit is thought to transport glutamate independently from the rest of the oligomer (Grewer et al., 2005;Koch and Larsson, 2005), it is presently unclear, if each subunit is also capable of anion transport by itself (Ryan et al., 2004;Grewer et al., 2005;Koch et al., 2007;Leary et al., 2007), or if the EAAT anion pore is jointly formed by several subunits (Eskandari et al., 2000). It has been postulated that the two functions of glutamate transporters arise from separate transmembrane domains. The C-terminal region is thought to be the substrate binding and glutamate translocation domain (Vandenberg et al., 1995;Kavanaugh et al., 1997;Bendahan et al., 2000;Ryan and Vandenberg, 2002;Seal et al., 2001), whereas the second transmembrane domain in the N-terminal half of the protein it has been postulated to play a role in chloride channel function (Ryan et al., 2004).

Different models have been proposed as how this two processes are structurally assembled, but there are principally two main concepts: 1) the chloride ions and transport substrate cross the membrane through the same conduction pathway (Wadiche et al., 1995;Larsson et al., 1996) or 2) the protein have two different pathways one for coupled transport, one for anion channel activity (Sonders and Amara, 1996)(Fig. 3.2). Although evidences that both processes do not affect to each other (Ryan and Vandenberg, 2002;Ryan et al., 2004) are strong arguments in favor of two different conduction pathways explanation, this remains as an open discussion. The data presented here in chapter 8 supports the idea of two different pathways, one for each transport process.

Heterologously expressing a neuronal, EAAT4, isoform in *Xenopus* oocytes and mammalian cells, and combining glutamate flux and anion current measurements, we here demonstrate an intersubunit interaction during EAAT4-associated anion channels activation (see chapter 8). Glutamate concentration dependence of radioactive glutamate uptake behaves as expected with a Michaleis-Menten relationship fashion, in agreement with the ability of an individual subunit to perform the coupled transport (Grewer et al., 2005;Koch and Larsson, 2005). In contrast, the glutamate dependence of the anion currents activation display a sigmoidal relationship arguing that the cooperative binding of at least more than one glutamate molecule is necessary to fully activate the EAAT4 anion channel (Fig. 8.3).

Since only one glutamate molecule is transported per transport cycle (Zerangue and Kavanaugh, 1996;Levy et al., 1998), the cooperativity between glutamate binding sites most likely arises from an interaction between different carrier domains. Two point mutations in the neighborhood of the glutamate binding site (Zhang and Kanner, 1999;Yernool et al., 2004) alter the substrate dependence of anion currents, leaving the concentration dependence of glutamate uptake unaffected (Figures 8.5 and 8.6), being another evidence in favor of

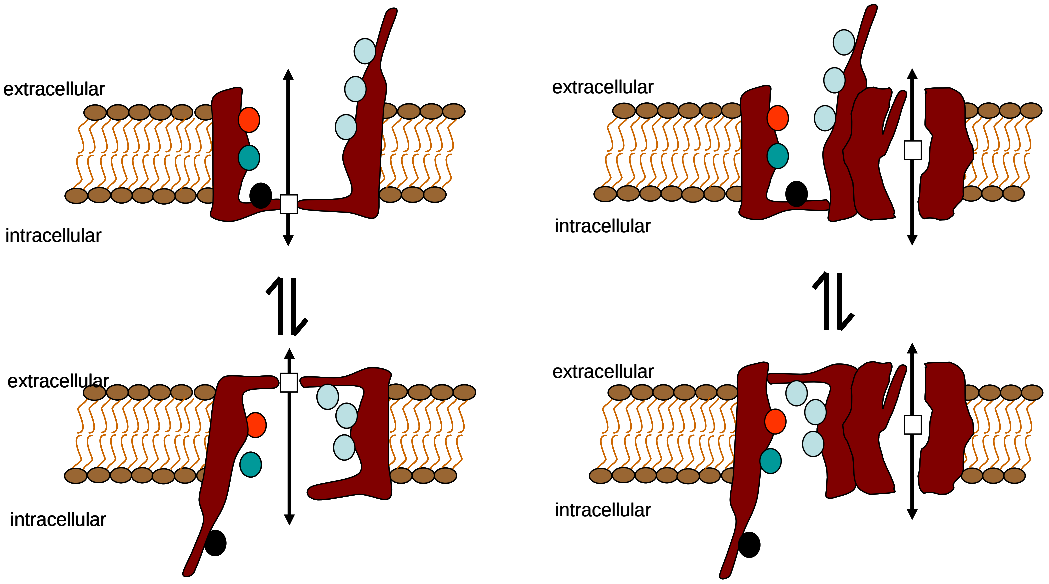
extracellular
intracellular
extracellular
intracellular
extracellular
intracellular
extracellular
intracellular

Wadiche *et al.* and Larsson *et al.*

Sonders and Amara

Figure 3.2 Schematic models for the glutamate translocation and chloride permeation pathways in glutamate transporters. Blue circles represent Na^+ ions, green circles represent H^+, black circles represent K^+ ions, red circle represent glutamate and white square represent Cl^-. Models adapted from (Wadiche et al., 1995;Larsson et al., 1996) and (Sonders and Amara, 1996)

intersubunit interaction during anion channel activation. These point mutations also affect time- and voltage-dependence of EAAT4-associated anion channels gating transitions (Fig. 8.7); again an interaction between the translocation regions with the pore would fit as a likely explanation for this observation.

In contrast with our results, Larsson's group have recently reported EAAT4-associated anion channels functioning independently on each monomer subunit of the protein (Koch et al., 2007). The difference of our results with Koch *et al.* could be explained by differences in the way we measured the anion currents, they measure steady state currents while we measure instantaneous. Since there are time- and voltage-dependent changes that at the same time depend on the glutamate concentration (Melzer et al., 2003), we believe that determining the glutamate dependence of the late current affects the accuracy of the measurement. On the other hand they observe such a small currents that probably could be contaminated by endogenous current that, in the conditions they are using, are more than 40% of the current amplitude they are measuring (unpublished observations). If the voltage dependence of the background current is different from the voltage dependence of the EAAT4 current, the glutamate induced EAAT4 anion current amplitude could be underestimated.

3.4 EAATs exhibit isoform specific gating properties

EAAT3 subunits functioning independently as anion channels has been observed by different groups (Ryan et al., 2004;Grewer et al., 2005;Leary et al., 2007). Although this also looks controversial with our results, an isoform specific channel function would be a likely explanation for the different results. This would be not surprising since there have been other important differences reported for these two isoforms. For example it have been observed that the anion current contribution to the total component of the current carried by EAAT is much smaller on EAAT3 (Wadiche et al., 1995) than on EAAT4 (Fairman et al., 1995). Another notable difference described is the huge difference in transport rates, which for EAAT3 have been reported to be 90 s^{-1} (Grewer et al., 2000) while for EAAT4 is smaller than 3 s^{-1} (Mim et al., 2005).

We studied uptake and anion currents of hEAAT3 and rEAAT4 heterologously expressed in mammalian and amphibian cells using voltage clamp approaches (see chapter 9). hEAAT3 shows a perfect hyperbolic glutamate dependence of the anion channel activation, while rEAAT4 exhibit the same sigmoidal relationship (Fig. 9.5A). In addition, two point mutations that affect the glutamate dependence of rEAAT4 (Fig. 8.6), affect the K_D as well as they do on rEAAT4 but did not affect de steepness of the curve (Fig. 9.5C). Time- and voltage-dependence of the anion channel gating were different on EAAT3 and EAAT4. In cells dialyzed with a Cl-based solution and perfused with a SCN-based solution, hEAAT3 shows a time- and voltage-dependent activation upon depolarizing potentials in the absence as well as in the presence of glutamate, while rEAAT4 display a time- and voltage-dependent deactivation (Fig. 9.2). Differences in the interaction of the pore forming regions could be a likely explanation for the observed differences in gating transition.

As we already discussed above, the anion current component to the total current carried by EAATs is much smaller on EAAT4 than on EAAT3. Until now, the functional basis for this difference was unknown. By a modification of a stationary noise analysis we here demonstrate that hEAAT3 and rEAAT4 display identical single channel amplitudes and very similar absolutes open probabilities in the absence as well as in the presence of glutamate (Fig. 9.3). These results are somehow surprising since the predominant macroscopic anion conductance of EAAT4 was always thought to originate from an associated anion channel with large single channel amplitude. However, this result does not argue against the general accepted physiological role of EAAT4 as anion channel in controlling neuronal excitability.

In contrast, the very low glutamate transport rate showed by EAAT4 might be necessary to allow this function. We report here a capacity of EAAT4-associated anion channels to switch mediating inhibitory and excitatory currents depending on the electrical state of the cell (see chapter 7). Excitatory currents will result in a depolarization that will cause an increase of the intracellular [Na^+] and consequently induce an inversion of the glutamate transporter direction. This process would produce an increase of the extracellular [glutamate] and could induce an excitotoxic process. However, the low transport capacity they display, allow them to regulate the cellular excitability without inducing a glutamatergic signal.

4. Conclusions

Our results demonstrate that EAAT glutamate transporters exhibit an evolutionarily conserved trimeric quaternary structure. Isoform specific subunit interactions modulate the gating of anion channels providing a likely explanation for their different activation mechanisms. Moreover, we demonstrate that different isoforms exhibit identical anion channels conductances, while they differ in ion transport rates. The differences between EAAT isoforms provide the basis for their specialized functions, preventing excitotoxicity through the glutamate transport and controlling neuronal excitability through the anion channel.

5. References

1. Amara SG, Fontana AC (2002) Excitatory amino acid transporters: keeping up with glutamate. Neurochem Int 41:313-318.

2. Arriza JL, Eliasof S, Kavanaugh MP, Amara SG (1997) Excitatory amino acid transporter 5, a retinal glutamate transporter coupled to a chloride conductance. Proc Natl Acad Sci U S A 94:4155-4160.

3. Arriza JL, Fairman WA, Wadiche JI, Murdoch GH, Kavanaugh MP, Amara SG (1994) Functional comparisons of three glutamate transporter subtypes cloned from human motor cortex. J Neurosci 14:5559-5569.

4. Arriza JL, Kavanaugh MP, Fairman WA, Wu YN, Murdoch GH, North RA, Amara SG (1993) Cloning and expression of a human neutral amino acid transporter with structural similarity to the glutamate transporter gene family. J Biol Chem 268:15329-15332.

5. Auger C, Attwell D (2000) Fast removal of synaptic glutamate by postsynaptic transporters. Neuron 28:547-558.

6. Bendahan A, Armon A, Madani N, Kavanaugh MP, Kanner BI (2000) Arginine 447 plays a pivotal role in substrate interactions in a neuronal glutamate transporter. Journal of Biological Chemistry 275:37436-37442.

7. Berger UV, Hediger MA (1998) Comparative analysis of glutamate transporter expression in rat brain using differential double in situ hybridization. Anat Embryol (Berl) 198:13-30.

8. Bergles DE, Diamond JS, Jahr CE (1999) Clearance of glutamate inside the synapse and beyond. Curr Opin Neurobiol 9:293-298.

9. Billups B, Rossi D, Attwell D (1996) Anion conductance behavior of the glutamate uptake carrier in salamander retinal glial cells. J Neurosci 16:6722-6731.

10. Brasnjo G, Otis TS (2004) Isolation of glutamate transport-coupled charge flux and estimation of glutamate uptake at the climbing fiber-Purkinje cell synapse. Proc Natl Acad Sci U S A 101:6273-6278.

11. Broer S, Brookes N (2001) Transfer of glutamine between astrocytes and neurons. J Neurochem 77:705-719.

12. Chaudhry FA, Lehre KP, Campagne MV, Ottersen OP, Danbolt NC, StormMathisen J (1995) Glutamate Transporters in Glial Plasma-Membranes - Highly Differentiated Localizations Revealed by Quantitative Ultrastructural Immunocytochemistry. Neuron 15:711-720.

13. Chen WZ, Aoki C, Mahadomrongkul V, Gruber CE, Wang GJ, Blitzblau R, Irwin N, Rosenberg PA (2002) Expression of a variant form of the glutamate transporter GLT1 in neuronal cultures and in neurons and astrocytes in the rat brain. Journal of Neuroscience 22:2142-2152.

14. Chen WZ, Mahadomrongkul V, Berger UV, Bassan M, DeSilva T, Tanaka K, Irwin N, Aoki C, Rosenberg PA (2004) The glutamate transporter GLT1a is expressed in excitatory axon terminals of mature hippocampal neurons. Journal of Neuroscience 24:1136-1148.

15. Conti F, DeBiasi S, Minelli A, Rothstein JD, Melone M (1998) EAAC1, a high-affinity glutamate transporter, is localized to astrocytes and gabaergic neurons besides pyramidal cells in the rat cerebral cortex. Cerebral Cortex 8:108-116.

16. Danbolt NC (2001) Glutamate uptake. Prog Neurobiol 65:1-105.

17. Danbolt NC, Storm-Mathisen J, Kanner BI (1992) An [Na+ + K+]coupled L-glutamate transporter purified from rat brain is located in glial cell processes. Neuroscience 51:295-310.

18. Dehnes Y, Chaudhry FA, Ullensvang K, Lehre KP, Storm-Mathisen J, Danbolt NC (1998) The glutamate transporter EAAT4 in rat cerebellar Purkinje cells: A glutamate-gated chloride channel concentrated near the synapse in parts of the dendritic membrane facing astroglia. Journal of Neuroscience 18:3606-3619.

19. Durand GM, Kovalchuk Y, Konnerth A (1996) Long-term potentiation and functional synapse induction in developing hippocampus. Nature 381:71-75.

20. Eliasof S, Arriza JL, Leighton BH, Amara SG, Kavanaugh MP (1998a) Localization and function of five glutamate transporters cloned from the salamander retina. Vision Res 38:1443-1454.

21. Eliasof S, Arriza JL, Leighton BH, Kavanaugh MP, Amara SG (1998b) Excitatory amino acid transporters of the salamander retina: identification, localization, and function. J Neurosci 18:698-712.

22. Eliasof S, Jahr CE (1996) Retinal glial cell glutamate transporter is coupled to an anionic conductance. Proc Natl Acad Sci U S A 93:4153-4158.

23. Eskandari S, Kreman M, Kavanaugh MP, Wright EM, Zampighi GA (2000) Pentameric assembly of a neuronal glutamate transporter. Proceedings of the National Academy of Sciences of the United States of America 97:8641-8646.

24. Eskandari S, Wright EM, Kreman M, Starace DM, Zampighi GA (1998) Structural analysis of cloned plasma membrane proteins by freeze-fracture electron microscopy. Proc Natl Acad Sci U S A 95:11235-11240.

25. Fairman WA, Vandenberg RJ, Arriza JL, Kavanaugh MP, Amara SG (1995) An excitatory amino-acid transporter with properties of a ligand-gated chloride channel. Nature 375:599-603.

26. Furness DN, Lehre KP (1997) Immunocytochemical localization of a high-affinity glutamate-aspartate transporter, GLAST, in the rat and guinea-pig cochlea. Eur J Neurosci 9:1961-1969.

27. Furuta A, Martin LJ, Lin CL, Dykes-Hoberg M, Rothstein JD (1997) Cellular and synaptic localization of the neuronal glutamate transporters excitatory amino acid transporter 3 and 4. Neuroscience 81:1031-1042.

28. Fyk-Kolodziej B, Qin P, Dzhagaryan A, Pourcho RG (2004) Differential cellular and subcellular distribution of glutarnate transporters in the cat retina. Visual Neuroscience 21:551-565.

29. Galli A, Blakely RD, DeFelice LJ (1996) Norepinephrine transporters have channel modes of conduction. Proc Natl Acad Sci U S A 93:8671-8676.

30. Galli A, Jayanthi LD, Ramsey IS, Miller JW, Fremeau RT, Jr., DeFelice LJ (1999) L-proline and L-pipecolate induce enkephalin-sensitive currents in human embryonic kidney 293 cells transfected with the high-affinity mammalian brain L-proline transporter. J Neurosci 19:6290-6297.

31. Galli A, Petersen CI, deBlaquiere M, Blakely RD, DeFelice LJ (1997) Drosophila serotonin transporters have voltage-dependent uptake coupled to a serotonin-gated ion channel. J Neurosci 17:3401-3411.

32. Grewer C, Balani P, Weidenfeller C, Bartusel T, Tao Z, Rauen T (2005) Individual subunits of the glutamate transporter EAAC1 homotrimer function independently of each other. Biochemistry 44:11913-11923.

33. Grewer C, Watzke N, Wiessner M, Rauen T (2000) Glutamate translocation of the neuronal glutamate transporter EAAC1 occurs within milliseconds. Proceedings of the National Academy of Sciences of the United States of America 97:9706-9711.

34. Haugeto O, Ullensvang K, Levy LM, Chaudhry FA, Honore T, Nielsen M, Lehre KP, Danbolt NC (1996) Brain glutamate transporter proteins form homomultimers. Journal of Biological Chemistry 271:27715-27722.

35. Hille B (1970) Ionic channels in nerve membranes. Prog Biophys Mol Biol 21:1-32.

36. Howland DS, Liu J, She YJ, Goad B, Maragakis NJ, Kim B, Erickson J, Kulik J, DeVito L, Psaltis G, DeGennaro LJ, Cleveland DW, Rothstein JD (2002) Focal loss of the glutamate transporter EAAT2 in a transgenic rat model of SOD1 mutant-mediated amyotrophic lateral sclerosis (ALS). Proceedings of the National Academy of Sciences of the United States of America 99:1604-1609.

37. Huang YHH, Dykes-Hoberg M, Tanaka K, Rothstein JD, Bergles DE (2004) Climbing fiber activation of EAAT4 transporters and kainate receptors in cerebellar Purkinje cells. Journal of Neuroscience 24:103-111.

38. Inage YW, Itoh M, Wada K, Takashima S (1998) Expression of two glutamate transporters, GLAST and EAAT4, in the human cerebellum: their correlation in development and neonatal hypoxic-ischemic damage. J Neuropathol Exp Neurol 57:554-562.

39. Ingram SL, Amara SG (2000) Arachidonic acid stimulates a novel cocaine-sensitive cation conductance associated with the human dopamine transporter. J Neurosci 20:550-557.

40. Ingram SL, Prasad BM, Amara SG (2002) Dopamine transporter-mediated conductances increase excitability of midbrain dopamine neurons. Nat Neurosci 5:971-978.

41. Kanai Y, Bhide PG, DiFiglia M, Hediger MA (1995) Neuronal high-affinity glutamate transport in the rat central nervous system. Neuroreport 6:2357-2362.

42. Kanai Y, Hediger MA (1992) Primary structure and functional characterization of a high-affinity glutamate transporter. Nature 360:467-471.

43. Kanner BI (1996) Structure/function relationships in glutamate transporters. Biochem Soc Trans 24:843-846.

44. Kanner BI, Schuldiner S (1987) Mechanism of transport and storage of neurotransmitters. CRC Crit Rev Biochem 22:1-38.

45. Kavanaugh MP, Bendahan A, Zerangue N, Zhang YM, Kanner BI (1997) Mutation of an amino acid residue influencing potassium coupling in the glutamate transporter GET-1 induces obligate exchange. Journal of Biological Chemistry 272:1703-1708.

46. Koch HP, Brown RL, Larsson HP (2007) The glutamate-activated anion conductance in excitatory amino acid transporters is gated independently by the individual subunits. J Neurosci 27:2943-2947.

47. Koch HP, Larsson HP (2005) Small-scale molecular motions accomplish glutamate uptake in human glutamate transporters. Journal of Neuroscience 25:1730-1736.

48. Komuro H, Rakic P (1993) Modulation of neuronal migration by NMDA receptors. Science 260:95-97.

49. Larsson HP, Picaud SA, Werblin FS, Lecar H (1996) Noise analysis of the glutamate-activated current in photoreceptors. Biophys J 70:733-742.

50. Leary GP, Stone EF, Holley DC, Kavanaugh MP (2007) The glutamate and chloride permeation pathways are colocalized in individual neuronal glutamate transporter subunits. J Neurosci 27:2938-2942.

51. Lehre KP, Danbolt NC (1998) The number of glutamate transporter subtype molecules at glutamatergic synapses: chemical and stereological quantification in young adult rat brain. J Neurosci 18:8751-8757.

52. Levy LM, Lehre KP, Rolstad B, Danbolt NC (1993) A monoclonal antibody raised against an [Na(+)+K+]coupled L-glutamate transporter purified from rat brain confirms glial cell localization. FEBS Lett 317:79-84.

53. Levy LM, Warr O, Attwell D (1998) Stoichiometry of the glial glutamate transporter GLT-1 expressed inducibly in a Chinese hamster ovary cell line selected for low endogenous Na+-dependent glutamate uptake. Journal of Neuroscience 18:9620-9628.

54. Mager S, Kleinberger-Doron N, Keshet GI, Davidson N, Kanner BI, Lester HA (1996) Ion binding and permeation at the GABA transporter GAT1. J Neurosci 16:5405-5414.

55. Mason DJ, Huggett JF (2002) Glutamate transporters in bone. J Musculoskelet Neuronal Interact 2:406-414.

56. Massie A, Vandesande F, Arckens L (2001) Expression of the high-affinity glutamate transporter EAAT4 in mammalian cerebral cortex. Neuroreport 12:393-397.

57. Matthews JC, Beveridge MJ, Malandro MS, Rothstein JD, Campbell-Thompson M, Verlander JW, Kilberg MS, Novak DA (1998) Activity and protein localization of multiple glutamate transporters in gestation day 14 vs. day 20 rat placenta. Am J Physiol 274:C603-C614.

58. Matute C, Melone M, Vallejo-Illarramendi A, Conti F (2005) Increased expression of the astrocytic glutamate transporter GLT-1 in the prefrontal cortex of schizophrenics. Glia 49:451-455.

59. Melzer N, Biela A, Fahlke C (2003) Glutamate modifies ion conduction and voltage-dependent gating of excitatory amino acid transporter-associated anion channels. Journal of Biological Chemistry 278:50112-50119.

60. Milton ID, Banner SJ, Ince PG, Piggott NH, Fray AE, Thatcher N, Horne CH, Shaw PJ (1997) Expression of the glial glutamate transporter EAAT2 in the human CNS: an immunohistochemical study. Brain Res Mol Brain Res 52:17-31.

61. Mim C, Balani P, Rauen T, Grewer C (2005) The glutamate transporter subtypes EAAT4 and EAATs 1-3 transport glutamate with dramatically different kinetics and voltage dependence but share a common uptake mechanism. J Gen Physiol 126:571-589.

62. Nicholls D, Attwell D (1990) The release and uptake of excitatory amino acids. Trends Pharmacol Sci 11:462-468.

63. Pearce IA, Cambray-Deakin MA, Burgoyne RD (1987) Glutamate acting on NMDA receptors stimulates neurite outgrowth from cerebellar granule cells. FEBS Lett 223:143-147.

64. Peghini P, Janzen J, Stoffel W (1997) Glutamate transporter EAAC-1-deficient mice develop dicarboxylic aminoaciduria and behavioral abnormalities but no neurodegeneration. EMBO J 16:3822-3832.

65. Picaud SA, Larsson HP, Grant GB, Lecar H, Werblin FS (1995) Glutamate-gated chloride channel with glutamate-transporter-like properties in cone photoreceptors of the tiger salamander. J Neurophysiol 74:1760-1771.

66. Pines G, Danbolt NC, Bjoras M, Zhang Y, Bendahan A, Eide L, Koepsell H, Storm-Mathisen J, Seeberg E, Kanner BI (1992) Cloning and expression of a rat brain L-glutamate transporter. Nature 360:464-467.

67. Plachez C, Danbolt NC, Recasens M (2000) Transient expression of the glial glutamate transporters GLAST and GLT in hippocampal neurons in primary culture. Journal of Neuroscience Research 59:587-593.

68. Rabacchi S, Bailly Y, haye-Bouchaud N, Mariani J (1992) Involvement of the N-methyl D-aspartate (NMDA) receptor in synapse elimination during cerebellar development. Science 256:1823-1825.

69. Rauen T (2000) Diversity of glutamate transporter expression and function in the mammalian retina. Amino Acids 19:53-62.

70. Rauen T, Fischer F, Wiessner M (1999) Glia-neuron interaction by high-affinity glutamate transporters in neurotransmission. Adv Exp Med Biol 468:81-95.

71. Rauen T, Kanner BI (1994) Localization of the glutamate transporter GLT-1 in rat and macaque monkey retinae. Neurosci Lett 169:137-140.

72. Rauen T, Rothstein JD, Wassle H (1996) Differential expression of three glutamate transporter subtypes in the rat retina. Cell and Tissue Research 286:325-336.

73. Rossi DJ, Oshima T, Attwell D (2000) Glutamate release in severe brain ischaemia is mainly by reversed uptake. Nature 403:316-321.

74. Rossi DJ, Slater NT (1993) The developmental onset of NMDA receptor-channel activity during neuronal migration. Neuropharmacology 32:1239-1248.

75. Rothstein JD, Dykes-Hoberg M, Pardo CA, Bristol LA, Jin L, Kuncl RW, Kanai Y, Hediger MA, Wang Y, Schielke JP, Welty DF (1996) Knockout of glutamate transporters reveals a major role for astroglial transport in excitotoxicity and clearance of glutamate. Neuron 16:675-686.

76. Rothstein JD, Martin L, Levey AI, Dykes-Hoberg M, Jin L, Wu D, Nash N, Kuncl RW (1994) Localization of neuronal and glial glutamate transporters. Neuron 13:713-725.

77. Ryan RM, Mitrovic AD, Vandenberg RJ (2004) The chloride permeation pathway of a glutamate transporter and its proximity to the glutamate translocation pathway. Journal of Biological Chemistry 279:20742-20751.

78. Ryan RM, Vandenberg RJ (2002) Distinct conformational states mediate the transport and anion channel properties of the glutamate transporter EAAT-1. Journal of Biological Chemistry 277:13494-13500.

79. Scott HL, Pow DV, Tannenberg AEG, Dodd PR (2002) Aberrant expression of the glutamate transporter excitatory amino acid transporter 1 (EAAT1) in Alzheimer's disease. Journal of Neuroscience 22.

80. Seal RP, Shigeri Y, Eliasof S, Leighton BH, Amara SG (2001) Sulfhydryl modification of V449C in the glutamate transporter EAAT1 abolishes substrate transport but not the substrate-gated anion conductance. Proceedings of the National Academy of Sciences of the United States of America 98:15324-15329.

81. Shayakul C, Kanai Y, Lee WS, Brown D, Rothstein JD, Hediger MA (1997) Localization of the high-affinity glutamate transporter EAAC1 in rat kidney. Am J Physiol 273:F1023-F1029.

82. Slotboom DJ, Konings WN, Lolkema JS (1999) Structural features of the glutamate transporter family. Microbiology and Molecular Biology Reviews 63:293-+.

83. Sonders MS, Amara SG (1996) Channels in transporters. Curr Opin Neurobiol 6:294-302.

84. Storck T, Schulte S, Hofmann K, Stoffel W (1992) Structure, expression, and functional analysis of a Na(+)-dependent glutamate/aspartate transporter from rat brain. Proc Natl Acad Sci U S A 89:10955-10959.

85. Sutherland ML, Delaney TA, Noebels JL (1996) Glutamate transporter mRNA expression in proliferative zones of the developing and adult murine CNS. J Neurosci 16:2191-2207.

86. Takayasu Y, Iino M, Kakegawa W, Maeno H, Watase K, Wada K, Yanagihara D, Miyazaki T, Komine O, Watanabe M, Tanaka K, Ozawa S (2005) Differential roles of glial and neuronal glutamate transporters in Purkinje cell synapses. J Neurosci 25:8788-8793.

87. Tanaka J, Ichikawa R, Watanabe M, Tanaka K, Inoue Y (1997a) Extra-junctional localization of glutamate transporter EAAT4 at excitatory Purkinje cell synapses. Neuroreport 8:2461-2464.

88. Tanaka K, Watase K, Manabe T, Yamada K, Watanabe M, Takahashi K, Iwama H, Nishikawa T, Ichihara N, Hori S, Takimoto M, Wada K (1997b) Epilepsy and exacerbation of brain injury in mice lacking the glutamate transporter GLT-1. Science 276:1699-1702.

89. Tolner B, Poolman B, Wallace B, Konings WN (1992) Revised nucleotide sequence of the gltP gene, which encodes the proton-glutamate-aspartate transport protein of Escherichia coli K-12. J Bacteriol 174:2391-2393.

90. van den Pol AN, Gao XB, Patrylo PR, Ghosh PK, Obrietan K (1998) Glutamate inhibits GABA excitatory activity in developing neurons. J Neurosci 18:10749-10761.

91. Vandenberg RJ, Arriza JL, Amara SG, Kavanaugh MP (1995) Constitutive ion fluxes and substrate binding domains of human glutamate transporters. J Biol Chem 270:17668-17671.

92. Veruki ML, Morkve SH, Hartveit E (2006) Activation of a presynaptic glutamate transporter regulates synaptic transmission through electrical signaling. Nat Neurosci 9:1388-1396.

93. Wadiche JI, Amara SG, Kavanaugh MP (1995) Ion fluxes associated with excitatory amino acid transport. Neuron 15:721-728.

94. Ward MM, Jobling AI, Puthussery T, Foster LE, Fletcher EL (2004) Localization and expression of the glutamate transporter, excitatory amino acid transporter 4, within astrocytes of the rat retina. Cell Tissue Res 315:305-310.

95. Yamada K, Watanabe M, Shibata T, Tanaka K, Wada K, Inoue Y (1996) EAAT4 is a post-synaptic glutamate transporter at Purkinje cell synapses. Neuroreport 7:2013-2017.

96. Yang W, Kilberg MS (2002) Biosynthesis, intracellular targeting, and degradation of the EAAC1 glutamate/aspartate transporter in C6 glioma cells. J Biol Chem 277:38350-38357.

97. Yernool D, Boudker O, Folta-Stogniew E, Gouaux E (2003) Trimeric subunit stoichiometry of the glutamate transporters from Bacillus caldotenax and Bacillus stearothermophilus. Biochemistry 42:12981-12988.

98. Yernool D, Boudker O, Jin Y, Gouaux E (2004) Structure of a glutamate transporter homologue from Pyrococcus horikoshii. Nature 431:811-818.

99. Zerangue N, Kavanaugh MP (1996) Flux coupling in a neuronal glutamate transporter. Nature 383:634-637.

100. Zhang YM, Kanner BI (1999) Two serine residues of the glutamate transporter GLT-1 are crucial for coupling the fluxes of sodium and the neurotransmitter. Proceedings of the National Academy of Sciences of the United States of America 96:1710-1715.

101. Zschocke J, Bayatti N, Clement AM, Witan H, Figiel M, Engele J, Behl C (2005) Differential Promotion of Glutamate Transporter Expression and Function by Glucocorticoids in Astrocytes from Various Brain Regions. J Biol Chem 280:34924-34932.

List of Included Publications

(1) Sandra Gendreau, Stephan Voswinkel, **Delany Torres-Salazar**, Niklas Lang, Hannelore Heidtmann, Silvia Detro-Dassen, Günther Schmalzing, Patricia Hidalgo, and Christoph Fahlke (2004) A trimeric quaternary structure is conserved in bacterial and human glutamate transporters. *J Biol Chem***.** 279 (38): 39505-39512

(2) Nico Melzer, **Delany Torres-Salazar** and Christoph Fahlke (2005) A dynamic switch between inhibitory and excitatory currents in a neuronal glutamate transporter. *Proc Natl Acad Sci USA*. 102 (52): 19214-19218

(3) **Delany Torres-Salazar** and Christoph Fahlke (2006) Inter-subunit interactions in EAAT4 glutamate transporters. *J Neurosci.* 26 (28): 7513-7522

(4) **Delany Torres-Salazar** and Christoph Fahlke (2007) Neuronal glutamate transporters vary in substrate transport rate, but not in unitary anion channel conductance. *J Biol Chem*. 282(48):34719-26

6. A trimeric quaternary structure is conserved in bacterial and human glutamate transporters

Sandra Gendreau,[1,*] Stephan Voswinkel,[2,*] **Delany Torres-Salazar**,[2] Niklas Lang[1], Hannelore Heidtmann,[2] Silvia Detro-Dassen[1], Günther Schmalzing,[1,#] Patricia Hidalgo[2,3,#], and Christoph Fahlke,[2,3,#]

[1]Department of Molecular Pharmacology and [2]Department of Physiology, RWTH Aachen, Pauwelsstr. 30, 52057 Aachen, Germany,
[3]Centro de Estudios Cientificos, Avendia Prat 514, Valdivia, Chile
*,# contributing equally

J Biol Chem. **2004 Vol. 279, No 38: 39505-39512**

6.1 Abstract

Neuronal and glial glutamate transporters play a central role in the termination of synaptic transmission and in extracellular glutamate homeostasis in the mammalian central nervous system. They are known to be multimers, however the number of subunits forming a functional transporter is controversial. We studied the subunit stoichiometry of two distantly related glutamate transporters, the human glial glutamate transporter, hEAAT2, and a bacterial glutamate transporter from *E.coli*, ecgltP. Using blue native polyacrylamide gel electrophoresis, analysis of concatenated transporters and chemical cross-linking, we demonstrated that human and prokaryotic glutamate transporters expressed in *Xenopus laevis* oocytes or in mammalian cells are assembled as trimers composed of three identical subunits. In an inducible mammalian cell line expressing hEAAT2 the glutamate uptake currents correlate to the amount of trimeric transporters. Overexpression and purification of ecgltP in *E.coli* resulted in a homogenous population of trimeric transporters that were functional after reconstitution in lipid vesicles. Our results indicate that an evolutionarily conserved trimeric quaternary structure represents the sole native and functional state of glutamate transporters.

6.2 Introduction

Glutamate is the major excitatory neurotransmitter in the mammalian central nervous system. After the release from glutamatergic nerve terminals, glial and neuronal glutamate transporters remove glutamate from the synaptic cleft to ensure low resting glutamate levels and to prevent neuronal damage by excessive glutamate receptor activation. Five mammalian glutamate transporters, EAAT1 to EAAT5, have been cloned (1-5) and shown to belong to a large family of membrane transport proteins, the sodium-dicarboxylate symporter family (6).

EAAT glutamate transporters sustain two fundamentally distinct transport mechanisms. They function as co-transporters of glutamate, sodium, potassium and protons ions ("coupled transport") (7;8) and as anion channels ("uncoupled transport") (4;9-12). The molecular basis for these diverse transport functions is not understood. Eskandari *et al.* (13) suggested that the coupled and the uncoupled transport functions are mediated by distinct oligomeric states of the same protein subunit, i.e. a multimeric assembly conducts anions while a single subunit suffices for coupled glutamate transport. EAAT transporters are known to be multimers (14), and a pentameric assembly has been proposed based on results obtained with freeze-fracture electron-microscopy (13). However, freeze-fracture electron-microscopy is only suitable to determine the subunit stoichiometry of membrane proteins with known transmembrane topology (15), a property that has not yet been established for glutamate transporters (16).

Here, we determined the subunit stoichiometry of two distantly related glutamate transporters, the human glial glutamate transporter hEAAT2 (2) and the bacterial glutamate transporter ecgltP from *E. coli* (17). The results from a variety of experimental approaches indicate that the two transporters assemble as homotrimers demonstrating an evolutionary conserved trimeric quaternary structure of glutamate transporters.

6.3 Experimental Procedures

6.3.1 Expression of His_6-tagged polypeptides in *Xenopus* oocytes and in mammalian cells

A pTLN2-hEAAT2 plasmid (18) was modified by adding a cDNA fragment encoding six histidine residues either NH_2- (His_{NT}EAAT2) or COOH-terminal (His_{CT}EAAT2) to the hEAAT2 coding region by PCR. A cDNA fragment encoding a His-tagged ecgltP was amplified by PCR from genomic *E. coli* DNA and subcloned into a pGEMHE vector using *BamHI* and *HindIII* restriction sites. To generate the ecgltP-ecgltP concatameric construct (pGEMHE-ecgltP-ecgltP), an N-terminal His-tagged coding region of ecgltP was linked to a non-tagged ecgltP with a cDNA sequence encoding a 20 amino acid linker sequence (SPLHPGLYPYDVPDYAISAV) in a single open reading frame. Mutations were inserted using the QuikChange™ site-directed mutagenesis kit (Stratagene) and confirmed by sequencing. Transcription of cRNAs and handling of oocytes was performed as described (19).

To generate an inducible stable cell line, a cDNA fragment encoding an N-terminal His-tagged hEAAT2 was subcloned into the pcDNA5/FRT/To vector (Invitrogen). Flp-In T-Rex 293 cells (Invitrogen) were co-transfected with pcDNA5/FRT/To-His_{NTh}EAAT2 and pOG44 (Invitrogen) using the calcium phosphate method, and oligoclonal cell lines were obtained by selection for the antibiotic hygromycin (Invitrogen). After 28 days, hygromycin-resistant clones were picked and tested for uptake of radioactive L-^{3}H-glutamate after 24h incubation with 1 µg/ml tetracycline. Six cell lines were positive, and one was used for the experiments reported here.

6.3.2 Electrophysiological examination of injected *Xenopus* oocytes and stably transfected mammalian cells

EAAT-associated currents in oocytes were recorded by two-electrode voltage clamp using a CA1 amplifier (Dagan, Minneapolis, MN, USA). Oocytes were held at –30 mV, and currents elicited by 200 ms voltage steps between –130 mV and +40 mV were filtered at 2kHz (-3dB) and digitized with a sampling rate of 10 kHz using a Digidata AD/DA converter (Axon Instruments, Union City, CA, USA). The standard external solution contained (in mM): 96 NaCl, 4 KCl, 0.3 $CaCl_2$, 1 $MgCl_2$, 5 HEPES, pH 7.4, and the glutamate-containing solution was supplied with 0.5 mM L-glutamate. Anion currents were determined after exchanging the external solution to (in mM) 96 NaSCN, 4 KCl, 0.3 $CaCl_2$, 1 $MgCl_2$, 5 HEPES, pH 7.4 in the absence and presence of 0.5 mM external glutamate without any current subtraction procedure (12). Anion currents were normalized by dividing current amplitudes by the Glu/Na^+/H^+/K^+ uptake current amplitude measured at –140 mV. Glutamate uptake currents in mammalian cells were measured through standard whole-cell patch clamp recordings using an Axopatch 200B (Axon Instruments, Union City, CA, USA) amplifier as described (12). Currents were filtered at 5kHz (-3dB) and digitized with a sampling rate of 50 kHz using a Digidata (Axon Instruments). Cells were clamped to 0 mV for at least 2 s between test sweeps. The intracellular solution contained (in mM) 115 KCl, 2 $MgCl_2$, 5 EGTA, 10 HEPES, pH 7.4, the extracellular (in mM) 140 NaCl, 4 KCl, 2 $CaCl_2$, 1 $MgCl_2$, 5 HEPES, pH 7.4. To elicit glutamate transport-associated currents, cells were moved into a stream of an external solution supplemented with 0.5 mM L-glutamate. The glutamate uptake current was determined as the difference between the current amplitude in the presence and in the absence of glutamate measured at a test step to –175 mV. Data were analyzed using pClamp (Axon Instruments, Union City, CA) and SigmaPlot (Jandel Scientific, San Rafael, CA, USA) programs.

6.3.3 Purification of [^{35}S]methionine-labeled protein form *Xenopus* oocytes and mammalian cells

cRNA-injected and non-injected control oocytes were incubated for the indicated time with Revidue™ L-[^{35}S]methionine (> 37 TBq/mmol, Amersham Biosciences) at ~25 Mbq/ml (~0.1 MBq/oocyte) in frog Ringer's solution at 19°C for metabolic labeling. Either immediately after the pulse or after an additional chase period, the radiolabeled oocytes were extracted with digitonin (1.0%) in 0.1 M Na-phosphate buffer, pH 7.4. His-tagged proteins were isolated by Ni^{2+}-NTA agarose (Qiagen, Koln, Germany) chromatography as detailed previously (19) with the modification that iodoacetamide was routinely included at 10 mM and 1 mM in the lysis and washing buffers (20).

Flp-In T-Rex HEK293 cells stably expressing the His-EAAT2 transporter were cultured at a range of tetracycline concentrations (0 – 1 µg/ml) for 24h at 37°C, then starved for 30 min in methionine- and serum-free minimum DMEM medium, and subsequently metabolically labeled with Revidue™ L-[^{35}S] methionine at ~4 Mbq/ml in methionine- and serum-free minimum DMEM medium for 2h at 37°C. His-EAAT2 was natively purified from digitonin extracts of these cells by Ni^{2+}-NTA chromatography as described above.

6.3.4 Chemical cross-linking

His-tagged proteins bound to Ni^{2+}-NTA beads (packed volume ~15 µl) were washed twice with imidazole-free Na-phosphate buffer (pH 8.0) supplemented with 0.2% digitonin. The Ni^{2+}-NTA beads were resuspended in 50 µl of 0.2 M triethanolamine/HCl (pH 8.5), 0.5% digitonin. The cross-linking reaction was initiated by adding DMA (dimethyl adipimidate•2 HCl, Pierce) or DMS (dimethyl suberimidate•2 HCl, Pierce) from a freshly prepared stock solution in distilled water or DMSO, respectively. After 60 min at the indicated temperature, the cross-linking reaction was terminated by washing the Ni^{2+}-NTA agarose beads once with imidazole-free Na-phosphate buffer/0.2% digitonin. Bound protein were released from the beads with the non-denaturing elution buffer.

6.3.5 SDS-PAGE and BN-PAGE analysis

[^{35}S]methionine-labeled proteins were denatured for 10 min at 56°C with SDS sample buffer containing 20 mM dithiothreitol (DTT) and electrophoresed in parallel with [^{14}C]-labeled molecular mass markers (Rainbow, Amersham Biosciences, Freiburg, Germany) on linear SDS polyacrylamide gels. To investigate the glycosylation status of the proteins, samples were treated for 1-2 h with either endoglycosidase H (Endo H) or PNGase F (New England Biolabs, Beverly, MA, USA) in the presence of reducing SDS sample buffer and 1% (w/v) NP-40 to counteract SDS inactivation of PNGase F. BN-PAGE was performed as described (19) immediately after protein purification. Molecular mass markers (Combithek II, Boehringer Mannheim) were run in two different lanes of the gel and subsequently visualized by Coomassie and silver staining. Gels containing purified ecgltP were stained with silver. Radioactive proteins were visualized by autoradiography using BioMax MS films (Eastman Kodak Co.) at –70°C. Both SDS- and BN-polyacrylamide gels were fixed and dried. For quantification, the dried gels were exposed to a PhosphorImager screen and scanned using a Storm 820 PhosphorImager (Amersham Biosciences). Individual bands were quantified with the ImageQuant software.

6.3.6 Expression, purification, and reconstitution of ecgltP

The pASK-ecgltP construct was generated by subcloning the cDNA encoding ecgltP into a pASK-IBA5 (IBA, Gottingen, Germany) vector to add an N-terminal strep-tag. Transformed BL-21 (DE-3) *E. coli* bacteria were induced with 200µg/l anhydrotetracycline at 37 °C for 2h, harvested by centrifugation and stored at –80 °C until use. Membranes were collected by centrifugation at 100,000 X g for 60 minutes at 4 °C in a Beckman 45 Ti rotor. The protein was extracted by solubilization in 15 mM dodecylmaltoside (DDM) for 2 h at 4°C followed by centrifugation at 100,000 X g for 60 minutes at 4 °C. EcgltP was purified in one step by strep-tactin™ (IBA) affinity chromatography according to the manufacturer instruction manual. Western blots were carried out using a strep-tag AP detection kit (IBA) following manufacturer´s instructions.

Strep-ecgltP was reconstituted into liposomes using standard methods (21;22). Proteoliposomes were resuspended in buffer A (20 mM morpholinoethanesulfonic acid (Mes), 100 mM potassium acetate, 5 mM $MgSO_4$, pH 6) and incubated for 2h on ice. The uptake was initiated by diluting 25 µl of the proteoliposomes in 650 µl of buffer B (120 mM MES, 100 mM NaOH, 5 mM $MgSO_4$, 2 µM L-[^{3}H]-glutamate, pH 6) at room temperature (22). Control experiments were performed with vesicles without ecgltP or by diluting the proteoliposomes in 650 µl buffer A supplemented with 2 µM L-[^{3}H]-glutamate. 100 µl probes were taken after various time periods and then poured into a 10-fold excess of ice-cold 0.1 M LiCl solution, followed by immediate filtration over cellulose nitrate filters. After washing with 0.1 M LiCl filters were assayed for radioactivity.

6.4 Results

6.4.1 His-tagged hEAAT2 transporters exhibit unaltered functional properties

We added an NH_2- or a COOH-terminal hexahistidine tag to hEAAT2 and ecgltP to purify the transporters by a single Ni^{2+}-metal affinity chromatography step. To test whether these sequence alterations affect transport functions, WT and His-tagged transporters were expressed in *Xenopus* oocytes and currents examined with two-electrode voltage clamp. We performed experiments in two distinct external anion compositions to separate the current components of the stoichiometrically coupled transport of glutamate Na^+ H^+, and K^+ from the pore-mediated anion conductance. In Cl^--based external solution, the conductance of the hEAAT2-associated anion channel is very small (9), and the Glu/Na^+/H^+/K^+ current amplitudes can therefore be approximated to the difference between currents in the presence and absence of external glutamate substrate. The so-calculated current amplitudes are similar in magnitude and voltage dependence for WT and His-tagged hEAAT2 (Fig. 6.1A). In a SCN^--based external solution, hEAAT2 exhibit anion currents that largely exceeded the Glu/Na^+/H^+/K^+ current component allowing to directly measure anion currents (12). For all tested hEAAT2 constructs, a comparable constitutive anion current was observed in the absence of glutamate (Fig. 6.1B) that was about two-fold increased by external glutamate (12). We conclude that the addition of the His-tag does not alter the coupled and the uncoupled current amplitudes of hEAAT2. Neither glutamate-induced inward currents nor glutamate-induced increases of anion currents were observed in oocytes injected with WT or His-tagged ecgltP cRNA.

6.4.2 SDS-PAGE analysis and glycosylation of glutamate transporters heterologously expressed in *Xenopus* oocytes

His-tagged hEAAT2 and ecgltP transporters expressed in *Xenopus* oocytes were metabolically labeled with [^{35}S] methionine, extracted with 1% (wt/vol) digitonin and purified

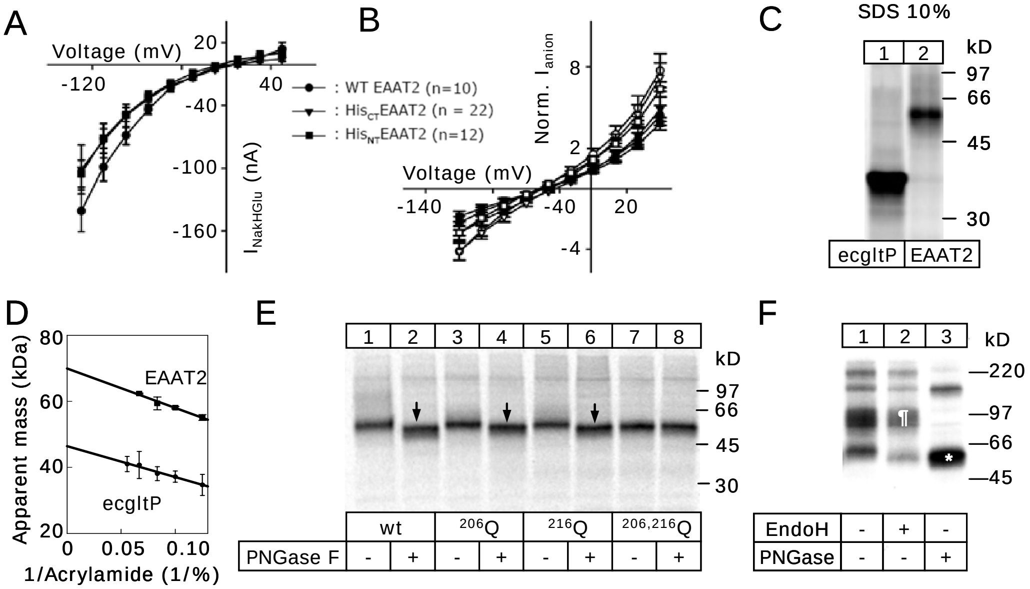

Figure 6.1. Basic functional and biochemical characterization of glutamate transporters expressed in *Xenopus* oocytes. ***A***, Voltage dependence of the absolute Glu/Na$^+$/H$^+$/K$^+$ uptake current component for WT EAAT2, His$_{NT}$EAAT2 and His$_{CT}$EAAT2. ***B***, Voltage dependence of the normalized anion current amplitude in the absence (closed symbols) and in the presence (open symbols) of 0.5 mM L-glutamate. Means ± SEM, n > 7. ***C***, EAAT2 and ecgltP transporters purified by Ni-NTA chromatography after a 4h [^{35}S]methionine pulse from *Xenopus* oocytes were resolved by reducing SDS-PAGE (10% acrylamide) in parallel with [^{14}C]-labeled molecular mass markers. ***D***, Plot of molecular masses of the hEAAT2 and ecgltP polypeptides determined by SDS-PAGE at various polyacrylamide concentrations versus the polyacrylamide concentration. ***E***, SDS-PAGE analysis of WT EAAT2 and N206Q and N216Q EAAT2 purified from *Xenopus* oocytes after a 4h [^{35}S]methionine pulse. ***F***, SDS-PAGE analysis after a 36h chase interval subsequent to the 4h [^{35}S]methionine pulse reveals the additional presence of an Endo H resistant EAAT2 polypeptide (¶), which can be reduced to the protein core by PNGase F. *, Endo H-sensitive EAAT2 polypeptide.

by metal affinity chromatography. Both proteins expressed at high levels in *Xenopus* oocytes and were metabolically stable during a sustained chase. When denatured by SDS and resolved by reducing SDS-PAGE, the hEAAT2 and the ecgltP polypeptides migrated both at 10-20% lower masses than calculated from the amino acid sequences (48 kDa for ecgltP and 63 kDa for hEAAT2) (Fig. 6.1C). However, a Ferguson analysis determining the apparent molecular mass in SDS-PAGE gels for several acrylamide concentrations (23) yielded molecular masses of 46 kDa for the His-tagged ecgltP and 69 kDa for His-hEAAT2 when extrapolated to high acrylamide concentration (Fig. 6.1D) demonstrating that the observed differences between the apparent and the calculated masses are caused by anomalous migration.

Membrane proteins are often N-glycosylated when expressed in eukaryotic cells. As oligosaccharide side chains are sequentially processed from a high mannose form in the endoplasmatic reticulum (ER) to the complex-glycosylated form in the Golgi apparatus, the presence of complex oligosaccharides can be used to monitor the efficiency of the exit of the protein from the ER. The hEAAT2 sequence encompasses two glycosylation sequences, ^{206}NATS and ^{216}NETV, which are both located on the predicted large ectodomain (residues 143-239) between transmembrane regions TM3 and TM4 (16). Complete deglycosylation of newly synthesized hEAAT2 polypeptide in *Xenopus* oocytes during a 4h pulse period resulted in a 3 kDa decrease of the molecular mass (Fig. 6.1E, lanes 1-2), corresponding to the mass of one single N-glycan. Moreover, glutamine substitution of only one of the two asparagine residues resulted in polypeptides migrating at the same position as the WT hEAAT2 (Fig. 6.1E, lanes 3 & 5) suggesting that one of the two glycosylation sites remain unused in WT EAAT2 presumably because of the small distance of only 10 amino acids. No mass shift by PNGaseF was observed when the asparagines residues of both N-glycosylation sequons were replaced by glutamine (lanes 7 & 8).

Posttranslational processes during a 36h chase interval lead to the occurrence of a prominent broad band (75-95 kDa) well above that of the core-glycosylated hEAAT2 polypeptide (~60 kDa) (Fig. 6.1E). This band could be reduced to the hEAAT2 apoprotein by incubation with PNGase F (~57 kDa in lane 3), but not with Endo H. Resistance to Endo H treatment distinguishes high-mannose from complex oligosaccharides and attributes the higher molecular weight band to the mature complex-glycosylated hEAAT2 polypeptide. Quantification by phosphorimage analysis demonstrated that 66% of the total hEAAT2 proteins leave the ER within the 36h chase interval. We conclude that the majority of hEAAT2 subunits are in a mature state located in post-ER compartments including the plasma membrane after the chase interval. The prokaryotic ecgltP polypeptide does not exhibit glycosylation sites precluding such an analysis for this particular transporter.

6.4.3 hEAAT2 transporters migrate as trimers in blue native PAGE gels

Blue native (BN) PAGE analysis (24;25) permits gel electrophoresis under non-denaturing conditions and thus the determination of the oligomeric structure of proteins (19;26;27). hEAAT2 transporters expressed in *Xenopus* oocytes migrated predominantly as a single band of ~200 kDa (Fig. 6.2A) in BN-PAGE, when compared with the defined membrane protein complexes generated by partial denaturing of the homopentameric α1 GlyR (26) or the homotrimeric P2X$_1$ receptor (19). These molecular masses are well above those of the respective monomers suggesting that hEAAT2 transporters exist exclusively as an homogenous population of multimers in *Xenopus* oocytes.

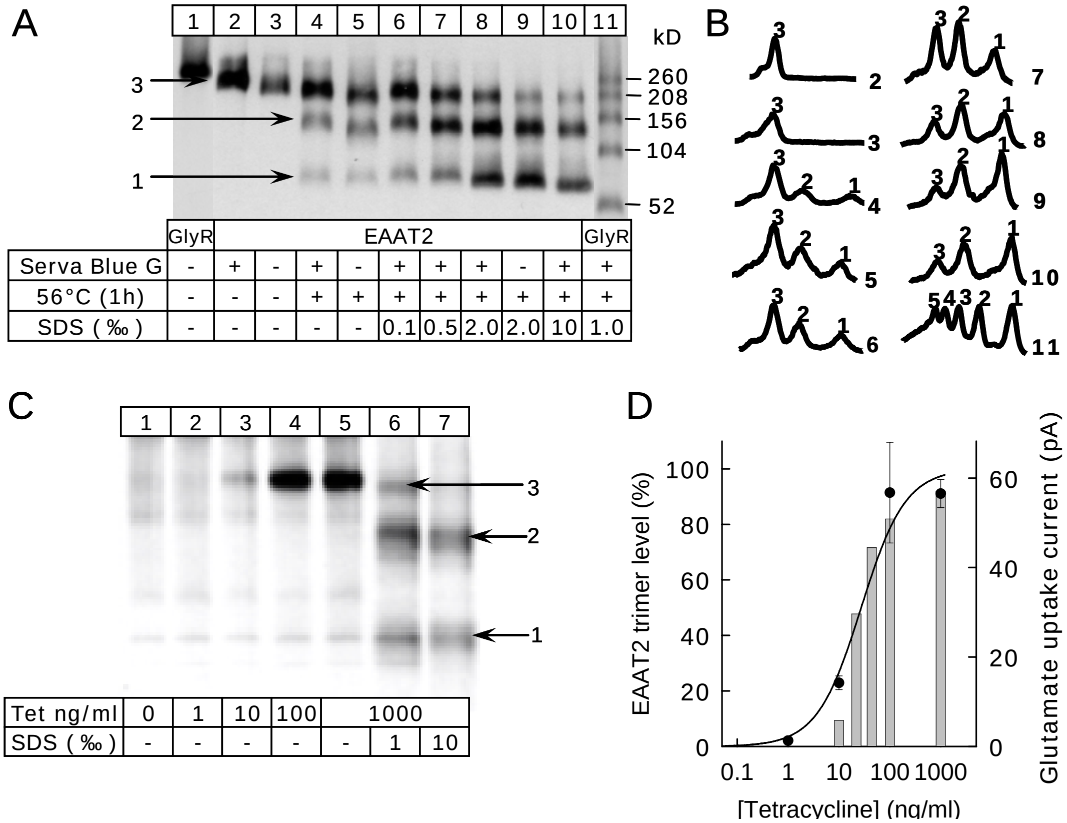
A
1 2 3 4 5 6 7 8 9 10 11
kD
3
2
1
260
208
156
104
52
GlyR
EAAT2
GlyR
Serva Blue G - + - + - + + + - + +
56°C (1h) - - - + + + + + + + +
SDS (‰) - - - - - 0.1 0.5 2.0 2.0 10 1.0
B
3 2
3 3
3 2 1 4
3 2 1 5
3 2 1 6
3 2 1 7
3 2 1 8
3 2 1 9
3 2 1 10
5 4 3 2 1 11
C
1 2 3 4 5 6 7
3
2
1
Tet ng/ml 0 1 10 100 1000
SDS (‰) - - - - - 1 10
D
EAAT2 trimer level (%)
0
20
40
60
80
100
Glutamate uptake current (pA)
0
20
40
60
0.1 1 10 100 1000
[Tetracycline] (ng/ml)

Figure 6.2. Oligomeric state of EAAT2 transporters in *Xenopus* oocytes and mammalian cells determined by BN-PAGE. ***A***, Autoradiography of a BN-PAGE gel containing EAAT2 purified from *Xenopus* oocytes. Samples were treated as indicated to induce dissociation into lower order intermediates including monomers. ***B***, Quantitative profiles of the gel lanes shown in A were obtained by PhosphorImager analysis and are marked by the same lane numbers. The origin of the abscissa corresponds to the top of the polyacrylamide gel. Numbers specify the oligomeric state of the corresponding protein peak. The five bands that became visible upon partial denaturing of the GlyR are consistent with its pentameric state. ***C,*** Autoradiography of a BN-PAGE gel containing EAAT2 transporter isolated from Flp-In T-Rex HEK293 cells. Various EAAT2 protein levels were adjusted by inducing the cells with the indicated concentrations of tetracycline. ***D***, Variation of normalized trimeric EAAT2 protein levels (bars, means from 2 experiments) and of mean glutamate uptake current amplitudes (symbols, means ± SEM from 3 – 8 cells) with the tetracycline concentration 24 h before the experiment. The solid line represents a fit of the tetracycline concentration dependence of the amount of the EAAT2 trimer with a Michaelis-Menten function.

The electrophoretic mobility of proteins is biased by dye binding and protein shape to an unclear extent, and therefore the exact number of monomers incorporated per protein complex cannot be readily deduced from mass estimates alone. A reliable approach to determine the number of polypeptide chains incorporated in one transporter complex is to dissociate protein complexes into lower order intermediates by weakening non-covalent subunit interactions by heat or low concentrations of SDS (19;26). For hEAAT2, a 1h incubation at 56°C both in the presence (Fig. 6.2A, lane 4) and absence (lane 5) of Coomassie dye generated a ladder-like pattern of three protein bands. Incubation in the additional presence of increasing concentrations of SDS (lanes 6-10) led to a gradual disappearance of the ~200 kDa protein and an enhanced appearance of two additional proteins of masses of ~130 kDa and ~65 kDa. At ≥ 0.05% SDS, the ~65 kDa band became the predominant one (lanes 9-10). Figure 6.2B shows PhosphorImager analysis of the gel shown in Figure 6.2A. All dissociating conditions caused the appearance of a total of three bands with masses corresponding to the assembly of three, two and one units with the monomer becoming the dominant species at increasing SDS concentrations (Fig. 6.2A). The complex-glycosylated hEAAT2 transporter also exhibits a trimeric structure as revealed by BN-PAGE (data not shown). The virtual absence of aggregated proteins and other multimerization states (Fig. 6.2) indicates that trimerization of hEAAT2 monomers occurs efficiently in oocytes during or shortly after synthesis of the individual subunits. A productive assembly process is further illustrated by the efficient exit of the hEAAT2 transporters from the ER inferred from the acquisition of complex-type carbohydrates (see above).

Oligomerization of EAAT transporters might be affected by the cellular environment or by unphysiologically high expression levels. To address these possibilities, we generated an inducible mammalian cell line that stably expresses N-terminal His-tagged hEAAT2 (Fig.

6.2C and D). This cell line allowed us to study oligomerization of hEAAT2 at different protein expression levels by simply varying the tetracycline concentration added to the culture medium 24 h prior to the experiment. hEAAT2 transporters expressed in mammalian cells were metabolically labeled with [^{35}S]methionine, extracted with 1% (wt/vol) digitonin and purified by metal affinity chromatography. Incubation of the cells with inducing tetracycline concentration between 0 and 1000 ng/ml resulted in pronounced changes of the amount of the purified hEAAT2 protein and glutamate uptake currents. BN-PAGE analysis demonstrates that the hEAAT2 protein exists exclusively in a trimeric state over a broad range of expression levels in HEK293 cells and those monomers are entirely absent (Fig. 6.2C). Figure 6.2D shows a plot of the intensity of the trimeric hEAAT2 band (bars) and the mean glutamate uptake currents (symbols) versus the tetracycline concentration. The solid line represents a fit of these data with a Michaelis-Menten relationship. Glutamate transport changes with the same dependence on the tetracycline concentration as the amount of purified trimeric hEAAT2 protein. Uptake and quantity of hEAAT2 trimers are highly correlated indicating that glutamate uptake is entirely mediated by hEAAT2 trimers. We conclude that a trimeric architecture of the hEAAT2 transporter is neither a result of overexpression nor of expression in non-mammalian host cells, but represents the sole native and functional state of the hEAAT2 transporter.

6.4.4 ecgltP transporters migrate as trimers in blue native PAGE gels

The ecgltP protein migrated predominantly at ~150 kDa in BN-PAGE gel electrophoresis (Fig. 6.3A, lane 3). In addition, a slower migrating distinct band, presumably an ecgltP hexamer, and an amorphous mass of proteins, most likely ecgltP aggregates, were visible. Oligomerization of ecgltP thus appears to be less complete than of hEAAT2. However, quantification of the various ecgltP forms by PhosphorImager analysis indicated that the 150 kDa band is the most prominent one (Fig. 6.3B). A 1h incubation at 56^{o}C both in the absence

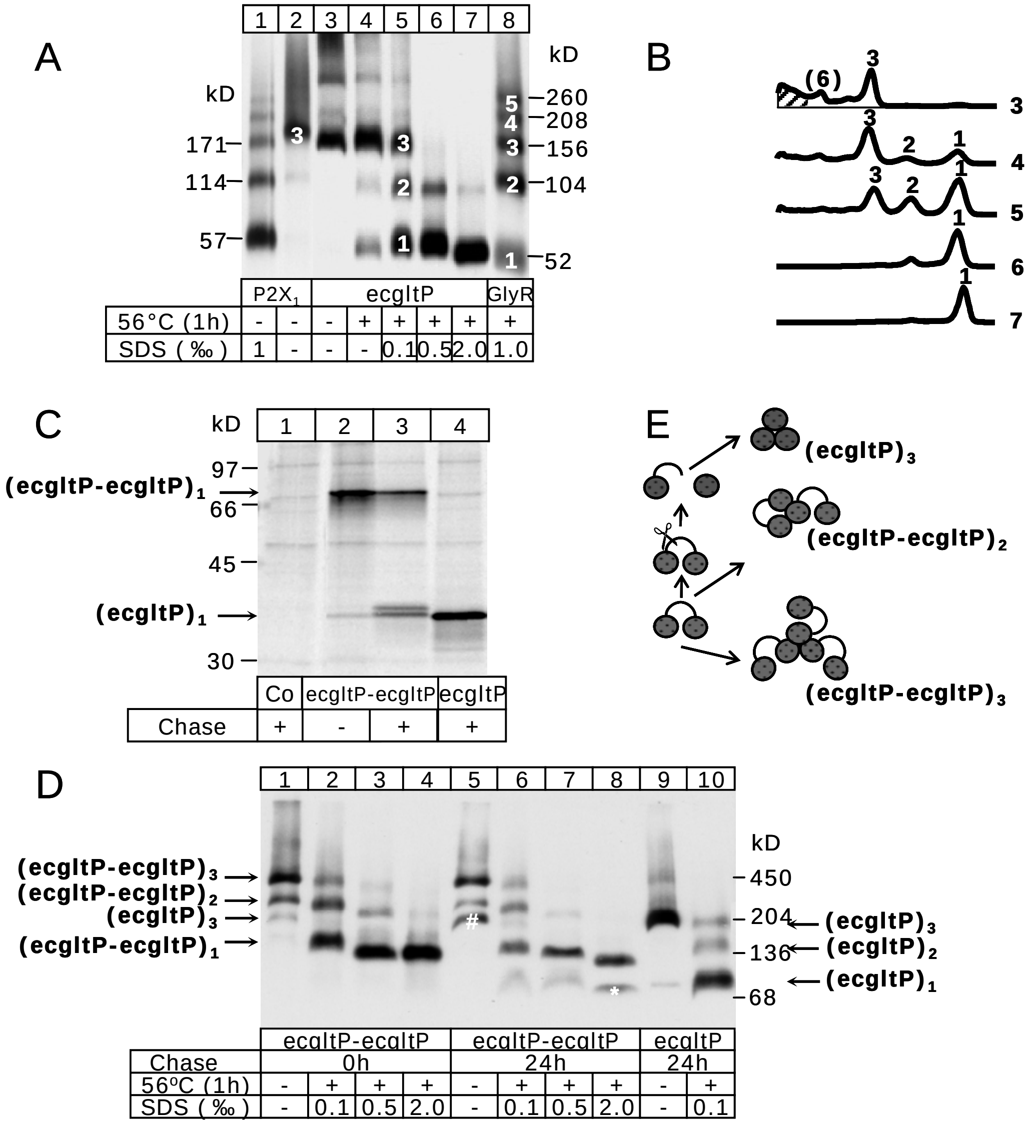
A
1 2 3 4 5 6 7 8
kD
171
114
57
3 3 2 1
5 4 3 2 1
kD
260
208
156
104
52
P2X1 ecgltP GlyR
56°C (1h) - - - + + + + +
SDS (‰) 1 - - - 0.1 0.5 2.0 1.0
B
(6) 3
3 2 1
3 2 1
1
1
3 4 5 6 7
C
kD
1 2 3 4
97
66
45
30
(ecgltP-ecgltP)1
(ecgltP)1
Co ecgltP-ecgltP ecgltP
Chase + - + +
E
(ecgltP)3
(ecgltP-ecgltP)2
(ecgltP-ecgltP)3
D
1 2 3 4 5 6 7 8 9 10
(ecgltP-ecgltP)3
(ecgltP-ecgltP)2
(ecgltP)3
(ecgltP-ecgltP)1
#
*
kD
450
204
136
68
(ecgltP)3
(ecgltP)2
(ecgltP)1
ecgltP-ecgltP ecgltP-ecgltP ecgltP
Chase 0h 24h 24h
56ºC (1h) - + + + - + + + - +
SDS (‰) - 0.1 0.5 2.0 - 0.1 0.5 2.0 - 0.1

Figure 6.3. Oligomeric state of ecgltP transporters in *Xenopus* oocytes determined by BN-PAGE. ***A***, Autoradiography of a BN-PAGE gel containing ecgltP. Samples were treated as indicated to induce dissociation into lower order intermediates including monomers. ***B***, Quantitative profiles of the gel lanes shown in A were obtained by PhosphorImager analysis and are marked by the same lane numbers. The origin of the abscissa corresponds to the top of the polyacrylamide gel. Numbers specify the oligomeric state of the corresponding protein peak. ***C***, Reducing SDS-PAGE analysis of isolated ecgltP-ecgltP concatamers expressed in *Xenopus* oocytes**.** During the chase interval two polypeptides appeared (lane 3) with masses corresponding to the ecgltP monomer that are barely detectable after the pulse (lane 2). Co, non-injected control oocytes. ***D***, Oligomeric state of the concatenated ecgltP dimer determined by BN-PAGE. The oligomeric state attained by expression of monomeric ecgltP is shown for comparison. Dissociation into lower order intermediates was induced by partial denaturing with SDS as indicated. The monomeric byproducts formed during the chase interval assemble into non-covalently linked trimeric ecgltP proteins (#). ***E***, Cartoon showing the assembly of full length concatenated ecgltP dimers and monomeric byproducts.

(not shown) as well as in the presence of Coomassie dye (Fig. 6.3A, lane 4) and denaturing with increasing concentrations of SDS (Fig. 6.3A, lanes 5-7) led to the dissociation of the 150 kDa band into the dimeric and monomeric ecgltP species.

Our results demonstrate that both hEAAT2 and ecgltP glutamate transporters are assembled as trimers from a minimal unit that migrates close to the expected molecular mass of the monomer in BN-PAGE. To rule out the possibility that the lowest molecular band corresponds to an unusually stable dimer and correspondingly the intermediate and higher molecular mass bands to tetramers and hexamers, we engineered a concatenated cDNA construct for one of the transporters (ecgltP-ecgltP) by linking two ecgltP coding regions in a single open reading frame. By reducing SDS-PAGE the ecgltP-ecgltP polypeptide was resolved as a 74 kDa polypeptide (Fig. 6.3C, lane 2), i.e. twice the mass of the apparent molecular mass of 37 kDa for the ecgltP monomer (lane 4). In BN-PAGE two major bands were observed (Fig. 6.3D, lane 1), and dissociating treatment with SDS led to the appearance of a third major non-further dissociable band of ecgltP-ecgltP (lane 2), which migrated at approximately the same position as the non-covalently associated ecgltP dimer, (ecgltP)$_2$ (lane 10). These results show that the intermediate molecular weight band dissociated from the ecgltP protein indeed corresponds to the dimeric form and, accordingly, the lower and higher molecular bands to the monomeric and trimeric forms, respectively.

Under non-denaturing conditions (lane 1) the two bands corresponding to (ecgltP-ecgltP)$_2$ and (ecgltP-ecgltP)$_3$ are prominent indicating that both conformations are stable and occur with comparable probability. This observation further corroborates a trimeric ecgltP structure that predicts two oligomeric populations assemble from dimeric concatamers (Fig. 6.3E): an assembly of two concatamers, one of them providing two subunits ((ecgltP-ecgltP)$_2$) or the association of three dimeric concatamers, each of them contributing one subunit ((ecgltP-ecgltP)$_3$) to the trimer interface.

An additional faint band (indicated by (ecgltP)$_3$ in lane 1 of Fig. 6.3D) migrating at exactly the same position as the ecgltP trimer assembled from three ecgltP monomers, (ecgltP)$_3$ (lane 9) became more abundant after an additional chase period (Fig. 6.3D, lane 5). The occurrence of this oligomeric complex is most likely due to a proteolytic digestion of ecgltP concatamers into monomers (28) giving rise to a trimer from proteolysis-derived monomers (Fig. 6.3E)). Upon treatment with SDS, this protein dissociated into a polypeptide migrating at the same position as the ecgltP monomer (Fig. 6.3D, lanes 6-8). This is confirmed in SDS-PAGE analysis where two byproducts besides the full length concatamer are observed after a chase period (Fig. 6.3C, lane 3), one migrating virtually at the same position as the ecgltP monomer, and a second one with a 1-2 kDa larger mass probably corresponding to the ecgltP monomer plus the 18 residues linker. The finding that two distinct concatameric constructs, the one used in this study and the one of Nicke et al. (28) are both subject to proteolytic digestion in *Xenopus* oocytes demonstrates the limitations of using tandem constructs to study multimeric proteins with defined composition in this expression system.

6.4.5 Cross-linking of hEAAT2 or ecgltP generates covalently bound dimers and trimers

We next used protein cross-linking to study intermolecular interactions within glutamate transporter subunits. Two homobifunctional imidoesters reagents, DMA and DMS were tested for their ability to covalently link transporter molecules extracted from *Xenopus* oocytes. At 22°C as well as 37 °C, DMA cross-linked ecgltP to dimers (Fig. 6.4A, lanes 2 to 4) and to trimers at higher reagent concentrations (lanes 3 and 5). DMS differs from DMA by a slightly longer spacer arm (11 Å *vs*. 8.6 Å) and was more efficient in cross-linking ecgltP to dimers and trimers at both 22°C (Fig. 6.4B, lanes 2-4) and 37°C (lanes 5-7). DMS also cross-linked

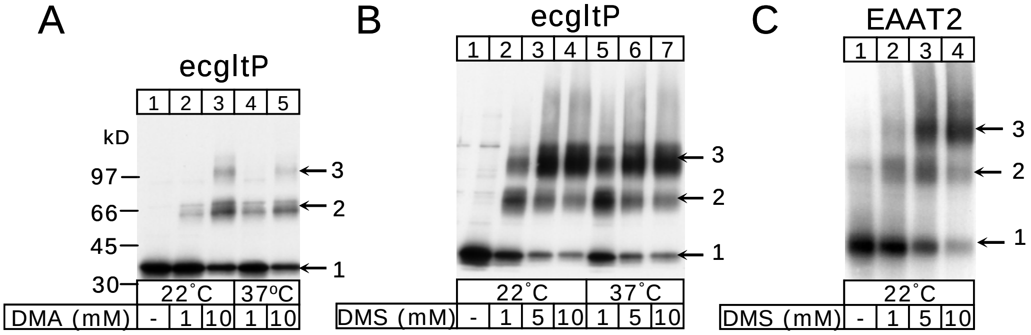
A
ecgltP
1 2 3 4 5
kD
97
66
45
30
3
2
1
22˚C
37ºC
DMA (mM) - 1 10 1 10
B
ecgltP
1 2 3 4 5 6 7
3
2
1
22˚C
37˚C
DMS (mM) - 1 5 10 1 5 10
C
EAAT2
1 2 3 4
3
2
1
22˚C
DMS (mM) - 1 5 10

Figure 6.4. Cross-linking of digitonin-solubilized purified glutamate transporters. EcgltP transporters (***A***, ***B***) and hEAAT2 transporters (***C***) were purified from [^{35}S]methionine labelled oocytes and incubated with cross-linkers as indicated while still bound to Ni-NTA beads. After elution with non-denaturing buffer, samples were supplemented with SDS sample buffer and 20 mM DTT and resolved by SDS–PAGE (4–10% acrylamide gradient gel) followed by autoradiography. Numbered arrows indicate positions of monomers, dimers and trimers.

hEAAT2 transporter subunits to dimers and to trimers preferentially at higher concentrations (Fig. 6.4C). Adducts larger than trimers were neither observed with ecgltP nor with hEAAT2 transporters, corroborating the trimeric quaternary structure determined by BN-PAGE analysis.

6.4.6 Purification and characterization of ecgltP

EcgltP tagged with a strep-tag (strep-ecgltP) was expressed in *E. coli* and purified after detergent-extraction by one affinity chromatography step using a strep-tactin superflow column. Reducing SDS-PAGE analysis of the purified protein demonstrated a single band with an apparent molecular mass of 37 kDa close to the metabolically labeled ecgltP expressed in *Xenopus* oocytes (Fig. 6.5A). The identity of the ecgltP was verified by western blot (Fig. 6.5B) and amino acid analysis (data not shown). The homogeneity of the purified protein was evaluated by FPLC-attached size exclusion chromatography (SEC) using a superdex 200 column pre-equilibrated with buffer containing 1 mM DDM (Fig. 6.5C). The strep-ecgltP eluted predominantly as a single symmetrical peak indicating that the majority of the purified protein (>95%) exists in one oligomeric conformation. The small peak eluting after the main fraction most likely corresponds to ecgltP monomers. Varying the DDM detergent concentration from 1 to 10 mM (corresponding to ~1 to 10 times the critical micellar concentration) had no effect on the oligomeric state as judged by SEC, indicating that conformation of the purified ecgltP is not due to artificial association promoted by a low detergent concentration.

We employed BN-PAGE analysis to determine the quaternary structure of the purified ecgltP. Strep-ecgltP migrates in BN-PAGE (Fig. 6.5D) mostly as a prominent band at the same position observed for the oocyte-expressed ecgltP (lane 1 and 2). Treatment with heat or SDS

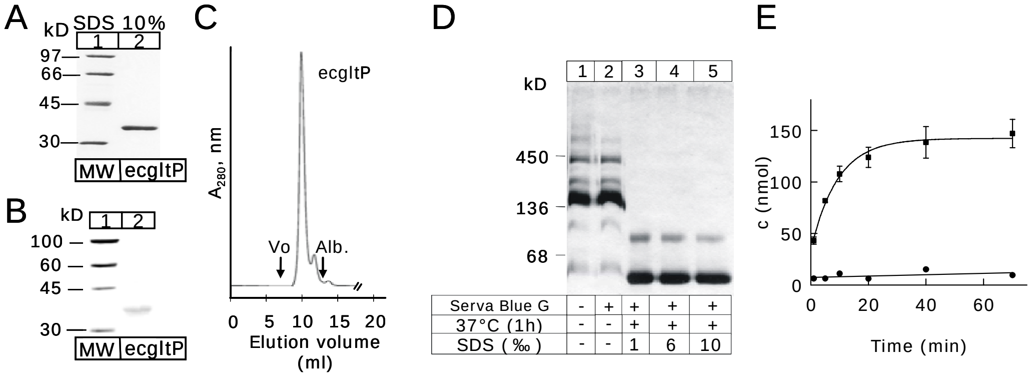

Figure 6.5. Biochemical and functional characterization of recombinant ecgltP produced in *E. coli.* A, Reducing SDS-PAGE of strep-tagged ecgltP purified from *E. coli.* Lane 1: protein markers, lane 2: ecgltP eluted from a strep-tactin™ column. B, Western blot of strep-tagged ecgltP detected with strep-tactin alkaline phosphatase conjugate. C, Elution profile monitored at 280 nm from size exclusion chromatography using a superdex^{TM} 200 column (24 ml bed volume) equilibrated with 50 mM phosphate buffer, 300 mM NaCl, 1 EDTA, 1 mM DDM, pH 7.0. The arrows show the void volume (Vo) and the elution volume of albumin (67 kDa). *D*, BN-PAGE (4-16% acrylamide) of purified strep-tagged ecgltP. The protein bands were visualized by silver staining. The numbers indicate the molecular weights of standards in kDa. *E*, Time course of the accumulation of L-[^{3}H]-glutamate in vesicles reconstituted with 10 µg ecgltP/mg lipid (■, means ± SEM, n =4)) or without protein (●, n =1).

causes a dissociation into lower order assemblies (lanes 3-5) resembling the one into dimers and monomers of the oocyte-expressed transporter. Thus, the ecgltP purified from *E. coli* exhibits the same oligomeric structure as ecgltP and hEAAT2 expressed in *Xenopus* oocytes and mammalian cells.

The purified strep-ecgltP protein is functionally active when reconstituted into liposomes. Proteoliposomes containing strep-ecgltP were loaded with a potassium acetate-solution, and the addition of L-[^{3}H]-glutamate to a sodium-containing external solution enabled glutamate uptake into the vesicles. Figure 6.5E shows the time course of radioactive glutamate accumulation by proteoliposomes containing purified ecgltP transporters. No glutamate uptake was observed when the intra- and extravesicular solution had the same salt content or in control vesicles without protein.

6.5 Discussion

Multimerization of EAAT transporters was first reported by Haugeto *et al.* (14). Using SDS-PAGE analysis and cross-linking of native rat brain or recombinant EAAT2 and EAAT3 transporters expressed in HeLa cells dimeric and trimeric assemblies were observed. These results demonstrated that EAAT transporters are multimers in native cells, however, the authors did not deduce the subunit stoichiometry from these experiments, as a larger number of subunits per single transporter could not be excluded. Later, Eskandari *et al.* (13) determined a cross-sectional area per unitary EAAT3 transporter that corresponds to a number of 35 transmembrane helices by freeze-fracture electron microscopy. Assuming 7 transmembrane helices per subunit, the authors assigned five subunits per transporter. In contrast to this pentameric assembly, a trimeric stoichiometry was recently reported for two prokaryotic glutamate transporters based on cross-linking and in-line laser light scattering, refractive index, and ultraviolet absorption measurements (29) raising the possibility that eukaryotic and prokaryotic transporters might exhibit distinct subunit stoichiometries.

We here demonstrate that this is not the case. BN-PAGE analysis and chemical cross-linking of transporters heterologously expressed in *Xenopus* oocytes revealed a conserved trimeric stoichiometry for prokaryotic and eukaryotic transporters. Expression of hEAAT2 in an inducible mammalian cell line demonstrated that trimerization is independent of the expression level and occurs in mammalian as well as in amphibian cells. No other oligomerization state was observed at all tested expression levels. Moreover, glutamate transport and hEAAT2 trimer quantity are highly correlated indicating that the trimer is the functional unit of glutamate transport under physiological conditions.

The experiments with single and concatenated ecgltP polypeptide units (Fig. 6.2 and 6.3) excluded a higher multimerization state than three. Under non-denaturing conditions, we did not observe monomers and dimers besides the trimeric state, and this result refutes the pentameric assembly suggested by Eskandari *et al.* (13). At present, we can not explain the distinct outcome of biochemical and microscopic approaches in determining the glutamate transporter stoichiometry. A possible reason for the observed differences is the currently unresolved transmembrane topology for EAAT transporters (16). A larger number of transmembrane helices per single glutamate transporter subunit would decrease the number of subunits necessary for the observed 35 transmembrane helices and might thus resolve the inconsistencies between our and Eskandari´s results. The results of our and of earlier studies are best explained by a trimeric subunit stoichiometry general to prokaryotic and eukrayotic glutamate transporters.

The conserved trimeric structure of glutamate transporters is in clear contrast to the situation observed in another family of neurotransmitter transporters, the GAT/NET transporter family including GABA, dopamine, serotonin, norepinephrine, solutes and amino acid transporters (30). A prokaryotic GABA transporter (31) and a mammalian glycine transporter (27) were shown to form monomers. There is evidence for the formation of tetrameric dopamine transporters (32), and serotonin transporters were shown to be dimers or tetramers (33-35). Similar to EAAT transporters, GAT/NET transporters not only exhibit a stoichiometric co-transport (36;37), but also current components that appear to be conducted by permeation pathways similar to that of ion channels (38-42). The channel-like activity was reported to become more apparent with increasing expression levels of rat and human serotonin transporters heterologously expressed in *Xenopus* oocytes (43). Ramsey and DeFelice interpreted this result as evidence for an endogenous regulatory protein that is necessary for the carrier transport mode (43). At low heterologous expression levels, virtually all serotonin transporters will contain this regulatory protein and thus function as carriers, while the endogenous protein is not sufficiently available at high expression levels resulting in homomultimeric serotonin transporters that function as channels. In support of this hypothesis, syntaxin A was recently identified as the first interacting protein that promotes stoichimetrically coupled serotonin transport (44). An alternative explanation might be the existence of multiple homo-oligomerization states with different function. At low expression levels, serotonin transporters might be formed by a smaller number of subunits than at high levels thus explaining the observed dependence of transporter function and protein expression (43). This hypothesis would also account for the multiple experimentally determined subunit stoichiometries within the GAT/NET family.

Glutamate transporters exhibit only a single oligomeric state formed by the assembly of three identical subunits. Our reconstitution experiments (Fig. 6.5) demonstrate that homotrimeric ecgltP is able to sustain coupled transport. The situation is not as clear for the pore-mediated uncoupled transport; however, several experimental results support the notion that accessory subunits are not involved in anion conduction by glutamate transporters. Coupled and uncoupled current components of heterologously expressed EAAT transporters differ little between distinct expression systems (9;45), and anion pores associated with distinct EAAT isoforms exhibit distinct pore properties (12). In SDS- or BN-PAGE gels only a single protein could be observed after expression and purification of hEAAT2 and ecgltP in *Xenopus* oocytes as well as in mammalian cells. The trimeric state of glutamate transporters is attained immediately after biosynthesis and appears to be the only significant oligomeric state in homologous and heterologous systems. These results taken together indicate that one quaternary structure of glutamate transporters supports two distinct transport processes. At present, we can not distinguish whether the three subunits contribute to the formation of a central anion conduction pathway or a central carrier domain mediating coupled transport or each subunit can mediate both transport modes.

Acknowledgements

We thank Dr. M. Hediger for providing expression constructs for hEAAT2, Dr. Benjamin Kaupp for the pGEMHE vector, insightful discussions, and critical reading of the manuscript, Drs Simon Hebeisen, Nico Melzer and Maike Warnstedt for help in generating the inducible EAAT2 cell line, and Barbara Poser for excellent technical assistance. These studies were supported by the Deutsche Forschungsgemeinschaft (FOR450/1 to P.H. (TP1) and Ch.F. (TP4), SCHM 536/6-1 to G. S.) and by a START grant of the medical faculty of the RWTH to P.H.

6.6 References

1. Storck, T., Schulte, S., Hofmann, K., and Stoffel, W. (1992) *Proc.Natl.Acad.Sci.USA* 89**,** 10955-10959
2. Pines, G., Danbolt, N. C., Bjoras, M., Zhang, Y., Bendahan, A., Eide, L., Koepsell, H., Storm-Mathisen, J., Seeberg, E., and Kanner, B. I. (1992) *Nature* **360,** 464-467
3. Kanai, Y. and Hediger, M. A. (1992) *Nature* **360,** 467-471
4. Fairman, W. A., Vandenberg, R. J., Arriza, J. L., Kavanaugh, M. P., and Amara, S. G. (1995) *Nature* **375,** 599-603
5. Arriza, J. L., Eliasof, S., Kavanaugh, M. P., and Amara, S. G. (1997) *Proc.Natl.Acad.Sci.USA* **94,** 4155-4160
6. Slotboom, D. J., Konings, W. N., and Lolkema, J. S. (1999) *Microbiology & Molecular Biology Reviews* **63,** 293-307
7. Levy, L. M., Warr, O., and Attwell, D. (1998) *J Neurosci* **18,** 9620-9628
8. Zerangue, N. and Kavanaugh, M. P. (1996) *Nature* **383,** 634-637
9. Wadiche, J. I., Amara, S. G., and Kavanaugh, M. P. (1995) *Neuron* **15,** 721-728
10. Larsson, H. P., Picaud, S. A., Werblin, F. S., and Lecar, H. (1996) *Biophys J* **70,** 733-742
11. Billups, B., Rossi, D., and Attwell, D. (1996) *J Neurosci* **16,** 6722-6731
12. Melzer, N., Biela, A., and Fahlke, Ch. (2003) *J Biol.Chem.* **278,** 50112-50119
13. Eskandari, S., Kreman, M., Kavanaugh, M. P., Wright, E. M., and Zampighi, G. A. (2000) *Proc.Natl.Acad.Sci.USA* **97,** 8641-8646
14. Haugeto, O., Ullensvang, K., Levy, L. M., Chaudhry, F. A., Honore, T., Nielsen, M., Lehre, K. P., and Danbolt, N. C. (1996) *J Biol Chem* **271,** 27715-27722
15. Eskandari, S., Wright, E. M., Kreman, M., Starace, D. M., and Zampighi, G. A. (1998) *Proc.Natl.Acad.Sci.USA* **95,** 11235-11240
16. Danbolt, N. C. (2001) *Progress in Neurobiology* **65,** 1-105
17. Tolner, B., Poolman, B., Wallace, B., and Konings, W. N. (1992) *Journal of Bacteriology* **174,** 2391-2393
18. Trotti, D., Rolfs, A., Danbolt, N. C., Brown, R. H., Jr., and Hediger, M. A. (1999) *Nature Neuroscience* **2,** 427-433
19. Nicke, A., Baumert, H. G., Rettinger, J., Eichele, A., Lambrecht, G., Mutschler, E., and Schmalzing, G. (1998) *EMBO J* **17,** 3016-3028
20. Sadtler, S., Laube, B., Lashub, A., Nicke, A., Betz, H., and Schmalzing, G. (2003) *J Biol Chem* **278,** 16782-16790

21. Knol, J., Veenhoff, L., Liang, W. J., Henderson, P. J. F., Leblanc, G., and Poolman, B. (1996) *J Biol Chem* **271,** 15358-15366

22. Gaillard, I., Slotboom, D. J., Knol, J., Lolkema, J. S., and Poolman, B. (1996) *Biochemistry* **35,** 6150-6156

23. Ferguson, K. A. (1964) *Metabolism* **13,** 985-1002

24. Schägger, H. and von Jagow, G. (1991) *Anal Biochem* **199,** 223-231

25. Schägger, H., Cramer, W. A., and von Jagow, G. (1994) *Anal Biochem* **217,** 220-230

26. Griffon, N., Büttner, C., Nicke, A., Kuhse, J., Schmalzing, G., and Betz, H. (1999) *EMBO J.* **18,** 4711-4721

27. Horiuchi, M., Nicke, A., Gomeza, J., Aschrafi, A., Schmalzing, G., and Betz, H. (2001) *Proc.Natl.Acad.Sci.USA* **98,** 1448-1453

28. Nicke, A., Rettinger, J., and Schmalzing, G. (2003) *Mol Pharmacol* **63,** 243-252

29. Yernool, D., Boudker, O., Folta-Stogniew, E., and Gouaux, E. (2003) *Biochemistry* **42,** 12981-12988

30. Blakely, R. D., De Felice, L. J., and Hartzell, H. C. (1994) *Journal of Experimental Biology* **196,** 263-281

31. Li, X. D., Villa, A., Gownley, C., Kim, M. J., Song, J., Auer, M., and Wang, D. N. (2001) *FEBS Lett* **494,** 165-169

32. Hastrup, H., Sen, N., and Javitch, J. A. (2003) *J Biol Chem* **278,** 45045-45048

33. Schmid, J. A., Scholze, P., Kudlacek, O., Freissmuth, M., Singer, E. A., and Sitte, H. H. (2001) *J Biol Chem* **276,** 3805-3810

34. Jess, U., Betz, H., and Schloss, P. (1996) *FEBS Lett* **394,** 44-46

35. Kilic, F. and Rudnick, G. (2000) *Proc.Natl.Acad.Sci.USA* **97,** 3106-3111

36. Hilgemann, D. W. and Lu, C. C. (1999) *J.Gen.Physiol.* **114,** 459-476

37. Galli, A., Jayanthi, L. D., Ramsey, I. S., Miller, J. W., Fremeau, R. T., Jr., and DeFelice, L. J. (1999) *J Neurosci* **19,** 6290-6297

38. Mager, S., Min, C., Henry, D. J., Chavkin, C., Hoffman, B. J., Davidson, N., and Lester, H. A. (1994) *Neuron* **12,** 845-859

39. Cammack, J. N. and Schwartz, E. A. (1996) *Proc. Natl. Acad. Sci. USA* **93,** 723-727

40. Galli, A., Petersen, C. I., deBlaquiere, M., Blakely, R. D., and DeFelice, L. J. (1997) *J Neurosci* **17,** 3401-3411

41. Lin, F., Lester, H. A., and Mager, S. (1998) *Biophys J* **71,** 3126-3531

42. Ingram, S. L., Prasad, B. M., and Amara, S. G. (2002) *Nature Neuroscience* **10,** 971-978

43. Ramsey, I. S. and DeFelice, L. J. (2002) *J Biol Chem* **277,** 14475-14482

44. Quick, M. W. (2003) *Neuron* **40,** 537-549

45. Otis, T. S. and Kavanaugh, M. P. (2000) *J Neurosci* **20,** 2749-2757

7. A dynamic switch between inhibitory and excitatory currents in a neuronal glutamate transporter

Nico Melzer[1,2], **Delany Torres-Salazar**[1,2], Christoph Fahlke[1,2,3]

[1]Abteilung Neurophysiologie, Medizinische Hochschule Hannover, Germany, [2]Abteilung Physiologie, RWTH Aachen, Germany, [3]Centro de Estudios Cientificos (CECS), Valdivia, Chile

Corresponding author: Christoph Fahlke, Abteilung Neurophysiologie, Medizinische Hochschule Hannover, Carl-Neuberg-Str. 1, 30625 Hannover, Tel +49 511 532 2777, Fax +49 511 532 2776, Email: fahlke.christoph@mh-hannover.de

***Proc Natl Acad Sci USA*. 2005 vol. 102, No 52: 19214-19218**

7.1 Abstract

Excitatory amino acid transporters (EAATs) terminate glutamatergic synaptic transmission and maintain extracellular glutamate concentrations in the central nervous system below excitotoxic levels. In addition to sustaining a secondary-active glutamate transport, EAAT glutamate transporters also function as anion-selective channels. Here, we report a gating process that makes anion channels associated with a neuronal glutamate transporter, EAAT4, permeable to cations and causes a selective increase of the open probability at voltages negative to the actual current reversal potential. The activation process is dependent on both membrane potential and extracellular glutamate concentration and causes an accumulation of EAAT4 anion channels in a state favoring cation influx and anion efflux. Gating of EAAT4 anion channels thus allows a switch between inhibitory currents in resting cells and excitatory currents in electrically active cells. This transporter-mediated conductance could modify the excitability of Purkinje neurons, providing them with an unprecedented mechanism for adaptation.

7.2 Introduction

EAAT transporters are known to function as glutamate carriers (1-4) and as anion channels (5-8). EAAT-mediated glutamate transport terminates glutamatergic synaptic transmission, ensures low resting extracellular glutamate levels and prevents neuronal damage by excessive glutamate receptor activation in the mammalian central nervous system. In contrast, the physiological function of EAAT-associated anion currents is not well understood. EAAT-associated anion currents are thought to support electrogenic glutamate uptake by clamping the membrane potential to negative values (6). Additionally, they might also inhibit neuronal excitability by increasing the resting membrane conductance and decreasing length constants of different neuronal compartments (2).

EAAT4 is predominantly expressed in dendritic spines of Purkinje neurons (7, 9, 10). It displays a significant anion conductance (7) and does not play a crucial role in cerebellar glutamate homeostasis (11), suggesting that its major role might be regulation of neuronal excitability as a glutamate-dependent anion channel (2). We studied functional properties of EAAT4 anion channels heterologously expressed in mammalian cells. Our experiments identified a novel voltage- and glutamate-dependent gating process that changes the selectivity of individual channels and permits EAAT4 anion channels to conduct excitatory currents under certain conditions and inhibitory under others.

7.3 Methods

7.3.1 Expression of EAAT4 and Whole-Cell Recordings

Heterologous expression of rEAAT4 in tsA201 cells was performed as described (12). In some of the experiments, a stable inducible cell line, generated by selecting Flp-In-T-Rex 293 cells (Invitrogen, Karlsruhe, Germany) transfected with pcDNA5-FRT-TO-rEAAT4, was used, 24h after incubation with 1 µg/ml tetracycline. Standard whole-cell and outside-out patch clamp recordings were performed using an EPC10 (HEKA Electronics, Lambrecht, Germany) amplifier (12). Pipettes were pulled from borosilicate glass and had resistances between 1.4 MΩ and 2.2 MΩ (1.8 ± 0.1 MΩ, n = 32). 60 - 80% of the series resistance was compensated by an analog procedure, so that the calculated voltage error due to access resistance was always < 2 mV. The whole-cell resistance under standard conditions was 300 ± 50 MΩ (n = 32). Pipettes were covered with dental wax to reduce their capacitance. Cells and patches were clamped to the reversal potential for at least 10 s between test sweeps. Standard solutions contained: extracellular (in mM) 140 $NaNO_3$, 4 KCl, 2 $CaCl_2$, 1 $MgCl_2$, 5 HEPES, pH 7.4, intracellular (in mM) 115 NaCl, 2 $MgCl_2$, 5 EGTA, 10 HEPES, pH 7.4. Unless otherwise stated, 500 µM L-glutamate was added to the external solution. In some experiments, $NaNO_3$ was replaced by NaSCN in the external solution. Under these ionic conditions, untransfected tsA201 cells (12), tsA201 cells expressing a non-functional anion channel (L590X hClC-1 (13)) or uninduced rEAAT4 Flp-In-T-Rex cells exhibit negligible current amplitudes. Junction potentials were corrected as described (12). The external solution in Fig. 7.3 contained (in mM): 150 $NaNO_3$, 2 $Ca(NO_3)_2$, 5 HEPES, pH 7.4. In the experiments shown in Fig. 7.3*E*, 20 mM $CaGluconate_2$ was added to this solution. Experiments shown in Fig. 7.3*D* were performed with cells that were externally perfused with three different solutions containing (in mM) X $NaNO_3$, 150 – X $NMDGNO_3$, 2 $Ca(NO_3)_2$, 5 HEPES, pH 7.4. MES was used to buffer pH 6.0 in Fig. 7.3*F*. In the experiments shown in Fig. 7.3*G*, the internal solution was modified by adding 5 mM NaGlutamate, or by replacing NaCl by KCl.

For Fig. 7.3*H*, intracellular Cl^- was substituted with NO_3^- and gluconate$^-$. Gluconate$^-$ was shown to remain impermeant during slow activation (data not shown). For the experiments with hClC-Kb, cells were co-transfected with pRcCMV-hClC-Kb and pcDNA3.1-Barttin. The standard extracellular solution contained (in mM): 140 NaCl, 4 KCl, 2 $CaCl_2$, 1 $MgCl_2$, 5 HEPES, pH 7.4; the standard intracellular (in mM): 115 NaCl, 2 $MgCl_2$, 5 EGTA, 10 HEPES, pH 7.4. Cells were held at 0 mV, and current amplitudes were measured at a test step to –20 mV without prepulse and after a 9.6 s prepulse to +60 mV, respectively (Fig. 7.2*C*).

7.3.2 Data Analysis

Data were analyzed with a combination of Pulse, Pulsefit, PulseTools (HEKA Electronics, Lambrecht, Germany) and SigmaPlot (Jandel Scientific, San Rafael, CA, USA) programs. Current amplitudes were used without subtraction procedure, and all summary data are shown as means ± SEM. Isochronal current amplitudes were measured 2 ms after the voltage step. Time constants of activation (Fig. 7.1*D*) were determined by fitting a monoexponential function to the dependence of the isochronal current amplitude measured at −120 mV on the length of the preceding membrane depolarization. The time course of slow gate deactivation (Fig. 7.1*E*) was measured at various negative potentials after a 3 s prepulse to +60 mV to open the gate. Permeability ratios were calculated from reversal potential measurements using the Goldman-Hodgkin-Katz (GHK) equation (14). Long depolarizations cause small changes of the intracellular anion concentration that need to be taken into account in the quantitative analysis of slow-gating induced alteration of EAAT4 anion channel selectivity. We calculated changes of the internal $[NO_3^-]$ from the measured NO_3^- influx using equation 3 (see *Supporting Text*, Fig. 7.5 which is published as *Supporting Information*) and inserted these values into the GHK equation. For non-stationary noise analysis (Fig. 7.4), a series of 300 records was recorded by pulsing to a certain voltage from the holding potential of –60 mV or 0 mV. Pairs of subsequent records were then subtracted to compute the ensemble variance

(15). Background noise was measured at the end of the experiment after taking the pipette out of the bath and subtracted from the ensemble variances. After normalization to the value determined at −180 mV following a holding potential of +60 mV, the square root of the ensemble variances was calculated and plotted versus the normalized mean current amplitudes. Current traces were sampled at 200 kHz and filtered using a Butterworth low pass filter with a cut off frequency of 10 kHz. For all experiments, the analysis was repeated after digital filtering at 5 kHz and at 2 kHz with similar results. For all statistic evaluations the Student's t-Test with $p < 0.05$ as level of significance was used.

7.4 Results

7.4.1 A novel gating process of EAAT4 anion channels

We expressed EAAT4 glutamate transporters heterologously in tsA201 cells and measured currents through whole-cell patch clamp experiments. The so-determined whole-cell currents are pure anion currents, as substitution of internal and external anions with gluconate results in current amplitudes comparable to background currents in non-transfected cells (Fig. 7.6 which is published as *Supporting Information*). EAAT4 anion channels are active with or without external glutamate; however, application of substrate increases the current amplitudes and modifies voltage-dependent gating (12) (Fig. 7.1*A-D*). In the presence of glutamate, positive voltages cause a pronounced increase of currents at a consecutive test step to a negative potential (Fig. 7.1*B*, arrow). Gradually incrementing the length of a depolarizing prepulse evokes a time-dependent increase of the current amplitude at a successive test step to –120 mV, while the amplitude at positive potentials remains basically unaltered (Fig. 7.1*D*). Without glutamate, there is only a small, if any, enhancement of the tail current amplitudes (Fig. 7.1*A*, arrow, *C*). The time course of activation (Fig. 7.1*D*) as well as the time course of deactivation during membrane hyperpolarization following a long activating prepulse (Fig. 7.1*E*) displays time constants in the range of seconds (Fig. 7.1*F*). Deactivation time constants depend on extracellular glutamate: when measured in a stream of glutamate-free solution after activation in a glutamate-containing solution, they are markedly slower (τ_{deact} (-80 mV) = 6.9 ± 0.5 s, n = 4) than those determined in the presence of glutamate (3.3 ± 0.4 s, n = 5).

A possible artifactual explanation for the observed changes of inward current amplitudes was that NO_3^- entering the cell during depolarization accumulated inside the cell and carried the inward current upon repolarization. We designed several experiments to test this possibility. In case of pure anion accumulation, the increases of the tail current amplitudes in pulse protocols such as in Fig. 7.1*D* should depend on the magnitude of anion influx and thus on the

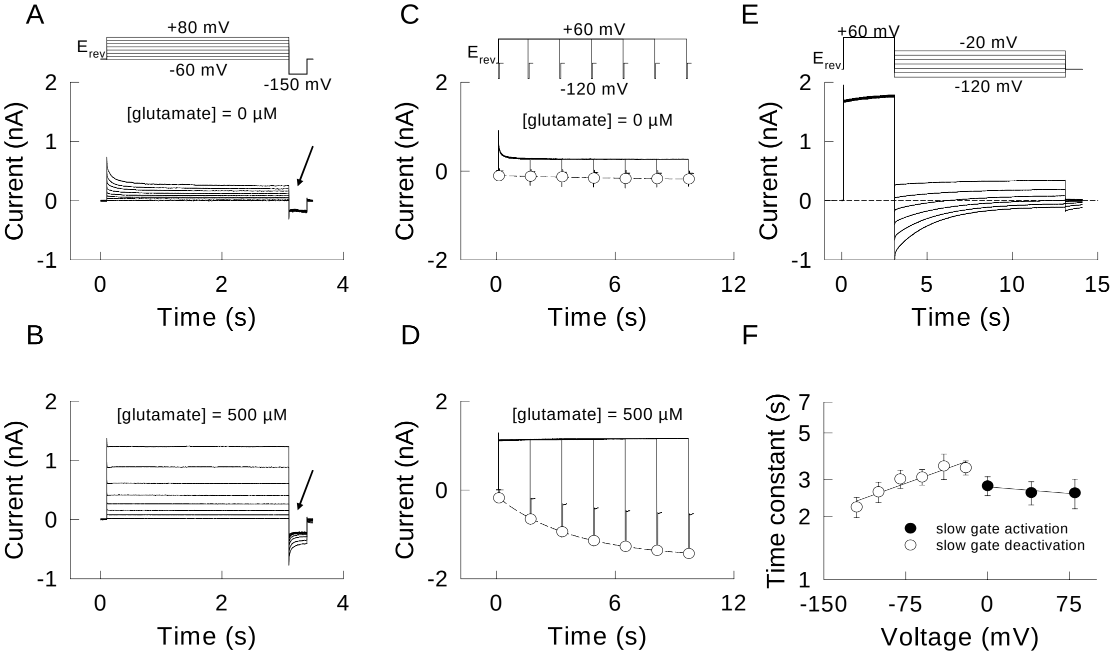

Figure 7.1. A novel gating transition in EAAT4 anion channels during prolonged membrane depolarizations. (*A,B*) Representative current recordings in the absence (*A*) or in the presence of glutamate (*B*). (*C,D*) Current responses to voltage steps to +60 mV of increasing durations followed by fixed test steps to –120 mV. Isochronal tail current amplitudes are represented by symbols and fits with monoexponential functions by dashed lines. (*E*) Current deactivation during hyperpolarizing voltage steps after a depolarizing prepulse. The dashed line gives zero current. (*F*) Voltage-dependence of activation and deactivation time constants (means ± SEM, n = 4-5).

expression levels of the channel. In contrast to this prediction, a comparison between cells expressing different EAAT4 levels (Fig. 7.2*A*) revealed that the ratios of tail current by prepulse current amplitude do not change for anion influx current amplitudes between 200 pA and 2 nA. Moreover, slow activation of EAAT4 anion channel depends on glutamate (Fig. 7.1). If the time- and voltage–dependent increase of the tail current amplitudes were solely caused by changes of the intracellular anion concentration, equal amounts of anions entering the cell would result in identical tail current amplitudes, regardless of the external glutamate concentration. However, in the absence of glutamate, similar time-dependent anion current increases were never observed, not even in cells with expression levels that result in large current amplitudes under these conditions (data not shown). EAAT4 anion currents are small when studied in excised outside-out patches (53 ± 19 pA, n = 5, at +60 mV), so that anion accumulation in the internal solution is virtually impossible. However, the typical prepulse-induced increases of the inward current could be also observed in this recording mode (Fig. 7.2*B*). The time constants (2.5 ± 0.9 s, n = 5, at +60 mV) and the magnitude of the depolarization-induced enhancement of inward currents were similar in patches and in whole-cell measurements (Fig. 7.1*F*, 7.2*C*). We performed additional whole-cell experiments with another type of anion channel, hClC-Kb together with its accessory subunit Barttin (Fig. 7.2*C*) (16). Although the anion influx into these cells during the prepulse (current amplitude at +60 mV 1.1 ± 0.3 nA, n = 5) was comparable to experiments with EAAT4 (1.3 ± 0.2 nA, n = 8), application of depolarizing prepulses of increasing durations resulted in only small time-dependent enhancements of the tail current amplitudes. If the increase of the after-depolarization inward current were caused by intracellular NO_3^- accumulation, identical anion influxes should result in similar enhancements of the tail current amplitude, independently of the underlying anion channel. Another argument stems from the voltage dependence of channel deactivation. If anion accumulation were the sole basis of the observed changes in current amplitude, the current decay at negative potentials must be caused by an outward

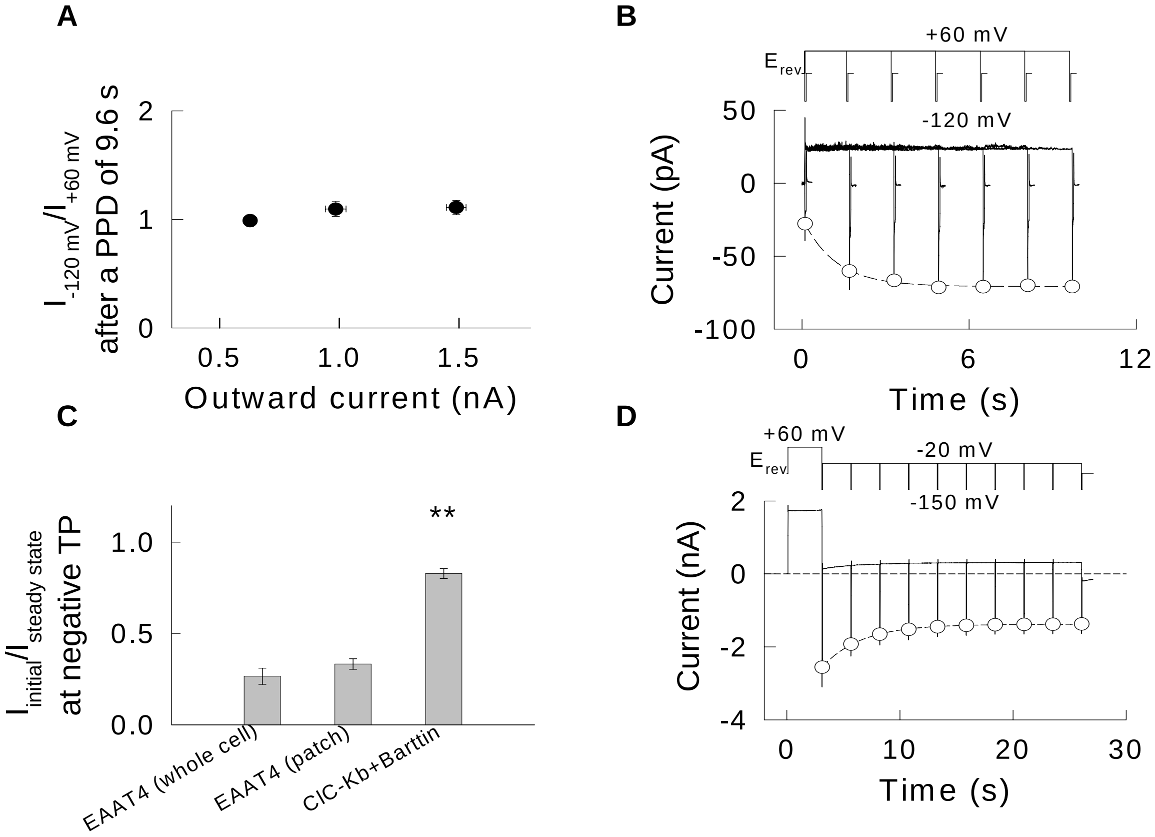
A
I-120 mV/I+60 mV after a PPD of 9.6 s
2
1
0
0.5
1.0
1.5
Outward current (nA)
B
+60 mV
Erev
-120 mV
50
0
-50
-100
Current (pA)
0
6
12
Time (s)
C
Iinitial/Isteady state at negative TP
1.0
0.5
0.0
**
EAAT4 (whole cell)
EAAT4 (patch)
ClC-Kb+Barttin
D
+60 mV
Erev
-20 mV
-150 mV
2
0
-2
-4
Current (nA)
0
10
20
30
Time (s)

Figure 7.2. Enhanced EAAT4 inward currents are not due to anion accumulation. (*A*) Isochronal tail current amplitudes at –120 mV after a 9.6 s prepulse normalized to the prepulse current amplitude from current responses to the pulse protocol shown in Fig. 7.1*C*. Data from 30 cells expressing different levels of EAAT4 were binned into 3 data groups that were statistically not different. (*B*) Current responses to voltage steps to +60 mV of increasing durations followed by fixed test steps to –120 mV in an outside-out patch from cells expressing EAAT4 transporters. Isochronal tail current amplitudes are represented by symbols and fits with monoexponential functions by a dashed line. The patch was clamped to –23 mV between test sweeps. Because of the larger contribution of leak current in outside-out patches, this value is more positive than reversal potentials in whole-cell experiments (–61.9 ± 0.9 mV, n = 32). (*C*) Ratio of the tail current amplitudes after stepping from the holding potential by the corresponding value after a prepulse of 9.6 s from current responses to the pulse protocol shown in *B*. Means ± SEM from cells (n = 19) and patches (n = 5) expressing EAAT4 and cells expressing hClC-Kb and barttin (n = 4), respectively. ** indicates a significant difference to EAAT4 at $p < 0.01$. (*D*) EAAT4 anion channel deactivation at potentials positive to the anion reversal potential. After an activating prepulse to +60 mV the cell was clamped to –20 mV and fixed test steps to –150 mV were applied every 1.6 s.

movement of anions and is therefore only possible at voltages negative to the anion reversal potential. However, application of a potential positive to the anion reversal potential (-20 mV) after a prepulse to +60 mV causes a decrease of tail current amplitudes at test steps to -150 mV (Fig. 7.2*D*). Taken together, these lines of evidence refute anion accumulation as the sole basis of the observed changes of EAAT4 anion current amplitudes and establish the existence of a novel gating process, designated slow activation in the following.

The experiments demonstrated so far were performed under non-physiological ionic conditions using voltage protocols that do not resemble the electrical activity of Purkinje neurons. However, slow activation also occurs under an approximately physiological anion gradient with $[Cl^-]_i$ of 10 mM and $[Cl^-]_o$ of 150 mM (data not shown), and with K^+ as the main internal cation (Fig. 7.3*G*). The slow gate is not only activated by long tonic depolarizations, but also by series of phasic depolarizations (see *Supporting Text***,** Fig. 7.7). These results taken together demonstrate that slow gating can occur in native Purkinje cells under physiological conditions.

7.4.2 Slow gating increases cation permeability of EAAT4 anion channels

To study slow gating-induced changes of EAAT4 channels in more detail, we applied voltage ramps after depolarizing prepulses of variable durations (Fig. 7.3*A*). Fig. 7.3*B* shows the voltage dependence of EAAT4 currents obtained from these pulse protocols. Depolarizing prepulses decrease outward and increase inward currents and shift the current reversal potential more positive indicating a time- and voltage-dependent variation of the selectivity of EAAT4 anion channels. The changes of the current reversal potential do not depend on the magnitude of anion influx (Fig. 7.3*C*), providing an additional argument against anion accumulation. The shift of ion selectivity can be directly demonstrated by applying hyperpolarizing voltage steps of –40 mV or –60 mV after a depolarizing prepulse. Under

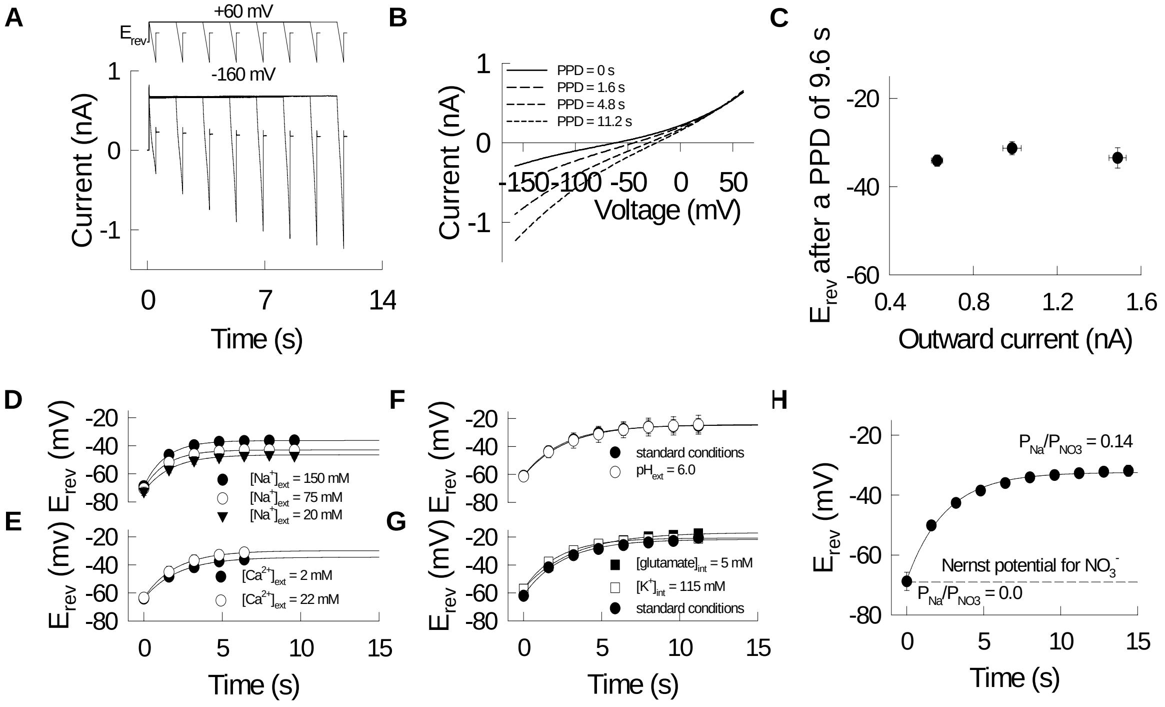
A
+60 mV
E_{rev}
-160 mV
Current (nA)
1
0
-1
0
7
14
Time (s)
B
PPD = 0 s
PPD = 1.6 s
PPD = 4.8 s
PPD = 11.2 s
Current (nA)
1
0
-1
-150 -100 -50 0 50
Voltage (mV)
C
E_{rev} after a PPD of 9.6 s
-20
-40
-60
0.4
0.8
1.2
1.6
Outward current (nA)
D
E_{rev} (mV)
-20
-40
-60
-80
$[Na^+]_{ext}$ = 150 mM
$[Na^+]_{ext}$ = 75 mM
$[Na^+]_{ext}$ = 20 mM
E
E_{rev} (mv)
-20
-40
-60
-80
$[Ca^{2+}]_{ext}$ = 2 mM
$[Ca^{2+}]_{ext}$ = 22 mM
0
5
10
15
Time (s)
F
E_{rev} (mV)
-20
-40
-60
-80
standard conditions
pH_{ext} = 6.0
G
E_{rev} (mV)
-20
-40
-60
-80
$[glutamate]_{int}$ = 5 mM
$[K^+]_{int}$ = 115 mM
standard conditions
0
5
10
15
Time (s)
H
E_{rev} (mV)
-20
-40
-60
-80
P_{Na}/P_{NO3} = 0.14
Nernst potential for NO_3^-
P_{Na}/P_{NO3} = 0.0
0
5
10
15
Time (s)

Figure 7.3. Activation of the slow gate is associated with increasing cation permeabilities of EAAT4 channels. (*A*) Current responses to voltage ramps after prepulses of variable duration. (*B*) Voltage dependence of the current amplitudes recorded during voltage ramps before and after different prepulse durations (PPD) from the experiment shown in *A*. (*C*) Plot of the corrected steady state reversal potential versus the outward current amplitude at +60 mV. Data from 30 cells were binned into 3 data groups that were statistically not different. (*D*) Time course of current reversal potentials determined from voltage ramp-experiments on 4 cells with different external $[Na^+]_o$. (*E*) Time course of current reversal potentials determined from voltage ramp-experiments on 4 cells with different external $[Ca^{2+}]_o$. (*F*) Time course of current reversal potentials determined from 4 cells perfused with standard solutions with pH 7.4 (●) and consequently with pH 6.0 (○). (*G*) Reversal potentials from cells under standard conditions (●, n = 14), cells dialyzed with an internal solution containing 5 mM glutamate (■, n = 2), and cells dialyzed with an internal solution in which Na^+ was completely replaced by K^+ (□, n = 4). (*H*) Time course of current reversal potential using an internal solution containing 10 mM NaNO and 100 mM NaGluconate. All reversal potentials are given as means ± SEM.

these conditions, the initial inward current decreases in amplitude and then reverses to an outward current (Fig. 7.1*E*).

To define the particular ions whose permeabilities change during slow activation, we performed ion substitution experiments. Cells were moved in the streams of different external solutions, and current reversal potentials were determined from voltage ramps after various durations of a prepulse to +60 mV. Reversal potentials were then plotted versus the prepulse duration (Fig. 7.3*D-H*), demonstrating that channel selectivity changes with the same time course as current amplitudes in Fig. 7.1*D*. Changing external [Na^+] (Fig. 7.3*D*) or external [Ca^{2+}] (Fig. 7.3*E*) affected the steady-state reversal potentials, but left the initial values unaffected, indicating that Na^+ and Ca^{2+} become permeant during slow activation. Neither protons nor glutamate are permeant under any tested condition (Fig. 7.3*F,G*). Activated EAAT4 channels do not select between monovalent cations, as intracellular substitution of Na^+ by K^+ does not modify current reversal potentials (Fig. 7.3*G*). To determine the cation to anion permeability ratio, experiments were performed with only one permeant anion, NO_3^-, on both sides of the membrane (Fig. 7.3*H*). After deactivation of the slow gate, EAAT4 currents reverse at the predicted anion reversal potential indicating ideal anion selectivity. Depolarizing prepulses result in reversal potentials that correspond to a P_{Na}/P_{NO3} of 0.14 ± 0.02 (n = 4). Using the NO_3^- to Cl^- permeability ratio determined from reversal potentials in the slow deactivated state (P_{NO3}/P_{Cl} = 9.4 ± 0.4; n = 30) and assuming that there is no change of the relative anion selectivity due to slow gate activation, these two values result in a P_{Na}/P_{Cl} permeability ratio of 1.3 ± 0.2. A P_{Ca}/P_{Cl} of 1.7 ± 0.2 (n = 4) was calculated from the measured steady state reversal potentials upon elevated $[Ca^{2+}]_o$ (Fig. 7.3*E*). These results demonstrate that, with Cl^- as the main anion, monovalent and divalent cations are considerably permeant through EAAT4 anion channels in the slow-activated state.

Cations could permeate the same ion conduction pathway as anions, or, alternatively, slow gating could open additional cation-permeable pores. We employed noise analysis to distinguish between these two possibilities (17). EAAT4 anion channels produce a Lorentzian noise that can be measured by whole-cell recordings (Fig. 7.4*A*) (see *Supporting Text*). At the current reversal potential, the unitary current amplitudes of a pore permeable to both anions and cations are zero. Therefore, current variances, determined before and after slow activation at the respective reversal potentials, will be identical for this scenario. In contrast, in case of separate anion- and cation-conducting pores, each pore would fluctuate between zero and non-zero current amplitudes resulting in an increased current variance at the apparent reversal potential after slow activation. We determined current variances at two different potentials: at –27 mV, the potential at which currents reverse on average after an activating prepulse to 0 mV, and at –61 mV, the reversal potential after a prepulse to –60 mV, respectively. The two current variances are not different ($\sigma^2 = 45 \pm 8$ pA^2 and $\sigma^2 = 41 \pm 9$ pA^2, n = 8) indicating that slow activation modifies the cation to anion selectivity of a single ion conduction pathway of EAAT4 anion channels (17). Cation currents are non-existent in the absence of permeant anions (Fig. 7.6 which is published as *Supporting Information*), indicating that cations can only permeate through this ion conduction pathway together with anions.

7.4.3 Slow gating alters the open probability of EAAT4 anion channels depending on the current direction

Ion substitution experiments demonstrated that slow gating functionally changes the anion conduction pathway of EAAT4. To test whether it also modifies the open probability, i.e. the proportion of time the EAAT4 anion channel is conducting anions, we employed a variation of non-stationary noise analysis. We determined isochronal standard deviations 2 ms after steps to various voltages from holding potentials of –60 mV and 0 mV, respectively (Fig. 7.4*B,C*), and plotted them versus the mean current amplitude. For such a plot, the slope of a

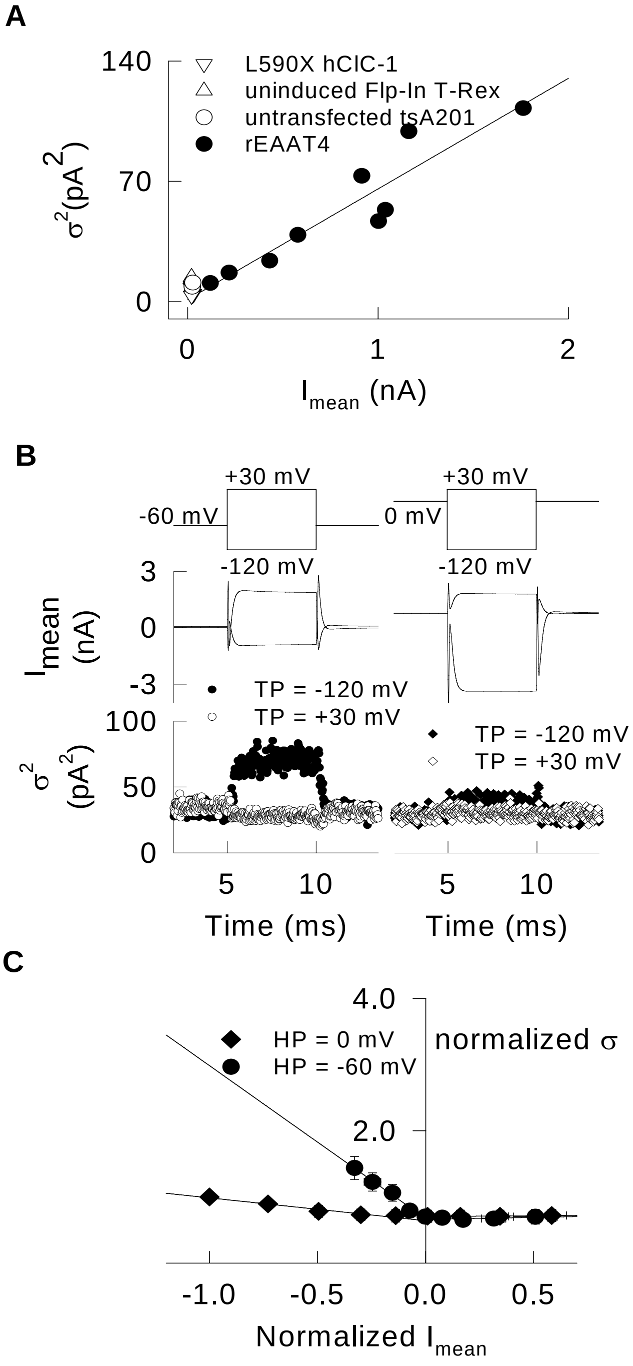
A
140
70
0
$\sigma^2 (pA^2)$
▽ L590X hClC-1
△ uninduced Flp-In T-Rex
○ untransfected tsA201
● rEAAT4
0
1
2
I_{mean} (nA)
B
+30 mV
-60 mV
-120 mV
+30 mV
0 mV
-120 mV
3
0
-3
I_{mean} (nA)
● TP = -120 mV
○ TP = +30 mV
◆ TP = -120 mV
◇ TP = +30 mV
100
50
0
$\sigma^2 (pA^2)$
5
10
Time (ms)
5
10
Time (ms)
C
4.0
2.0
normalized σ
◆ HP = 0 mV
● HP = -60 mV
-1.0
-0.5
0.0
0.5
Normalized I_{mean}

Figure 7.4. Activation of the slow gate increases the open probability of the EAAT4 anion channels. (*A*) Plot of the current variance at –120 mV versus the mean current amplitude determined from 9 tsA201 cells transiently transfected with cDNA encoding for EAAT4 transporters (●), 4 tsA201 cells transiently transfected with cDNA encoding for a non-conducting hClC-1 mutant (L590X hClC-1,∇), 5 untransfected tsA201 cells (○), and 4 uninduced Flp-In T-Rex HEK293 cells (Δ). The correlation coefficient between both parameters in rEAAT4-transfected cells is r = 0.93. (*B*) Time course of mean currents and variances measured at test potentials of –120 mV (filled symbols) and +30 mV (open symbols) stepping from holding potentials of –60 mV and 0 mV. The external solution contained NaSCN. (*C*) Plot of the normalized isochronal current standard deviation versus the normalized mean current amplitude, determined at test steps to potentials between –180 mV and +60 mV from holding potentials of –60 mV (●) and 0 mV (♦) (means ± SEM, n = 8), respectively.

linear regression depends on the absolute open probability ($\sigma(V) = I(V)\sqrt{\frac{\frac{1}{p(V)}-1}{N}}$) (18) (see *Supporting Text*), i.e. an increased absolute open probability results in a less steep relationship between standard deviation and current amplitude. For both holding potentials, the plots can be well described with two lines having different slopes at positive and at negative current amplitudes, demonstrating that the absolute open probability after a prescribed prepulse can assume two different values, one at potentials positive and another one at potentials negative to the current reversal potential. For EAAT4 anion channels, a holding potential of 0 mV causes an isolated increase of the open probability at potentials negative the current reversal potential, but leaves current amplitudes and current variances at positive potentials virtually unaffected. Thus, slow activation increases only the number of open channels permitting an inward current, but not of those conducting an outward current.

7.5 Discussion

EAAT4 transporters are known to mediate three different transport processes. They function as secondary-active glutamate transporters and as anion-selective ion channels. Additionally, they display a glutamate- and arachidonic acid-activated proton conductance (19). We here report that the selectivity of EAAT4 anion channels can be changed from ideally anion-selective to partially cation-permeable by a glutamate- and voltage-dependent gating process. Inward and outward anion currents are independently gated (Fig. 7.4C), allowing a selective modification of the inward current amplitude without affecting outward currents. Slow gating does not modify the proton permeability (Fig. 7.3G), indicating that the EAAT4 proton channel is not controlled by the slow gate.

The two unique qualities of the associated anion channel give EAAT4 transporters the remarkable ability to either inhibit or excite neuronal cells, depending on conditions and history. Under resting conditions, EAAT4 anion channels are ideally anion-selective and thus inhibit cell excitability. Trains of phasic depolarizations as well as long lasting depolarizations (20, 21) cause slow activation and change the number and selectivity of open channels. Since deactivation is extremely slow, Purkinje cell excitation is followed by an excitatory inward current of several seconds through slow activated EAAT4 channels.

EAAT4 transporters are primarily expressed in spines of Purkinje dendrites (10), precluding a detailed analysis of slow gating in native tissue. However, functional properties of EAAT4 anion channels in heterologous expression systems are very similar to those found in native cells (22). Thus, the here reported slow-gating induced changes of EAAT4 currents, together with EAAT4 densities in spines (10, 22) and estimates of passive electric properties of these neuronal compartments allow an approximation of slow activation-induced changes of the spinal membrane potential (see *Supporting Text*). Spines in Purkinje cell dendrites are small units with a high input resistance (23), and the estimated EAAT4 inward cation current will depolarize the spine membrane potential by about 25 mV (see *Supporting Text*). Since Ca^{2+} influx through activated EAAT4 channels potentially modifies Ca^{2+} release from intracellular stores (24), EAAT4 anion channels might also play a role in neuronal plasticity (24, 25). The unusual features of slow activation thus allow EAAT4 to modify excitability, firing frequency and Ca^{2+} signaling in Purkinje neurons.

In all known ion channels involved in electrical signaling, changes in open probability modify the membrane conductance for permeant ions over the whole voltage range. In such cases, the effect of channel activation on the membrane potential depends on the ion concentration on both sides and is therefore, in most cases, an invariable property of the channel. EAAT4 transporter-associated anion channels exhibit a totally novel behavior. They conduct inhibitory as well as excitatory currents, and they switch between inhibitory and excitatory action in short periods of time, without requiring energetically costly alterations of bulk solution ion concentrations. Slow gating of EAAT4 anion channels most likely obtains its glutamate- and voltage-dependence from the association to the glutamate carrier. The novel gating process defines a likely physiological role of EAAT4 transporter-associated ion channels and demonstrates the impact of the tight coupling of anion channel and glutamate carrier in this class of membrane proteins.

Acknowledgments

We would like to thank Drs. A.L. George, D. Naranjo and J. Rothstein for providing the expression construct for hClC-Kb, barttin, F425GΔ6-46 *Shaker* and rEAAT4, respectively, Drs. Louis DeFelice, Patricia Hidalgo, JP Johnson, Günther Schmalzing, and the participants of the Ion Channel Carnival, December 2004, Valdivia, Chile, for helpful discussions, and Hannelore Heidtmann and Barbara Poser for excellent technical assistance. These studies were supported by the Deutsche Forschungsgemeinschaft and by the Studienstiftung des Deutschen Volkes.

7.6 References

1. Danbolt, N. C. (2001) *Progress in Neurobiology* **65**, 1-105.
2. Amara, S. G. & Fontana, A. C. (2002) *Neurochem. Int.* **41**, 313-318.
3. Kanner, B. I. (1996) *Biochem. Soc Trans.* **24**, 843-846.
4. Billups, B., Rossi, D., Oshima, T., Warr, O., Takahashi, M., Sarantis, M., Szatkowski, M. & Attwell, D. (1998) *Progress in Brain Research* **116**, 45-57.
5. Larsson, H. P., Picaud, S. A., Werblin, F. S. & Lecar, H. (1996) *Biophys J* **70**, 733-742.
6. Wadiche, J. I., Amara, S. G. & Kavanaugh, M. P. (1995) *Neuron* **15**, 721-728.
7. Fairman, W. A., Vandenberg, R. J., Arriza, J. L., Kavanaugh, M. P. & Amara, S. G. (1995) *Nature* **375**, 599-603.
8. Billups, B., Rossi, D. & Attwell, D. (1996) *J Neurosci* **16**, 6722-6731.
9. Yamada, K., Watanabe, M., Shibata, T., Tanaka, K., Wada, K. & Inoue, Y. (1996) *Neuroreport* **7**, 2013-2017.
10. Dehnes, Y., Chaudhry, F. A., Ullensvang, K., Lehre, K. P., Storm-Mathisen, J. & Danbolt, N. C. (1998) *J Neurosci.* **18**, 3606-3619.
11. Huang, Y. H., Dykes-Hoberg, M., Tanaka, K., Rothstein, J. D. & Bergles, D. E. (2004) *J Neurosci.* **24**, 103-111.
12. Melzer, N., Biela, A. & Fahlke, Ch. (2003) *J Biol. Chem.* **278**, 50112-50119.
13. Hebeisen, S., Biela, A., Giese, B., Muller-Newen, G., Hidalgo, P. & Fahlke, Ch. (2004) *J Biol. Chem.* **279**, 13140-13147.
14. Lewis, C. A. (1979) *J Physiol (London)* **286**, 417-445.
15. Heinemann, S. H. & Conti, F. (1992) *Method Enzymol* **207**, 131-148.
16. Estevez, R., Boettger, T., Stein, V., Birkenhager, R., Otto, E., Hildebrandt, F. & Jentsch, T. J. (2001) *Nature* **414**, 558-561.
17. Dionne, V. E. & Ruff, R. L. (1977) *Nature* **266**, 263-265.
18. Hebeisen, S., Heidtmann, L., Cosmelli, D., Gonzalez, C., Poser, B., Latorre, R., Alvarez, O. & Fahlke, Ch. (2003) *Biophys J* **84**, 2306-2318.
19. Fairman, W. A., Sonders, M. S., Murdoch, G. H. & Amara, S. G. (1998) *Nat. Neurosci.* **1**, 105-113.
20. Canepari, M., Auger, C. & Ogden, D. (2004) *J Neurosci.* **24**, 3563-3573.
21. Tempia, F., Alojado, M. E., Strata, P. & Knopfel, T. (2001) *J Neurophysiol.* **86**, 1389-1397.

22. Otis, T. S., Kavanaugh, M. P. & Jahr, C. E. (1997) *Science* **277**, 1515-1518.

23. Rapp, M., Segev, I. & Yarom, Y. (1994) *J Physiol (London)* **474**, 101-118.

24. Berridge, M. J. (1998) *Neuron* **21**, 13-26.

25. Sabatini, B. L., Maravall, M. & Svoboda, K. (2001) *Curr. Opin. Neurobiol.* **11**, 349-356.

7.7 Supporting Text

7.7.1 Time-Dependent Changes of the Intracellular Anion Composition

The long depolarizations necessary to activate the slow gate (Fig. 7.1) might cause changes of the intracellular anion composition that could contribute to the time-dependent changes of the current amplitude and affect the accuracy in determining relative cation to anion permeabilities. Changes of the intracellular anion concentration (c_i) of a cell in the whole-cell mode at a constant anion influx (j) depend on the volume of the cell V_i, the series resistance R_s, the diffusion coefficient D and the resistivity ρ of the intracellular solution (1 - 3). c_p denotes the anion concentration in the pipette.

$$\frac{dc_i}{dt} = \frac{1}{V_i} j - \frac{1}{\tau_p}(c_p - c_i) \qquad [1]$$

with τ_p given by

$$\tau_p = \frac{R_s V_i}{D\rho} \qquad [2]$$

This equation can be solved when the anion flux j across the membrane is constant.

$$c_i(t) = c_i(0) + \frac{j}{V_i}\tau_p(1 - e^{-\frac{t}{\tau_p}}) \qquad [3]$$

In our experiments, τ_p is ≈ 60 s, based on average values of the series resistance R_s (≈ 4 MΩ, ref. 3), the cell volume V_i (≈ 20 x 10^{-15} m^3, calculated from reported tsA201 capacitances, ref. 4) the diffusion coefficient D (19 x 10^{-10} m^2/s for NO_3^-, ref. 5) and the resistivity ρ (0.7 Ωm, ref. 6) of the intracellular solution. The calculated time constant is ≈ 20 times larger than the activation and deactivation time constants of slow gating (Fig. 7.1*F*) and thus represents an additional argument against anion accumulation as the sole basis of the observed changes of the inward current and reversal potential.

The analysis does predict small changes of the intracellular anion concentration that need to be taken into account in the quantitative analysis of slow-gating induced alteration of EAAT4 anion channel selectivity. Based on the anion current amplitude during the depolarizing prepulse, we calculated changes of the internal anion concentration and corrected the measured reversal potential for this value (Fig. 7.5). This correction resulted in an average subtraction of 7.5 ± 0.5 mV (n = 30) from the steady state reversal potential. Fig. 7.3*C* gives the plot of corrected current reversal potentials determined at different cells versus the EAAT4 current amplitudes. There is no dependence of the reversal potentials on the current amplitude demonstrating that the correction is adequate and that the corrected values allow an accurate determination of anion to cation permeability ratios.

7.7.2 Trains of Phasic Depolarizations Cause Slow Activation

Application of repetitive short voltage steps of different frequencies, followed by a fixed 10s test step to –80 mV, cause a time and frequency-dependent increase of the tail current amplitude (Fig. 7.7). Increasing the frequency of the transient depolarizations (Fig. 7.7 *A* and *B*) augmented the current amplitudes at negative, but not at positive potentials. Fig. 7.7*C* gives a plot of the instantaneous tail current amplitude at –80 mV (arrows in Fig. 7.7*A* and *B*) charted against several excitation frequencies. Within a frequency range typical of spontaneous burst firing of Purkinje cell dendrites (7, 8), current amplitudes at negative potentials increase threefold.

7.7.3 The Observed Current Variance Is EAAT4 Channel-Associated Noise

We determined current variances in transfected tsA201 cells, as well as in untransfected tsA201 cells, tsA201 cells expressing a non-functional anion channel (L590X hClC-1, ref. 9), and in uninduced rEAAT4 Flp-In-T-Rex cells. For tsA201 cells expressing EAAT4, we observed a clear correlation between EAAT4 current levels and current variance (r = 0.93),

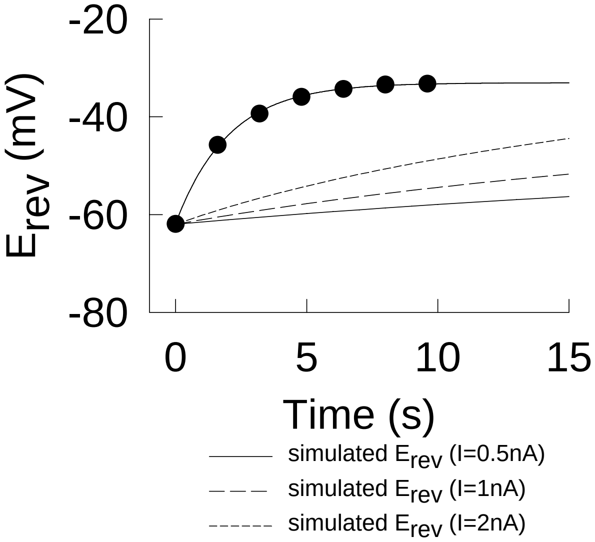

Figure 7. 5. Slow gating-induced alterations of the reversal potentials are much larger than those predicted for anion accumulation. Time course of the simulated reversal potential shift caused by alteration of the intracellular anion composition due to anion influx of 0.5 nA (solid line), 1 nA (long dashed line) and 2 nA (short dashed line) and measured means ± SEM of the reversal potential (●) from cells with inward current amplitudes between 0.5 and 2 nA.

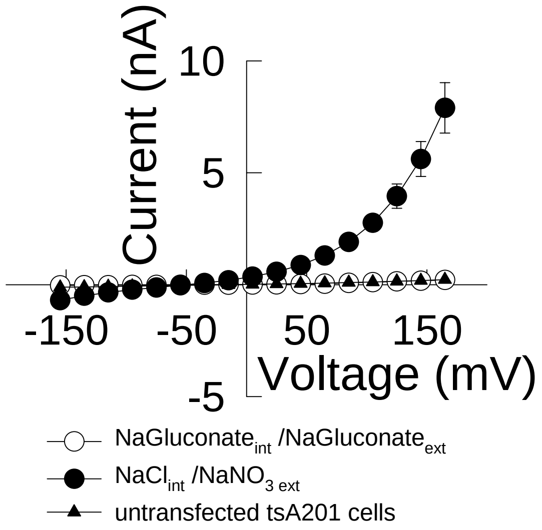

Figure 7.6. Whole-cell currents in EAAT4-expressing cells represent glutamate transporter-associated anion currents. Current-voltage relationships of EAAT4 whole-cell currents under standard conditions (●) and in the absence of permeant anions (○), and of whole-cell currents of untransfected cells under standard conditions (▲). Means ± SEM, n > 4.

while untransfected and uninduced cells, as well as cells expressing large quantities of a non-conducting membrane protein (9) have markedly reduced current variances (Fig. 7.4 *A*). Moreover, in cells that do not express EAAT4, the current variance at a test potential of –120 mV is independent from the holding potential (data not shown). These results demonstrate that the current variance measured in transfected cells is caused by EAAT4 channels and not by endogenous ion channels. Increased current amplitudes at negative test potentials after depolarizing prepulses are associated with reduced current variances (Fig. 7.4), demonstrating that the measured current variance is not thermal noise associated with the recording pipettes, shunt resistances, membrane impedances or electrical circuits, but rather Lorentzian noise associated with gating of EAAT4-associated channels.

To study slow gating induced changes of the open probability of EAAT4-associated anion channels, the current standard deviation was determined as the square root of the non-stationary noise measured 2 ms after the voltage step for various voltages and plotted versus the mean current amplitudes determined at the same time (Fig. 7.4 *B* and *C)*. Lorentzian noise depends on the number of channels (*N*), the unitary current amplitude (*i*) and the absolute open probability (*p*). The measured variance is equal to:

$$\sigma^2(V) = Ni^2(V)\, p(V)\, (1 - p(V)) + \sigma_0^2 \qquad [4]$$

with σ_0^2 being the background noise.

In this experiment, the unitary current amplitude is not constant and substitution of

$$i(V) = \frac{I(V)}{Np(V)} \qquad [5]$$

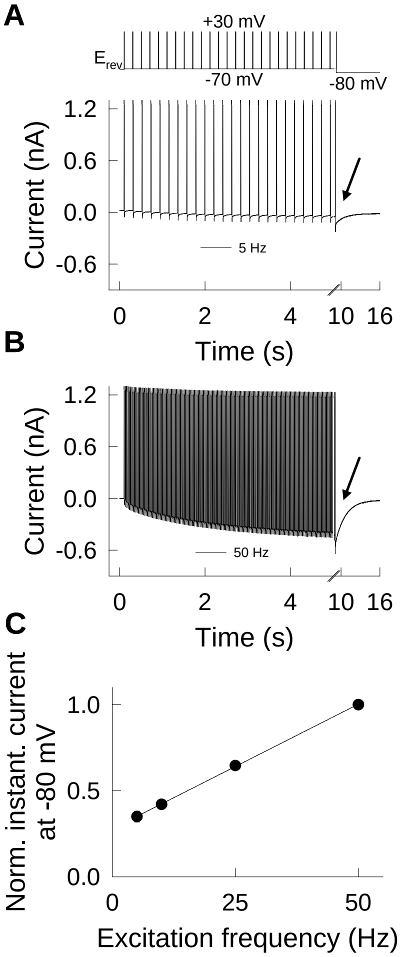

Figure 7.7. Slow activation during repetitive short depolarisations. (*A, B*) Current responses to repetitive depolarisations at frequencies of 5 Hz (*A*) and 50 Hz (*B*) followed by a fixed test step to –80 mV. The cell was perfused with a NaSCN-based solution. (*C*) Frequency dependence of the normalized isochronal tail current amplitude (arrows) (means ± SEM, n = 5).

into Eq. 4 yields:

$$\sigma^2 = \frac{I^2(V)}{N} \left(\frac{1}{p(V)} - 1 \right) + \sigma_0^2 \qquad [6]$$

After subtraction of the background noise, Eq. 6 can be transformed to Eq. 7:

$$\sigma_{app} = \sqrt{\sigma^2 - \sigma_0^2} = I(V)\sqrt{\frac{\frac{1}{p(V)} - 1}{N}} \qquad [7]$$

This analysis shows that the slope of a straight line fitted to the standard deviation-mean current plot solely depends on the open probability and that the observed change of the slope by a depolarizing prepulse (Fig. 7.4*C*) is due to a change of the open probability of EAAT4 channels. Control experiments with voltage-gated potassium channels (10) provide identical open probabilities for inward and outward currents (Fig. 7.8), demonstrating that this behavior is specific for glutamate transporter-associated channels.

7.7.4 Approximation of EAAT4 Current Amplitudes and Resulting Voltage Changes in Spines of Purkinje Cell Dendrites

Published values (11) of the EAAT4 transporter density, their distribution and the mean spine surface area (12) predict ≈ 4900 transporters per spine that are in direct vicinity to the presynaptic glutamate release sites and thus face synaptically released glutamate. Transporters in the dendritic membrane adjacent to the spine were not included in our analysis.

A single channel amplitude of 25 fA in external NO_3^- in the presence of glutamate at 0 mV was calculated using published unitary current amplitudes (13). This value was then used to scale the current-voltage relationships shown in Fig 7.3*B*. The so-obtained voltage dependence of unitary, slow activated EAAT4 current amplitudes was multiplied by the number of transporters in a single synaptic spine and the absolute open probability resulting in

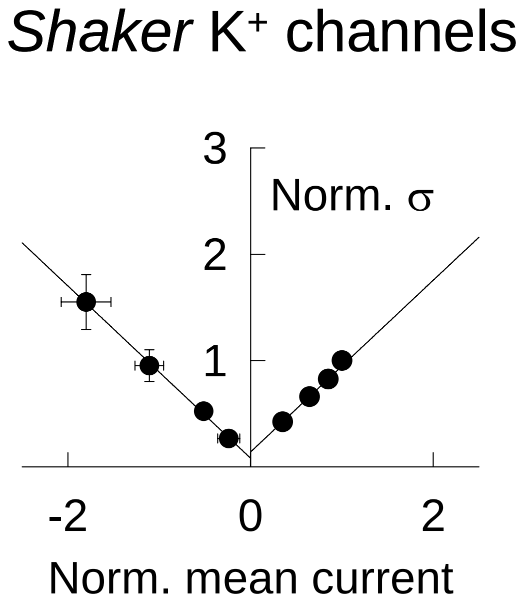

Figure 7. 8. Plot of normalized isochronal current standard deviations versus normalized mean current amplitudes of F425G *Shaker* potassium channels (means ± SEM, n = 6). tsA201 cells were transfected with pMTO3-F425G *Shaker* K^+ channels, and studied using whole-cell patch clamp recordings with an internal solution containing (in mM) 120 KCl, 2 $MgCl_2$, 5 EGTA, 10 HEPES, pH 7.4, and an external solution of (in mM) 144 KCl, 2 $CaCl_2$, 1 $MgCl_2$, 5 HEPES, pH 7.4. Cells were held at –80 mV, channels were activated at 0 mV for 3 ms, and isochronal currents and standard deviations were determined 1 ms after stepping to various voltages.

a total spine current amplitude of about 175 pA at –60 mV (14) carried entirely by slowly activated EAAT4 transporters. Assuming an input resistance of a single spine R_{in} = 400 MΩ (14), this current flow gives rise to a membrane depolarization of ≈ 25 mV, demonstrating a physiological relevance of slow activation of EAAT4 inward currents in synaptic transmission.

7.8 Supporting text References

1. Oliva, C., Cohen, I. S. & Mathias, R. T. (1988) *Biophys. J.* **54**, 791-799.
2. Mathias, R. T., Cohen, I. S. & Oliva, C. (1990) *Biophys. J.* **58**, 759-770.
3. Marty, A. & Neher, E. (1995) in *Single-Channel Recording*, eds. Sakmann, B. & Neher, E. (Plenum, New York), pp. 31-52.
4. Santos-Sacchi, J., Shen, W., Zheng, J. & Dallos, P. (2001) *J. Physiol. (London)* **531**, 661-666.
5. Hille, B. (1992) *Ionic Channels of Excitable Membranes* (Sinauer, Sunderland, MA).
6. DeFelice, L. J. (1981) in *Introduction to Membrane Noise* (Plenum, New York), pp. 115-230.
7. Llinas, R. & Sugimori, M. (1980) *J. Physiol. (London)* **305**, 171-195.
8. Llinas, R. & Sugimori, M. (1980) *J. Physiol. (London)* **305**, 197-213.
9. Hebeisen, S., Biela, A., Giese, B., Müller-Newen, G., Hidalgo, P. & Fahlke, Ch. (2004) *J. Biol. Chem.* **279**, 13140-13147.
10. Goldstein, S. A., Pheasant, D. J. & Miller, C. (1994) *Neuron* **12**, 1377-1388.
11. Takahashi, M., Sarantis, M. & Attwell, D. (1996) *J. Physiol. (London)* **497**, 523-530.
12. Dehnes, Y., Chaudhry, F. A., Ullensvang, K., Lehre, K. P., Storm-Mathisen, J. & Danbolt, N. C. (1998) *J. Neurosci.* **18**, 3606-3619.
13. Melzer, N., Biela, A. & Fahlke, Ch. (2003) *J. Biol. Chem.* **278**, 50112-50119.
14. Rapp, M., Segev, I. & Yarom, Y. (1994) *J. Physiol. (London)* **474**, 101-118.

8. Inter-subunit interactions in EAAT4 glutamate transporters

Delany Torres-Salazar[1,2,3], Christoph Fahlke[1,2,3,4]

[1]Abteilung Neurophysiologie, Medizinische Hochschule Hannover, Germany, [2]Institute of Physiology, RWTH Aachen, Germany, [3]Zentrum für Systemische Neurowissenschaften Hannover (ZSN), Germany, [4]Centro de Estudios Cientificos (CECS), Valdivia, Chile

Corresponding author: Christoph Fahlke, Abteilung Neurophysiologie, Medizinische Hochschule Hannover, Carl-Neuberg-Str. 1, 30625 Hannover, Tel +49 511 532 2777, Fax +49 511 532 2776, Email: fahlke.christoph@mh-hannover.de

Running title: Inter-subunit interactions in glutamate transporters

Keywords: glutamate transporter, chloride channel, synaptic transmission, patch clamp, neurotransmitter, cell excitability

J Neurosci. **2006 Vol. 26, No 28: 7513-7522**

8.1 Abstract

Excitatory amino acid transporters (EAATs) play a central role in the termination of synaptic transmission and in extracellular glutamate homeostasis in the mammalian central nervous system. A functional transporter is assembled as oligomer consisting of three subunits, each of which appears to transport glutamate independently from the neighboring subunits. EAATs do not only sustain a secondary-active glutamate transport, but also function as anion channel. We here address the question whether inter-subunit interactions play a role in pore-mediated anion conduction. We expressed a neuronal isoform, EAAT4, heterologously in *Xenopus* oocytes and mammalian cells and measured glutamate flux and anion currents under various concentrations of Na^+ and glutamate. EAAT4 anion channels are active in the absence of both substrates, and increasing concentrations activate EAAT4 anion currents with a sigmoidal concentration dependence. Since only one glutamate molecule is co-transported per uptake cycle, the cooperativity between glutamate binding sites most likely arises from an interaction between different carrier domains. This interaction is modified by two point mutations close to the putative glutamate binding site, G464S and Q467S. Both mutations alter the dissociation constants and Hill coefficient of the substrate dependence of anion currents, leaving the concentration dependence of glutamate uptake unaffected. Our results demonstrate that glutamate carriers cooperatively interact during anion channel activation, suggesting that several subunits contribute to the formation of the EAAT anion channel.

8.2 Introducion

Excitatory amino acid transporters (EAATs) sustain two fundamentally distinct transport mechanisms. They function as co-transporters of glutamate, sodium, potassium and protons ions ("coupled transport") (Zerangue and Kavanaugh, 1996; Levy et al., 1998) and as anion channels ("uncoupled transport") (Fairman et al., 1995; Wadiche et al., 1995; Billups et al., 1996; Larsson et al., 1996; Melzer et al., 2003). The coupled glutamate transport ensures low resting extracellular glutamate levels and prevents neuronal damage by excessive glutamate receptor activation in the mammalian central nervous system. EAAT-associated anion currents were suggested to support electrogenic glutamate uptake by clamping the membrane potential to negative values (Wadiche et al., 1995). Additionally, EAAT anion channels might play a direct role in electric signaling of certain excitable cells (Amara and Fontana, 2002; Melzer et al., 2005).

The high-resolution structure of a bacterial glutamate transporter (Yernool et al., 2004) and recent fluorescence resonance energy transfer (FRET) analysis (Koch and Larsson, 2005) provided first insights into likely conformational changes underlying glutamate transport. In contrast, the molecular function of the EAAT-associated anion channel is only poorly understood. EAAT glutamate transporters assemble as homotrimeric complexes (Haugeto et al., 1996; Gendreau et al., 2004; Yernool et al., 2004; Koch and Larsson, 2005; Grewer et al., 2005). Trimerization of monomers occurs efficiently during or shortly after synthesis of the individual subunits resulting in stable trimers as the sole native and functional oligomeric state (Gendreau et al., 2004). The trimeric structure thus mediates carrier- as well as pore-mediated transport processes. While each subunit is thought to transport glutamate independently from the rest of the oligomer (Grewer et al., 2005; Koch and Larsson, 2005), it is presently unclear, if each subunit is also capable of anion transport by itself (Ryan et al., 2004, Grewer et al., 2005), or if the EAAT anion pore is jointly formed by several subunits

(Eskandari et al., 2000). We here study glutamate uptake and anion conduction at various concentrations of transporter substrates such as Na^+ and glutamate. Experiments were performed with WT EAAT4 as well as with mutant channels bearing two point mutations, G464S and Q467S, that are located in the neighborhood of the glutamate binding pocket (Zhang and Kanner, 1999; Yernool et al., 2004). We demonstrate that several cooperatively interacting glutamate binding sites need to be occupied in order to activate the anion channel. G464S and Q467S alter the apparent dissociation constants, the binding cooperativity and gating of the EAAT4 anion channels. Our results demonstrate that individual subunits interact in activating EAAT4 anion channels, fully consistent with the notion of anion channels that are either jointly formed by three subunits or consist of three cooperatively interacting protopores.

8.3 Materials and Methods

8.3.1 Expression of EAAT4 in mammalian cells

The pcDNA3.1-rEAAT4 construct was kindly provided by Dr. J. Rothstein, John Hopkins University, Baltimore, USA. Transient transfection of tsA201 cells using the $Ca_3(PO_4)_2$ technique was performed as previously described (Melzer et al., 2003). To identify cells with a high probability of expressing recombinant transporters, cells were co-transfected with a plasmid encoding the CD8 antigen and incubated 5 min before use with polystyrene microbeads precoated with anti-CD8 antibodies (Dynabeads M-450 CD 8, Dynal, Great Neck, NY). The CD8/EAAT4 cDNA ratio was adjusted to ensure that almost every cell with beads exhibited currents with the characteristic properties shown in Fig. 8.1. Point mutations were introduced by PCR-based strategies. For each construct, two independent recombinants from the same transformation were examined and shown to exhibit indistinguishable functional properties. Co-transfection experiments with WT and R501C EAAT4 were performed at a 1:1 and a 1:4 molar ratio of WT and mutant EAAT4 cDNA.

8.3.2 Electrophysiology

Standard whole-cell patch clamp recordings were performed using an Axopatch 200B (Axon Instruments, Union City, CA, USA) amplifier. Borosilicate pipettes were pulled with resistances of 1.0 - 2.2 MΩ. To reduce voltage errors due to uncompensated series resistances, we routinely compensated more than 80% of the series resistance by an analog procedure and excluded cells with more than 10 nA maximum anion currents from the analysis. This procedure results in a calculated voltage error below 5 mV in all analyzed cells under all conditions. Mean maximum current amplitudes in the presence of 140 mM external Na^+ and 0.5 mM glutamate were 5.6 ± 0.4 nA (n = 25) at +165 mV with standard NaCl-based internal and standard $NaNO_3$-based external solution, and -4.0 ± 0.3 nA (n =55) at –175 mV with standard $NaNO_3$-based internal and standard NaCl-based external solution. The mean maximum voltage error was calculated to be 2.6 ± 0.2 mV (n=80). Currents were filtered at 5kHz (-3dB) and digitized with a sampling rate of 50 kHz using a Digidata (Axon Instruments) AD/DA converter. Cells were clamped to 0 mV for at least 5s between test sweeps. For all these experiments, we used an external and/or internal agar salt bridge to connect the Ag/AgCl electrode, made from a plastic tubing filled with 3 M KCl in 0.3% agar. If not otherwise stated, standard solutions were used that contained (in mM): 140 $NaNO_3$ (standard $NaNO_3$-based external solution) or NaCl (standard NaCl-based external solution), 4 KCl, 2 $CaCl_2$, 1 $MgCl_2$, 5 HEPES, pH 7.4, intracellular (in mM) 115 NaCl (standard NaCl-based internal solution) or $NaNO_3$ (standard $NaNO_3$-based external solution), 2 $MgCl_2$, 5 EGTA, 10 HEPES, pH 7.4. For the concentration dependences of Na^+ and glutamate (Fig. 8.2, 8.3, 8.4 and 8.6), external Na^+ was substituted equimolarly with K^+, or a given concentration of L-glutamate was added to the external solution, respectively. For determination of external anion permeability ratios, cells were moved into a stream of solutions containing various sodium salts (in mM) 140 NaX, 4 KCl, 2 $CaCl_2$, 1 $MgCl_2$, 5 HEPES, pH 7.4; X denotes Cl^-, NO_3^- and SCN^-.

8.3.3 Data Analysis

Data were analyzed with a combination of pClamp9 (Axon Instruments) and SigmaPlot (Jandel Scientific, San Rafael, CA, USA) programs. Current amplitudes were used without applying a subtraction procedure. Current-voltage relationships at various substrate concentrations were constructed by plotting isochronal current amplitudes determined 1 ms after the voltage step versus the membrane potential. To obtain the concentration dependence of anion channel activation by Na^+ and glutamate, isochronal anion current amplitudes were measured at various concentrations at a given test potential. The so-obtained substrate dependences were normalized to the maximum current amplitude, fit with Hill equations

($I = \frac{I_{\max}[substrate]^n}{[substrate]^n + K_D{}^n} + I_o$) and averaged after normalization to the maximum current amplitude (I_{max} + I_o). The Hill coefficients (n) were determined as fit parameter with the restriction to be an integer. The residual errors of these fits (< 0.001) were not significantly different from fits in which the Hill coefficient was allowed to assume non-integer values and were significantly different compared to residual errors from the fit with a fixed hill coefficient of 1 (>0.01). In Fig. 8.3, various Hill equations with given Hill parameters were fitted to the experimental values. For each membrane potential, apparent dissociation constants (K_Ds) were determined at several cells and averaged. The voltage dependence of the relative open probability (Fig.8.7, Table 8.1) was determined by plotting the normalized isochronal current amplitude at +135 mV or –135 mV after 0.2 s prepulses to different voltages versus the preceding potential. Activation curves obtained in this manner were then fit with a single Boltzmann term plus a voltage-independent value ($I(V) = Amp/(1 + e^{(V - V0.5)/kV}) + P_{min}$). To determine the time course of current activation, deactivation or inactivation (Table 8.1), a sum of two exponentials and a time-independent value ($I(t) = a_1\exp(-t/\tau_{fast}) + a_2\exp(-t/\tau_{slow}) + c$) were fit to data recorded during a series of voltage steps from a holding potential of 0 mV. Permeability ratios were calculated from reversal potential measurements using the Goldman-Hodgkin-Katz (GHK) equation (Hodgkin and Katz, 1949) as described (Melzer et al., 2003). The ratio of coupled and uncoupled transport (Fig. 8.5D) was calculated by dividing the mean glutamate-induced current increases determined in the presence of internal K^+ by mean values of current increases in its absence determined in a different group of cells and by subsequent subtraction of 1 (see Results section). For statistic evaluation the Student's t-Test was used. Insight II (Accelrys, Cambridge, UK) was used to generate the ribbon presentation shown in Fig. 8.5B and to determine distances between the α-carbones of different residues.

8.3.4 Expression in *Xenopus* oocytes and radiotracer flux experiments

Uptake of L-[^{3}H]glutamate (Amersham Biosciences Europe, Freiburg, Germany) was measured in oocytes expressing WT, G464S and Q467S EAAT4. WT and mutant rEAAT4 were subcloned into the pGEMHE vector (Liman et al., 1992) using EcoRI and HindIII sites. Capped cRNA was synthesized from NheI- or SpHI-linearized pGEMHE-rEAAT4 templates through use of the MESSAGE machine (Ambion, Austin, TX), resuspended in 10 µl of water, and stored in 2-µl aliquots at –80 °C until use. The cRNA was injected using a nanoliter injector (nanoliter 2000, World Precision Instruments, Sarasota, FL), and oocytes were kept at 18 °C in ND-96 solution supplemented with 2.5 mM sodium pyruvate and 100 µg/ml gentamycin sulfate until recording (Neely et al., 2004). 5 days after cRNA injection, oocytes were placed into a tube with 100 µl $ND_{SCN}96$ buffer containing (in mM) 96 NaSCN, 4 KCl, 1.3 $CaCl_2$, 5 HEPES, and various concentrations of L-[^{3}H]glutamate and L-glutamate in a ratio of 1: 6000 above 300 µl mineral oil. After 30 min, L-[^{3}H]glutamate uptake was terminated by centrifuging the oocytes into the mineral oil layer. Uptake of L-[^{3}H]glutamate was linear for at least 40 min at the highest used concentration (data not shown). Oocytes were transferred to 0.5% SDS and subjected to scintillation counting after lysis. For each tested experimental condition, uptake was also determined for at least two uninjected oocytes. These control values were averaged and subtracted from radioactive uptake levels measured on injected oocytes. Subtracted uptake values were normalized to values obtained with 100 µM L-glutamate and averaged. The so-obtained concentration dependences of glutamate uptake were fitted with Hill equations. The Hill coefficients were determined as fit parameter with the restriction to be an integer. In Fig. 8.3E, Hill equations with given Hill parameters were fitted to the experimental values.

8.4 Results

8.4.1 Transporter substrates increase the amplitudes and change the voltage dependence of EAAT4 anion currents

We expressed EAAT4 glutamate transporters heterologously in tsA201 cells and measured currents through whole-cell patch clamping. Cells were intracellularly dialyzed with K^+-free solutions to abolish the glutamate uptake current. The so-obtained whole-cell currents predominantly represent EAAT4 anion currents, as complete substitution with impermeant anions results in negligible current amplitudes (current amplitudes at +165 mV at 140 mM external $NaNO_3$ and 115 mM internal NaCl with 0.5 mM glutamate: 5.6 ± 0.4 nA (n = 25), compared to 0.2 ± 0.04 nA (n = 5) after complete substitution of internal and external anions with gluconate in the presence of 0.5 mM glutamate, (Amara and Fontana, 2002; Melzer et al., 2005).). Fig. 8.1 shows representative current responses and mean current amplitudes from transfected tsA201 cells at two different anion compositions. In Fig. 8.1A and B, cells were internally dialyzed with a NaCl-based solution and perfused with a solution containing NO_3^- constituting the main external anion. In Fig. 8.1C and D, an inverted anion distribution with NO_3^- as main internal and Cl^- as main external anion was used. To each cell, three external solutions were consecutively applied: a solution lacking Na^+ and glutamate with K^+ as main extracellular cation, a solution with a physiological external Na^+ concentration without glutamate, and one containing both glutamate and Na^+. Currents were small in the absence of external Na^+, and markedly increased after the application of substrates (Fig. 8.1). For all tested ionic conditions, current amplitudes were significantly larger than in untransfected tsA201 cells (Fig. 8.1B and D). Moreover, all currents can be completely blocked, i.e. to the levels of background currents, by 100 µM L-threo-beta-benzyloxyaspartate (L-TBOA), a known blocker of EAAT4-associated anion channels (Shimamoto et al., 1998) (Fig. 8.1B).

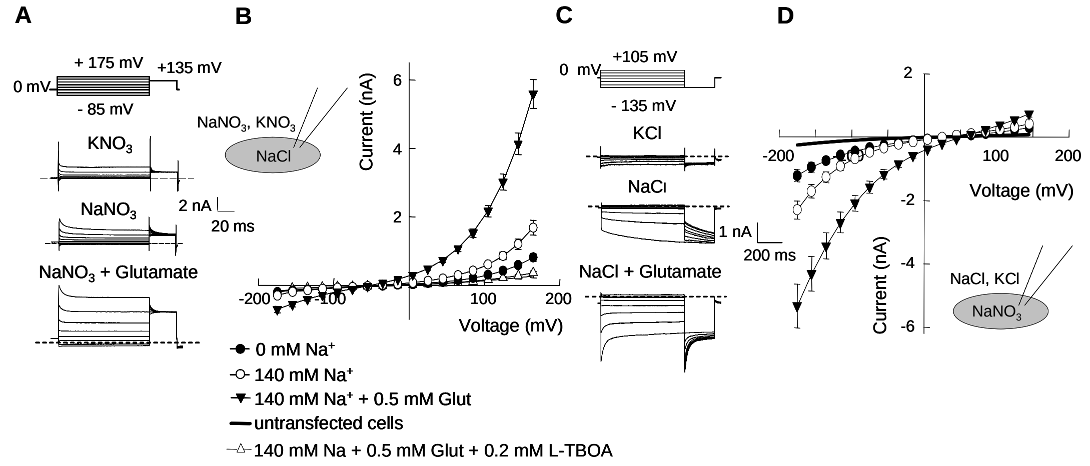

Figure 8.1. Activation of EAAT4 anion channels by transporter substrates. ***A***,***C***, Pulse protocols and representative whole-cell current traces recorded from tsA201 cells expressing EAAT4 transporters. Cells were dialyzed with NaCl- (***A***) or $NaNO_3$- (***C***) based internal solutions and perfused with the indicated solutions. Dashed lines represent zero current amplitude. ***B***,***D***, Mean current-voltage relationships in the absence of Na^+ with K^+ as the main extracellular cation (closed circles, n = 5), in the presence of 140 mM Na^+ (open circles, n = 13 in B and n = 12 in D) and in the presence of 140 mM Na^+ and 0.5 mM glutamate (inverted closed triangles, n = 25 in B and n = 13 in D). Open triangles give mean current amplitudes from cells perfused with 0.1 mM L-TBOA (n=5) and the solid line represent current amplitudes from untransfected tsA201 cells measured in 140 mM Na^+-containing external solutions in the presence of 0.5 mM glutamate (n = 5).

Cells were held at 0 mV, and voltage steps between –175 mV and +165 mV were applied. With NO_3^- on the extracellular membrane site, EAAT4-associated anion currents rise instantaneously upon voltage-steps to negative and positive potentials (Fig. 8.1A). At positive potentials, this instantaneous rise is followed by a time- and voltage-dependent current decay in the presence of sodium, as well as in the presence of both sodium and glutamate, but not in the absence of both substrates. Application of glutamate changes the time course of inactivation and makes steady-state inactivation less complete (Melzer et al., 2003). Gating of EAAT4 anion channels is completely different when studied with internal NO_3^- and external Cl^- (Fig. 8.1C). In the absence of transporter substrates, currents are inwardly rectifying and time-independent. Na^+ and glutamate increase the amplitude and alter the time- and voltage-dependence of EAAT4 anion currents. Upon application of a Na^+-containing external solution lacking glutamate, voltage step to more negative voltages elicit a time-dependent increase of current amplitudes. Depolarizing steps result in time-independent current amplitudes (Fig. 8.1C). Application of glutamate causes an inversion of the activation curve of EAAT4 anion channels. Under these conditions, negative voltage steps elicit an instantaneous rise of the current amplitude followed by a time-dependent decrease (Fig. 8.1C).

8.4.2 Concentration dependence of external Na^+ and glutamate

We next measured EAAT4 anion currents at various concentrations of external Na^+ and glutamate (Fig. 8.2 and 8.3). Isochronal current amplitudes determined at one cell at a fixed membrane potential under different [Na^+] and [glutamate] were normalized, averaged and plotted versus the ligand concentration. Fig. 8.2A shows the current responses to voltage steps between -175 mV and +165 mV of a single cell, consecutively exposed to standard NO_3^--based and glutamate-containing external solutions with three different [Na^+], of 0, 20 mM and 140 mM. In all these experiments, the external glutamate concentration was 0.5 mM. Fig.

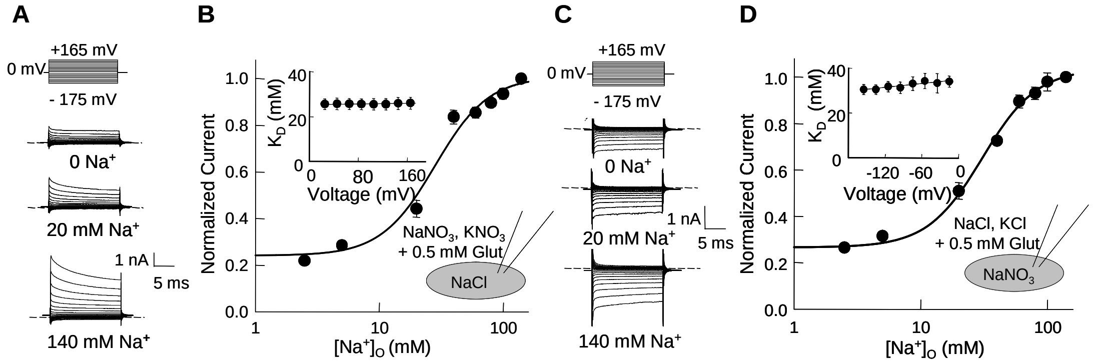

Figure 8.2. Sodium dependence of EAAT4 anion currents. *A*, *C*, Pulse protocols and representative whole-cell current traces recorded from tsA201 cells expressing EAAT4 transporters at different external sodium concentration. Cells were either dialyzed with a NaCl-(***A***) or $NaNO_3$-(***C***) based internal solution, respectively. ***B***, ***D***, Sodium dependences of isochronal anion current amplitudes measured at +165 mV and –175 mV, respectively. Means ± SEM, n = 6 (***B***) and n = 5 (***D***). The solid lines represent fits with the Hill. Inserts, plot of apparent dissociation constants (K_{Ds}) for various voltages *versus* the test potentials. In all experiments, 0.5 mM glutamate is present, and the extracellular [Na^+] was modified by eqimolar substitution of Na^+ by K^+.

8.2B gives the sodium dependence of the isochronal EAAT4 anion current at a test potential of 165 mV obtained from such recordings. Na^+ increases EAAT4 anion currents in sigmoidal relationship with a K_D of 31.6 ± 2.6 mM ($n > 4$) and a Hill coefficient of 3. Apparent dissociation constants were determined for various other test potentials between +25 mV and +165 mV without appreciable voltage dependence (Fig. 8.2B, insert). In the absence of external Na^+, the current amplitude is about 20% of the maximum current amplitude. These currents are not contaminations by endogenous channels, since addition of L-TBOA reduces this anion current amplitude to 3.5% of the maximum current amplitude and since the relative current amplitude in the absence of Na^+ is independent of the EAAT4 expression level (data not shown). Similar results were obtained in experiments in which cells were dialyzed with $NaNO_3$-based internal and NaCl–based external solutions (Figs. 8.2C and D). Fig. 8.3 gives the glutamate dependence of anion currents with NaCl-based internal and $NaNO_3$-based external solution (8.3A and B) or $NaNO_3$-based internal and NaCl–based external solution (8.3C and D). Again, glutamate binds with voltage-independent K_Ds of 35.0 ± 0.3 µM (with internal Cl^- and external NO_3^-, $n = 5$) and 51.0 ± 3.0 µM (with internal NO_3^- and external Cl^-, $n > 4$, $p > 0.05$) (Fig. 8.3). At both anion distributions, there is a marked cooperativity in the glutamate dependence which results in a Hill coefficient of 3 when fitted with a Hill equation (Fig. 8.3B and D). EAAT4 anion channels are active in the absence of glutamate, conducting around 20% of the maximum current amplitude. The glutamate dependence of anion currents were repeated with cells dialyzed with a K^+-containing solution without change of apparent dissociation or Hill coefficient (data not shown). In contrast, substitution of external NO_3^- with SCN^- caused an increase of the Hill coefficient from 3 to 5 (data not shown), demonstrating a role of the permeating anion in determining the cooperativity of the glutamate dependence.

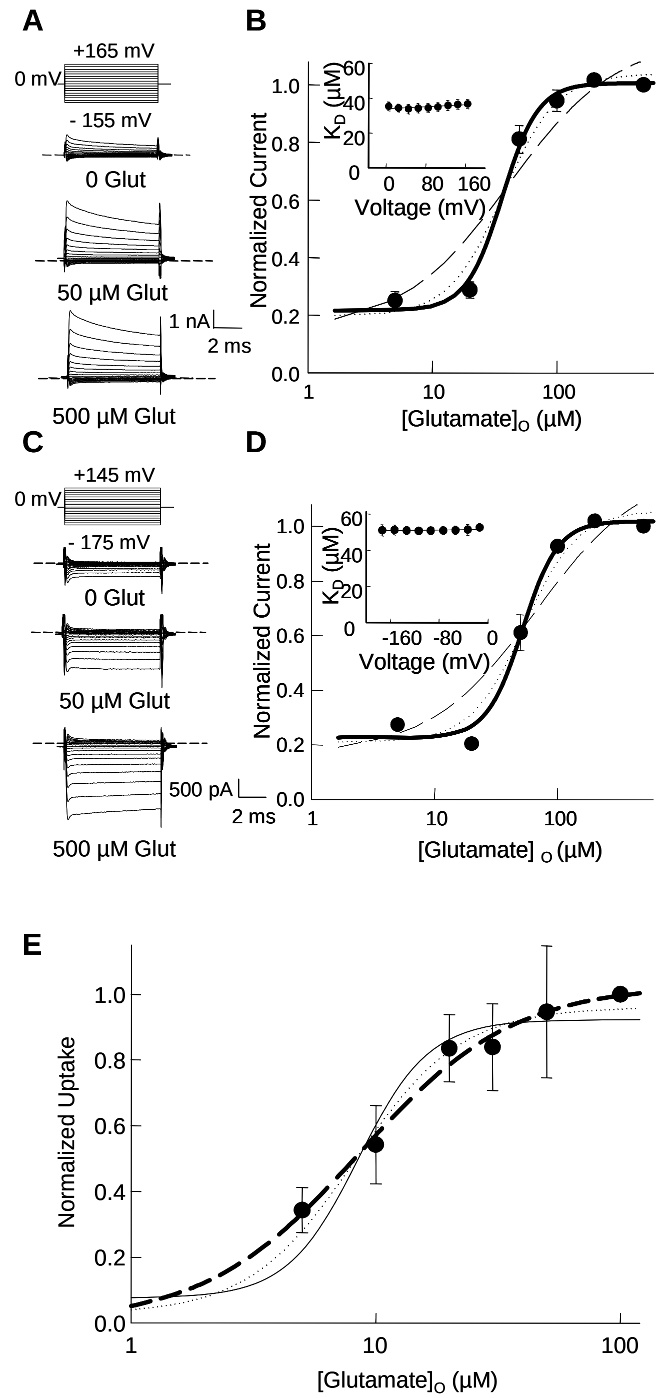
A
+165 mV
0 mV
- 155 mV
0 Glut
50 µM Glut
1 nA
2 ms
500 µM Glut
B
Normalized Current
1.0
0.8
0.6
0.4
0.2
0.0
1
10
100
[Glutamate]$_O$ (µM)
K_D (µM)
60
40
20
0
0
80
160
Voltage (mV)
C
+145 mV
0 mV
- 175 mV
0 Glut
50 µM Glut
500 pA
2 ms
500 µM Glut
D
Normalized Current
1.0
0.8
0.6
0.4
0.2
0.0
1
10
100
[Glutamate] $_O$ (µM)
K_D (µM)
60
40
20
0
-160
-80
0
Voltage (mV)
E
Normalized Uptake
1.0
0.8
0.6
0.4
0.2
0.0
1
10
100
[Glutamate]$_O$ (µM)

Figure 8.3. Glutamate dependence of EAAT4 anion currents and glutamate uptake. ***A***, ***C***, Pulse protocols and representative whole-cell current traces recorded from tsA201 cells expressing EAAT4 transporters at different glutamate concentration. Cells were either dialyzed with 115 mM NaCl- (***A***) or $NaNO_3$-(***C***) based internal solutions and externally perfused with 140 $NaNO_3$- and NaCl- based solutions respectively. ***B***, ***D***, Glutamate dependence of anion currents for NaCl- (***B***) and $NaNO_3$-based (***D***) internal solutions. Means ± SEM, n = 5 (***B***) and n = 8 (***D***), respectively. Lines represent fits with the Hill equation with different fixed Hill coefficients (n = 1, dashed line; n = 2, dotted line; and n= 3, solid line). Inserts give the voltage dependences of the apparent dissociation constants for glutamate (K_{Ds}). (***E***) Glutamate dependence of the normalized radioactive glutamate uptake into oocytes expressing EAAT4 glutamate transporters in 96 mM NaSCN external-based solution. Means ± SEM from 8 oocytes. Fits with the Hill equation with different Hill coefficients are shown as dashed (n = 1), dotted (n = 2) and solid (n = 3) lines. In the experiments shown in ***A***-***D*** the extracellullar $[Na^+]$ was 140 mM, in ***E*** 96 mM.

While the measured sodium-dependence of anion currents is in agreement with the idea of multiple co-transported Na^+ ions (Fig. 8.2) (Watzke et al., 2001), the cooperativity of the glutamate dependence is at first glance surprising. EAAT2 and EAAT3 transport one glutamate together with three Na^+, one K^+ and one proton (Zerangue and Kavanaugh, 1996; Levy et al., 1998). The observed glutamate dependence of the EAAT4 anion current might be due to a different transport stoichiometry in this particular isoform, or alternatively, to a cooperative interaction of several carrier domains in regulating the anion current. To distinguish between these two possibilities, we determined the concentration dependence of EAAT4 glutamate uptake using radiotracer flux measurements (Fig. 8.3E). *Xenopus* oocytes were incubated in different glutamate concentrations at a fixed ratio of radioactive and non-radioactive glutamate, and the amount of transported ^{3}H-L-glutamate was determined after 30 min. With an external solution containing 140 mM NaSCN, the anion current largely exceeds the glutamate uptake current (Melzer et al., 2003), clamping the oocyte membrane to the anion reversal potential. This procedure prevents membrane depolarization by electrogenic glutamate uptake and thus improves the accuracy in determining the concentration dependence of glutamate uptake. Fig. 8.3E gives the results of such experiments with different glutamate concentrations. Glutamate uptake increases with the extracellular glutamate concentration following a Hill equation with a Hill coefficient of 1 and an apparent K_D of 8.5 ± 0.8 μM. In contrast to the glutamate dependence of anion currents, there are no indications for cooperativity in glutamate uptake. We conclude from these experiments that only one glutamate is transported in each transport cycle of EAAT4, and that several cooperatively interacting glutamate binding sites need to be occupied in order to activate an EAAT4 anion channel.

Apparent dissociation constants and the cooperativity of glutamate and sodium dependences are additionally modified by the concentration of the other transporter substrate (Fig. 8.4). Fig. 8.4A gives the sodium dependence of the anion current for two different external glutamate concentrations (0.05 and 0.5 mM). The cells were dialyzed with a $NaNO_3$-based standard internal solution and externally perfused with a NaCl-based external solution. A reduction of the external glutamate concentration leads to increased apparent dissociation constants of sodium binding (from 31.7 ± 2.6 mM (0.5 mM) to 67.6 ± 1.4 mM (0.05 mM) without obvious change of cooperativity (Fig. 8.4A). For the glutamate dependence a reduction of $[Na^+]$ from 140 mM to 40 mM causes an increase of the K_D from 51.1 ± 2.7 µM to 206 ± 20.7 µM and a change of the Hill coefficient from 3 to 1 (Fig. 8.4B). Under all conditions, apparent dissociation constants are voltage-independent (Fig. 8.4, inserts).

8.4.3 Point mutations affecting glutamate and Na^+ binding and anion channel gating

The results presented so far suggest cooperativity between separate sodium and glutamate binding sites in the activation of the EAAT4 anion channels. We evaluated two mutant EAAT4 transporters, G464S and Q467S EAAT4, to study this phenomenon in more detail. Rat and human EAAT2 differ from all other mammalian EAAT isoforms in two serine residues at position 440 and 443 (in the EAAT2 numbering) (Fig. 8.5A) located between hairpin 2A and 2B in the structure of the *P. horikoshii* glutamate transporter (Yernool et al., 2004) (Fig. 8.5B). These positions were postulated to play a role in glutamate and sodium binding (Zhang and Kanner, 1999). Assuming that the three-dimensional structures of EAAT4 and the *P. horikoshii* glutamate transporter are comparable, these residues have distances of about 20 Å (G464) or 24 Å (Q467), respectively, to the center of the protein and of 37 Å (G464) or 41Å (Q467), respectively, to the corresponding residue in neighboring subunits. We expressed G464S and Q467S EAAT4 transporters in *Xenopus* oocytes and

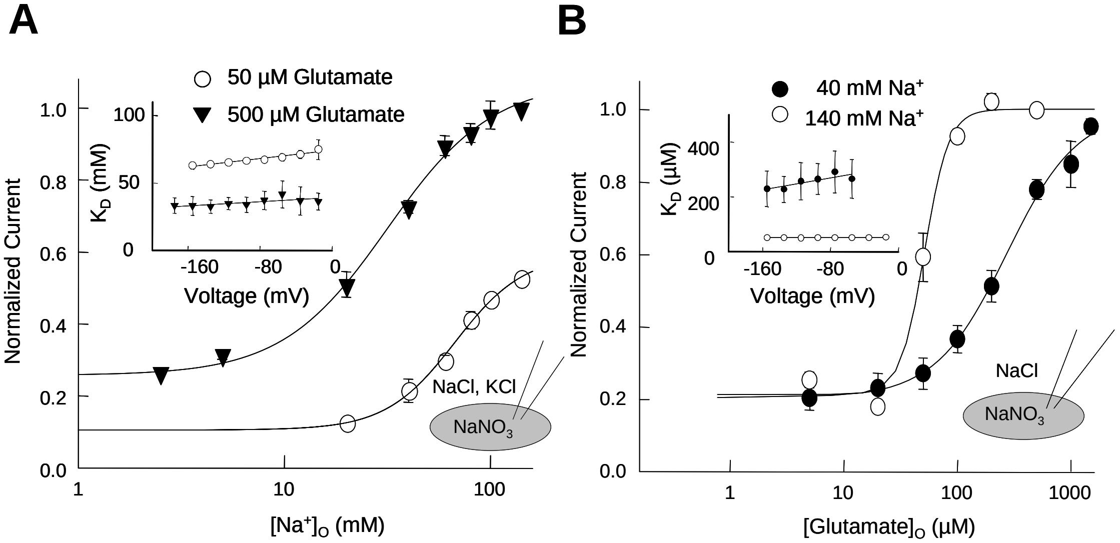

Figure 8.4. **Sodium and glutamate interact in activating EAAT4 anion channels. A**, Sodium dependence of EAAT4 anion currents determined for two external glutamate concentrations (five cells each). **B**, Glutamate dependence of EAAT4 anion currents for two external sodium concentrations; 40 mM Na^+, closed circles (n=6) and 140 mM Na^+ open circles (n=8). Solid lines represent fits with Hill equations. Inserts give the voltage dependence of apparent dissociation constants. Cells were internally dialyzed with $NaNO_3$-based solution and externally perfused with NaCl-based solution. The external $[Na^+]$ was changed by equimolar substitution of NaCl by KCl.

tsA201 cells and studied radioactive glutamate uptake (Fig. 8.5) and anion currents (Fig. 8.5, 8.6 and 8.7) associated with mutant transporters.

Absolute values as well as the glutamate-dependence of L-^{3}H-glutamate uptake are comparable for WT and mutant EAAT4 (K_D = 8.6 ± 0.8 µM (WT), 12.5 ± 4.0 µM (G464S), and 7.9 ± 1.7 µM (Q467S), $p > 0.5$; (Fig. 8.5C)). To calculate the ratios of coupled and uncoupled currents, glutamate-induced current increases were measured in transfected tsA201 cells internally dialyzed with a K^+-containing solution and in cells with an internal K^+-free solution, respectively. For these experiments, Cl^- was chosen to be the main anion to increase the relative amplitude of the uptake current compared to the EAAT4 anion current. Since a lack of internal K^+ abolishes the coupled uptake current ($I_{GluNaHK}$) (Bergles et al., 2002), and since the chloride current in the absence of glutamate ($I_{chloride(-glu)}$) is independent of the internal cation (Melzer et al., 2003), one can calculate the ratio of uncoupled to coupled current by comparing relative current increases in the presence of internal K^+ divided by the corresponding values in its absence as follows.

$$\frac{current\ \ increase}{current\ \ increase}\,\frac{\left([K^+]_{\text{int}}=115mM\right)}{\left([K^+]_{\text{int}}=0\right)}=\frac{\dfrac{I_{GluNaHK}+I_{chloride(+glu)}}{I_{chloride(-glu)}}}{\dfrac{I_{chloride(+glu))}}{I_{chloride(-glu)}}}=\frac{I_{GluNaHK}+I_{chloride(+glu)}}{I_{chloride(+glu)}}=\frac{I_{GluNaHK}}{I_{chloride(+glu)}}+1$$

Current increases were measured from cells dialyzed with a K^+-containing or a K^+-free solution, respectively, mean values were calculated, and the ratio of the respective values determined. This calculation reveals that, at –175 mV with Cl^- as permeant anion, the glutamate uptake current measures about 40% of the anion current in the presence of glutamate (Fig. 8.5). In agreement with the known voltage-dependence of coupled glutamate transport (Zerangue and Kavanaugh, 1996), this analysis predicts a zero glutamate uptake at +125 mV. Neither G464S nor Q467S affect the so-obtained ratios of $I_{GluNaHK}$ by $I_{anion(+glu)}$ (at –175 mV, WT: 0.40 ± 0.01, n=8; G464S: 0.42 ± 0.03, n=7; Q467S: 0.45 ± 0.03, n=7, $p > 0.1$)

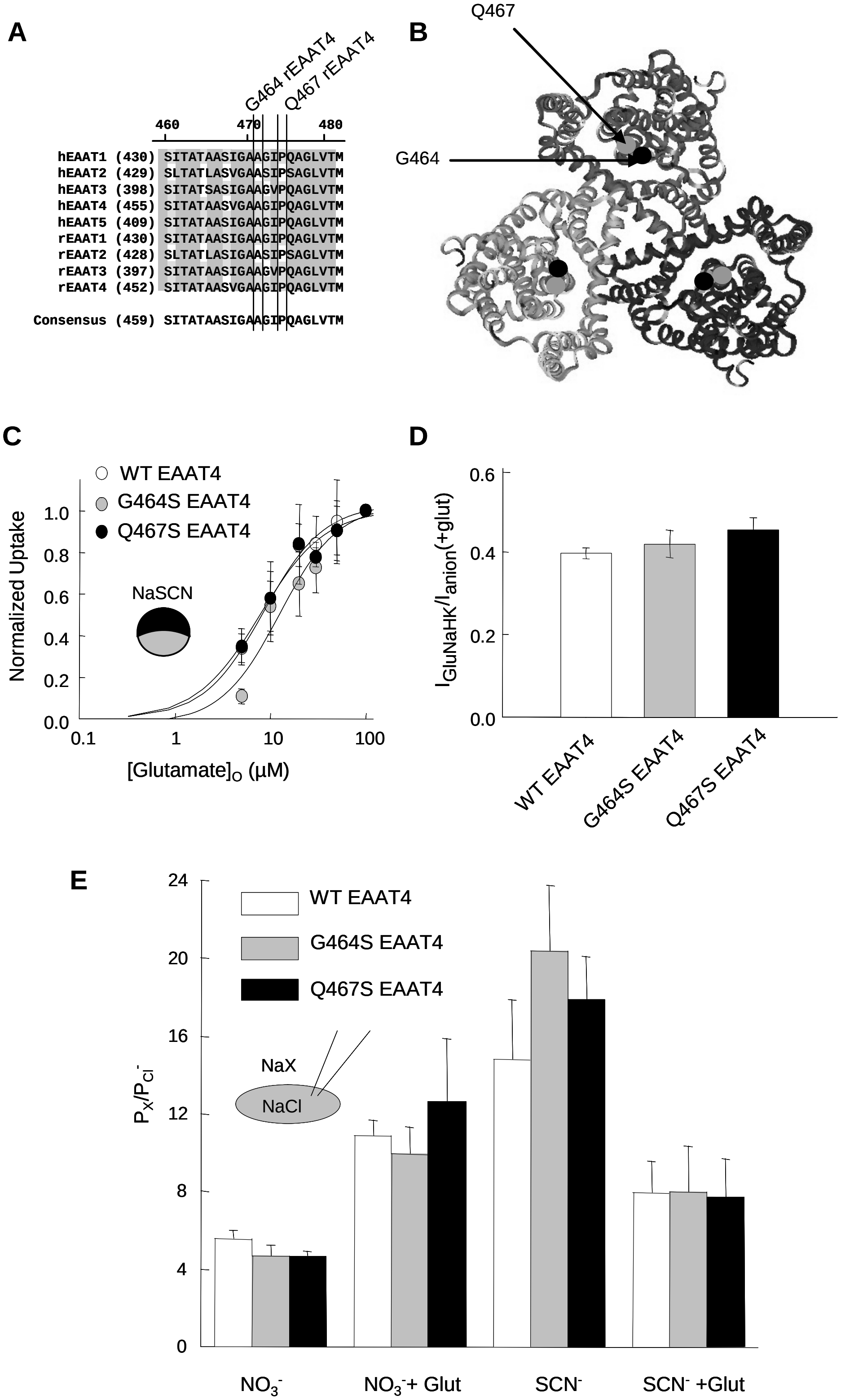
A
G464 rEAAT4
Q467 rEAAT4
460
470
480
hEAAT1 (430) SITATAASIGAAGIPQAGLVTM
hEAAT2 (429) SLTATLASVGAASIPSAGLVTM
hEAAT3 (398) SITATSASIGAAGVPQAGLVTM
hEAAT4 (455) SITATAASVGAAGIPQAGLVTM
hEAAT5 (409) SITATAASIGAAGIPQAGLVTM
rEAAT1 (430) SITATAASIGAAGIPQAGLVTM
rEAAT2 (428) SLTATLASIGAASIPSAGLVTM
rEAAT3 (397) SITATAASIGAAGVPQAGLVTM
rEAAT4 (452) SITATAASVGAAGIPQAGLVTM
Consensus (459) SITATAASIGAAGIPQAGLVTM
B
Q467
G464
C
○ WT EAAT4
● G464S EAAT4
● Q467S EAAT4
NaSCN
Normalized Uptake
1.0
0.8
0.6
0.4
0.2
0.0
0.1
1
10
100
[Glutamate]$_O$ (µM)
D
$I_{GluNaHK}/I_{anion}(+glut)$
0.6
0.4
0.2
0.0
WT EAAT4
G464S EAAT4
Q467S EAAT4
E
WT EAAT4
G464S EAAT4
Q467S EAAT4
NaX
NaCl
P_X/P_{Cl^-}
24
20
16
12
8
4
0
NO_3^-
NO_3^-+ Glut
SCN^-
SCN^- +Glut

Figure 8.5. Effects of two point mutations close to the putative glutamate binding site on coupled and uncoupled transport. ***A***, Alignment of the region containing G464 and Q467 in various human and rat EAAT isoforms. ***B***, Localization of the residues corresponding to G464 (black) and Q467 (grey) of EAAT4 in the ribbon presentation of the three-dimensional structure of the *P. horikoshii* glutamate transporter (Yernool et al., 2004), viewed from the external membrane site. ***C***, Glutamate dependence of radioactive glutamate uptake by WT and mutant EAAT4. Means + SEM from 8 cells for each glutamate concentration. ***D***, Ratio of uptake current to anion current amplitudes from at least 5 cells for WT and mutant EAAT4 transporters at 0.5 mM glutamate. ***E***, Anion permeability ratios for WT and mutant EAAT4 in the presence of 0.5 mM glutamate for at least 4 cells.

(Fig. 8.5D). Mutant transporters exhibit anion currents of comparable amplitude (without external glutamate at +175 mV with Cl_{int}/NO_{3ext}: 3.6 ± 0.3 nA, WT (n = 47), 3.6 ± 0.3 nA, G464S (n = 44), and 4.1 ± 0.4 nA, Q467S (n = 36), and at -175 mV with NO_{3int}/Cl_{ext}: -2.6 ± 0.2 nA, WT (n = 54), -2.1 ± 0.3 nA, G464S (n = 16), and -2.4 ± 0.3 nA, Q467S (n = 16)) and similar relative anion permeabilities (Fig. 8.5E). We conclude that the two mutations neither modify the amplitudes of coupled nor of uncoupled transport.

The mutations do alter apparent dissociation constants and cooperativity of the glutamate and sodium concentration dependence of the anion current amplitude (Fig. 8.6). Fig. 8.6A shows the glutamate concentration dependence of WT, G464S and Q467S EAAT4 anion currents. G464S causes an increase of the glutamate dissociation constant from 51.0 ± 3.0 µM to 183.5 ± 3.4 µM (n > 4), while Q467S decreases the apparent dissociation constant to 41.3 ± 3.4 µM (n > 3). Both mutations affect the cooperativity of glutamate binding. While G464S increases the Hill coefficient from 3 to 15, the glutamate concentration dependence of Q467S EAAT4 is so steep that it cannot be satisfactorily fitted. In the presence of glutamate, G464S causes an increase of the apparent sodium dissociation constant from 31.7 ± 2.6 mM to 70.2 ± 2.5 mM (n > 3) and Q467S a decrease to 8.7 ± 0.8 mM (n = 3). The sodium dependence of G464S fitted with a Hill equation gives a Hill coefficient of 4, in contrast to a Hill coefficient of 2 for Q467S and of 3 for WT EAAT4. All concentration dependences were identical for the two tested anion distributions (data not shown).

The two point mutations also alter anion channel gating (Fig. 8.7). So far, no coherent model of EAAT4 anion channel gating has been developed, and we therefore restrict the kinetic analysis to the experimentally observed time- and voltage-dependences of macroscopic currents (Table 8.1). At the two tested anion compositions, the mutations have distinct effects

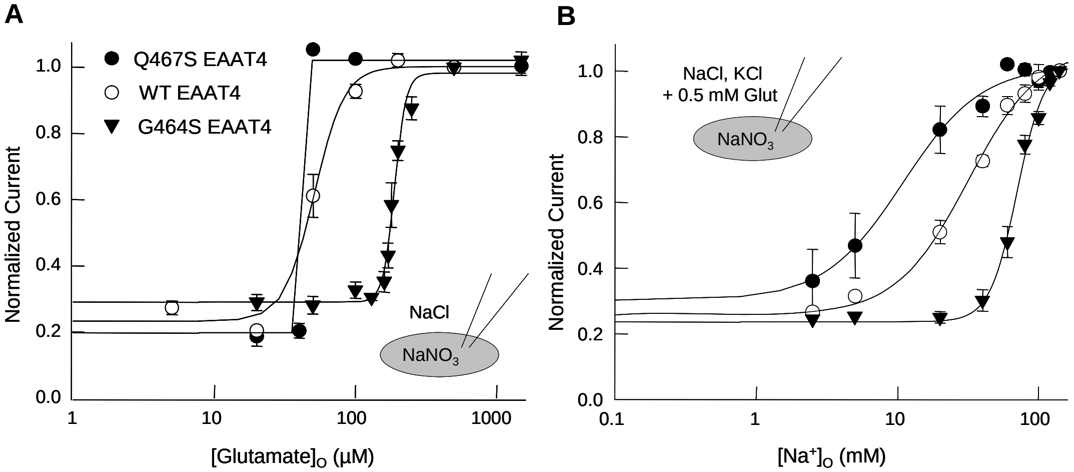

Figure 8.6. G464S and Q467S modify the intersubunit cooperativity in the EAAT4 anion channel activation. Plots of the normalized anion currents at –155 mV versus the glutamate (***A***) and the Na^+ (***B***) concentration for WT, G464S and Q467S EAAT4. Means ± SEM ofrom at least 3 (***A***) or 4 cells (***B***), respectively. The cells were dialyzed with a $NaNO_3$-based standard internal and perfused with a NaCl-based standard external solution.

			V_{50} (mV)	P_O min	Time Constant (ms)		n
					fast	slow	
int NaCl$^-$/ext NaNO$_3^-$	140 mM Na$^+$	**WT EAAT4**	42.0 ± 0.5	0.2 ± 0.003	3.8 ± 0.20	41.3 ± 1.75	19
		G464S EAAT4	-107.9 ± 15.8 **	0.13 ± 0.005	3.5 ± 0.1	36.9 ± 1.74	3
		Q467S EAAT4	- 97.9 ± 3.5 **	0.12 ± 0.012	4.4 ± 0.03	40.1 ± 0.47	3
	140 mM Na$^+$ + 0.5 mM Glutamate	**WT EAAT4**	108.6 ± 3.6	0.47 ± 0.018	2.6 ± 0.14	10.1 ± 0.59	12
		G464S EAAT4	66.2 ± 2.1 **	0.33 ± 0.014	3.4 ± 0.05 **	33.1 ± 0.92 **	9
		Q467S EAAT4	78.1 ± 1.0 **	0.38 ± 0.006	5.9 ± 0.21 **	31.0 ± 0.26 **	3
int NaNO$_3^-$/ext NaCl$^-$	140 mM Na$^+$	**WT EAAT4**	- 4.6 ± 1.17	0.37 ± 0.008	-	181.5 ± 3.82	11
		G464S EAAT4	-125.1 ± 22.7 **	0.23 ± 0.013	-	114.2 ± 10.08 **	6
		Q467S EAAT4	51.9 ± 12.9 **	0.68 ± 0.053	-	-	5
	140 mM Na$^+$ + 0.5 mM Glutamate	**WT EAAT4**	-69.9 ± 2.8	0.50 ± 0.015	24.5 ± 0.29	342.2 ± 6.05	14
		G464S EAAT4	-58.2 ± 6.2	0.53 ± 0.031	30.6 ± 0.43 **	1690 ± 140.2 **	7
		Q467S EAAT4	-101.2 ± 8.7 **	0.70 ± 0.037	-	2032 ± 62.0 **	9

Table 8.1. Gating properties for EAAT4 wild type and mutants in the absence and presence of glutamate for two anion conditions. * indicates a significant difference to WT at $p<0.05$, and ** at $p< 0.01$, respectively.

on channel gating. With external NO_3^-, WT and mutant channels inactivate upon depolarising voltage steps on a bi-exponential time course (Fig. 8.7A). While deactivation time constants of G464S and Q467S EAAT4 anion channels are similar to WT without external glutamate, they are significantly increased in the presence of glutamate (Table 8.1). At the inverted anion distribution, WT and G464S EAAT4 anion channels activate upon hyperpolarisation in the absence of glutamate, and deactivate at the same voltages in its presence. Activation was fit with a monoexponential and deactivation with a biexponential time course. The so determined time constants are increased by G464S. For Q467S, activation in the absence of glutamate is basically absent (Fig. 8.7C), and there is no fast component of deactivation after application of glutamate. (Table 8.1). We next plotted instantaneous current amplitudes at a fixed test step *versus* the preceding potential (Fig. 8.7B and D). These instantaneous current amplitudes depend on the number of anion channels per cell (N), the unitary current amplitude (i) and the absolute open probability at the end of the preceding voltage step (p) ($I = Nip$). Assuming that no change in the open probability occurs during the voltage step to the test potential and that the unitary conductance is independent from the prepulse potential, the normalized instantaneous test step current amplitude is proportional to the absolute open probability at the end of the prepulse and thus gives the voltage dependence of the so-called relative open probability. The voltage dependence of the relative open probabilities of WT and mutant channels can be well described by a Boltzmann function for all constructs and conditions (Fig. 8.7B and D). With NO_3^- on the external membrane site, both mutations shift the voltage dependence of inactivation to more negative potentials, in the presence as well as in the absence of glutamate. With internal NO_3^-, G464S shift the activation curve determined without glutamate to more negative voltages, leaving the voltage dependence of activation in the presence of glutamate unaffected. Q467S increases the minimum open probability, and shifts the voltage dependence of activation to more negative potential in the presence of glutamate. Without glutamate, the activation curve of Q467S EAAT4 anion channels has its

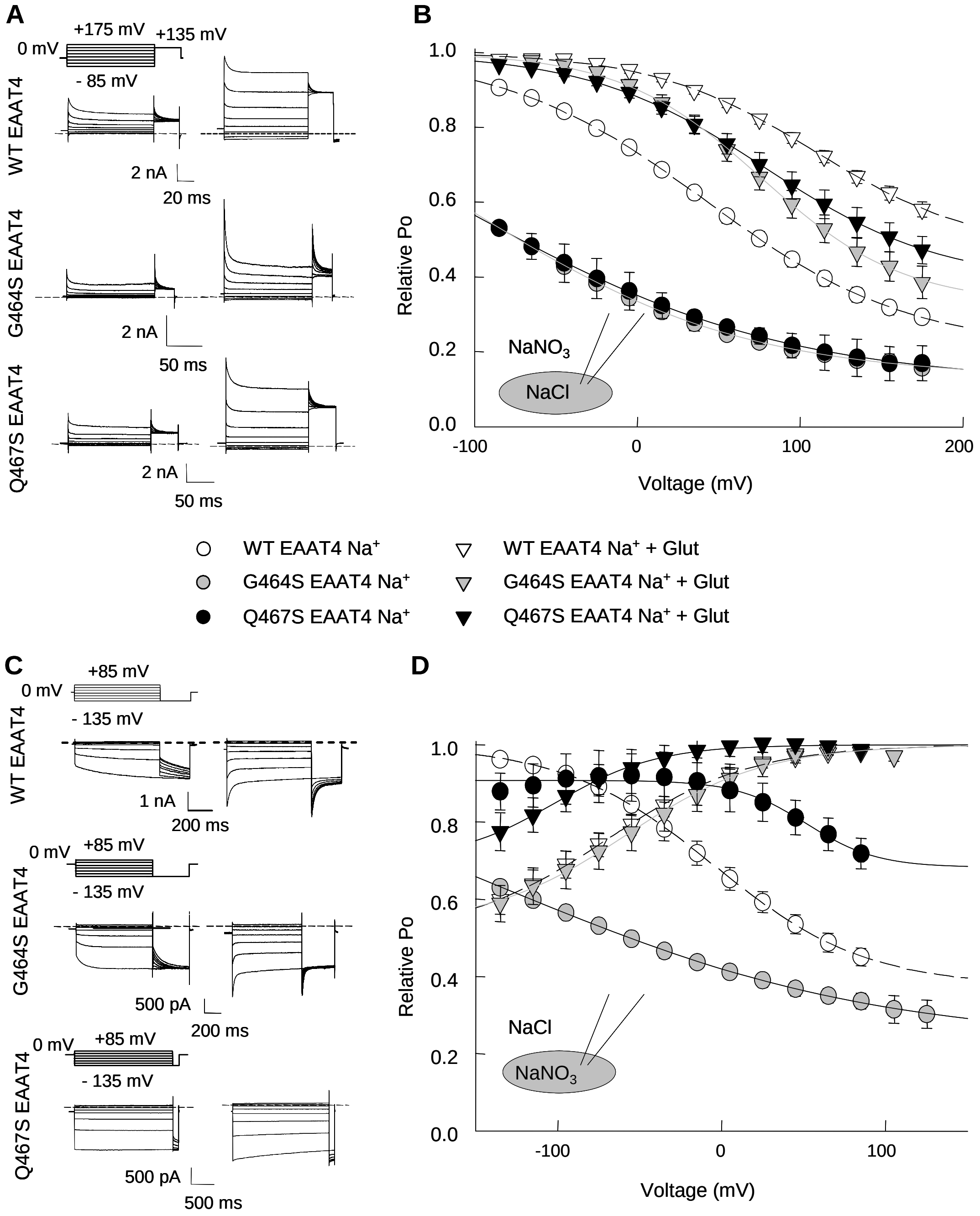
A
+175 mV
+135 mV
0 mV
- 85 mV
WT EAAT4
2 nA
20 ms
G464S EAAT4
2 nA
50 ms
Q467S EAAT4
2 nA
50 ms
B
Relative Po
Voltage (mV)
NaNO$_3$
NaCl
○ WT EAAT4 Na$^+$
▽ WT EAAT4 Na$^+$ + Glut
● G464S EAAT4 Na$^+$
▽ G464S EAAT4 Na$^+$ + Glut
● Q467S EAAT4 Na$^+$
▼ Q467S EAAT4 Na$^+$ + Glut
C
+85 mV
0 mV
- 135 mV
WT EAAT4
1 nA
200 ms
G464S EAAT4
500 pA
200 ms
Q467S EAAT4
500 pA
500 ms
D
Relative Po
Voltage (mV)
NaCl
NaNO$_3$

Figure 8.7. G464S and Q467S modify gating of EAAT4 anion channels. Representative current recordings for WT and mutant transporters for external (***A***) or internal NO_3^- (***C***). Recordings in the left column were done in the absence of glutamate and those in the right column after applying 0.5 mM L-glutamate. ***B***, ***D***, Voltage dependence of the relative open probability for WT, G464S and Q467S EAAT4 at the same anion conditions as in the corresponding left panel. Means ± SEM from at least 6 cells (***B***) and (***D***).

midpoint at more positive potentials than WT channels. Our results demonstrate that mutations affecting binding of Na^+ and glutamate modify voltage- and anion-dependent gating processes in EAAT4 anion channels.

8.4.4 Mixed heterotrimers of WT and mutant EAAT4 with altered substrate selectivity

The results presented so far indicate allosteric interactions between glutamate binding sites. Since each subunit is thought to function as independent glutamate transporter (Grewer et al., 2005; Koch and Larsson, 2005), our data support the concept of the three subunits cooperating in activating anion channels. This interpretation is in disagreement with a recent report by Grewer et al. (2005) who studied anion currents of mixed EAAT3 heterotrimers consisting of WT and a mutant with changed substrate selectivity (R446Q). In these experiments, the amplitudes of anion currents elicited at 0 mV by the mixture of two substrates were identical to the sum of the anion current amplitudes activated by the application of individual substrates. The authors concluded that each subunit forms an independently functioning anion conduction pathway.

To resolve this difference, we performed analogous experiments with EAAT4 (Fig. 8.8). We constructed a mutant EAAT4 plasmid that causes the substitution of arginine by cysteine at position 501 (corresponding to position 446 in rEAAT3). R501C EAAT4 expressed in tsA201 cells exhibit anion currents that are activated by serine, but not by glutamate (supplemental Fig. 8.9), in agreement with results on similar EAAT3 mutants (Bendahan et al., 2000). If individual subunits formed separate and independent anion channels, one would expect additive effects of serine and glutamate on anion currents in cells co-expressing WT and R501C EAAT4. Fig. 8.8 shows a representative recording and current voltage relationships from such an experiment. The cell was held at 0 mV, and current responses to voltages between – 155 mV and +165 mV were determined in the presence of 1mM serine, 1mM glutamate or both substrates, respectively. Fig. 8.8B gives the voltage dependences of the current amplitudes measured at these conditions, together with the voltage dependence of the sum of the glutamate- and serine-induced current amplitudes. In this experiment, serine and glutamate do not exert additive effects. A comparison of mean values from ten cells revealed that anion amplitudes in the presence of serine and glutamate were significantly smaller than the sum of the current amplitudes with only one substrate at all positive test potentials and at all potentials negative to -50 mV (Fig. 8.8C). Hence, our experiments do not support the notion of a functional independence of EAAT4 subunits in activating anion currents.

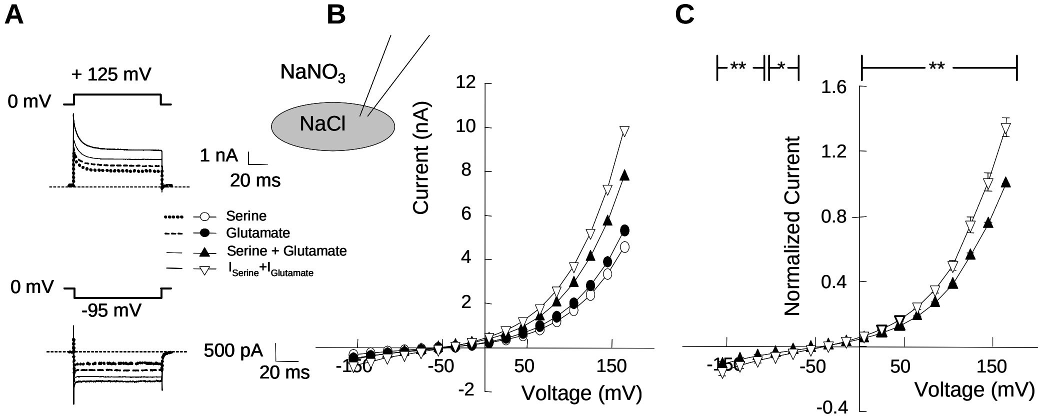

Figure 8.8. Mixed heterotrimers consisting of WT and R501C EAAT4 exhibit functional properties that are intermediate to WT and R501C homotrimers. A, Representative current responses to voltage steps to -95 mV and +125 mV, respectively, from a cell co-transfected with WT and R501C EAAT4 in the presence of 1 mM serine (dotted line), 1 mM glutamate (dashed line) and both together (solid line). The bold solid line gives the sum of the current amplitudes observed after application of individual substrates. **B**, Voltage-dependence of current amplitudes from the experiment shown in ***A***. **C**, Voltage dependence of normalized mean current amplitudes upon the application of both substrates (closed triangles) compared to the predicted value assuming independence of individual subunits forming an anion conduction pathway (open inverted triangles). Means ± SEM from 10 cells.

8.5 Discussion

All mammalian EAAT isoforms do not only sustain a secondary-active glutamate transport, but also a pore-mediated anion current. EAAT-associated anion currents were observed in native cells (Larsson et al., 1996) as well as in various heterologous expression systems (Wadiche et al., 1995; Wadiche and Kavanaugh, 1998; Watzke et al., 2001; Melzer et al., 2003), and ratios between coupled and uncoupled current amplitudes are largely independent of the expression levels and the expression system. Moreover, separate EAAT isoforms exhibit different anion selectivities (Melzer et al., 2003), and mutations in EAAT3 affect anion permeability ratios of the associated anion currents (Ryan et al., 2004). The EAAT protein itself is therefore thought to form the underlying anion-selective ion conduction pathway.

EAAT4 anion channels are active in absence of glutamate (Fig. 8.1), and extracellular glutamate increases anion current amplitudes with a sigmoidal concentration dependence. Fitting Hill equations to these concentration dependences result in Hill coefficients larger than 1 pointing towards the existence of more than one binding site and to a cooperativity between these multiple sites. Such as EAAT2 and EAAT3, EAAT4 appears to transport only one glutamate together with Na^+, K^+ and proton (Zerangue and Kavanaugh, 1996; Levy et al., 1998), indicating that each carrier domain exhibit only a single glutamate binding site. Assuming that each subunit transports glutamate by itself (Grewer et al., 2005; Koch and Larsson, 2005), the cooperativity in glutamate binding in activating the anion channel must result from interactions between multiple subunits. Two tested point mutations, G464S and Q467S, modify the steepness of the glutamate dependence of the anion current amplitude, although both are far away from the center of the protein and the corresponding residue in neighboring subunits (Fig. 8.5B). The effects of these amino acid substitutions thus indicate that conformational changes of one subunit are sensed by its neighbors. Despite the pronounced effects on EAAT4 anion channels, G464S and Q467S have no effect on glutamate transport (Fig. 8.5), in agreement with the notion that glutamate transport occurs without inter-subunit interactions (Grewer et al., 2005; Koch and Larsson, 2005).

Additional support for the idea of inter-subunit interactions in EAAT anion transport comes from the finding that, in mixed heterotrimers consisting of WT and mutant EAAT4 with modified substrate selectivity, WT and mutant subunits do not conduct anions independently (Fig. 8.8). Our results differ from those reported by Grewer et al. (2005) who performed similar experiments with the result that different substrates have additive effects on heterotrimers out of WT and mutant EAAT3. The reasons for this discrepancy are not clear. Isoform-specific differences between EAAT3 and EAAT4 are possible. Moreover, the trimeric structure of EAAT transporters results in four different population transporters in co-transfection experiments, and the functional properties of the heterotrimers are not known. Since EAAT4 anion current activation by substrate including substrate-, voltage- and anion-dependent gating processes is very complex, two substrates might have an additive effect on transporter currents under certain conditions in co-transfection experiments, although there are interactions between subunits. In contrast, every deviation from independence indicates that heterotrimeric transporters exhibit a novel substrate sensitivity, due to cooperative interactions between subunits. We conclude that, at least for EAAT4, glutamate binding sites cooperate in activating glutamate transporter-associated anion channels.

In contrast to our results, two earlier publications reported glutamate or aspartate dependences of EAAT4 currents that were well fit with a Hill coefficient of 1 (Lin et al. 1998, Mitrovic et al. 2001). While we determined the glutamate dependence of isolated anion currents, these experiments were performed in *Xenopus* oocytes under conditions that allow anion current as well as glutamate uptake current flow. Hence, an incomplete separation of these two current components is the most likely basis for the differences of the published and our results. *Xenopus* oocytes exhibt a $[Cl^-]_{int}$ of 30 mM (Cooper and Fong, 2001), resulting in an approximately fourfold lower unitary anion conductance of EAAT4 anion channels than under our conditions. The ratio of $I_{GluNaHK}$ /$I_{chloride(+glu)}$ will be therefore considerably larger than the value determined in dialyzed mammalian cells (0.4 at negative voltages at $[Cl^-]$ = 119 mM), and the uptake current amplitude will dominate the substrate dependence at this experimental condition. Alternatively, the cooperativity of the glutamate effect might be caused by the absence of K^+ in the intracellular solution and the use of NO_3^- or SCN^- as permeant anion. While no difference in the glutamate dependence of the anion current was observed between cells dialyzed with K^+-containing and K^+-free solution, we can currently not exclude that the use of Cl^- as only permeant anion in our experiments might have resulted in a less steep glutamate dependence.

The EAAT-associated anion channel has been conceived as a glutamate-gated channel with a tight coupling of channel opening and closing to conformational changes of the glutamate carrier domain (Larsson et al., 1996; Wadiche et al., 1995; Fairman et al., 1995; Billups et al., 1996; Arriza et al., 1997; Wadiche and Kavanaugh, 1998; Watzke et al., 2001). In this model, only certain carrier conformations are associated with conducting anion pores. During transitions through various conformational states of the glutamate carrier the anion channel is thought to cycle between conducting and non-conducting states. Recently, Ryan et al. (2004) demonstrated that many residues involved in anion selectivity are in close spatial proximity to regions presumed to play a role in substrate binding. The finding that engineered cysteines at these positions form intra- but not inter subunit disulfide bridges (Ryan et al., 2004) suggested that anion conduction pathways are formed by individual EAAT subunits that switch between glutamate transporting and anion conducting states.

The here reported interactions between neighboring subunits that occur during activation of the EAAT4 anion channel, but not during glutamate transport, argue against this model. Moreover, the anion- and voltage-dependence of EAAT4 anion currents, shown here and in an earlier report (Melzer et al., 2003), is inconsistent with a strict coupling of glutamate transport and anion channel activation. We did not see any decrease of the instantaneous or the steady state anion current amplitudes up to an external glutamate concentration of 2 mM (data not shown). Time- and voltage-dependent current relaxations are observed in the absence of glutamate as well as at all glutamate concentrations. These results demonstrate that the voltage-dependent relaxations of EAAT4 anion currents are not caused by voltage-dependent glutamate binding resulting in changed percentages of EAAT4 transporters binding glutamate, but rather by a voltage-dependent gating process.

Inversion of the anion gradient across the membrane changes gating of EAAT4 anion channels (Fig. 8.1), but does not modify binding of Na^+ and glutamate (Fig. 8.2 and 8.3). Hence, there must exist conformational changes of the anion channel that are not related to transitions between separate carrier states. EAAT4 anion channels can open and close in the absence of conformational changes of the glutamate carrier. The dependence of the anion distribution on the EAAT4 current relaxation is much more pronounced than for other channels (Marchais and Marty, 1979; Pusch et al., 1995; Chen and Miller, 1996). While the channels´ open probability increase with more positive potentials in the presence of internal NO_3^- and external glutamate (Fig. 8.1C), in all other tested conditions channels deactivate upon depolarization (Fig. 8.1A) or activate upon hyperpolarization (Fig. 8.1C). One mutation, Q467S, alters the time course of anion currents in cells intracellularly dialyzed with the more permeant anion, but affect channel gating only minimally under the inverse anion gradient (Fig. 8.7). A possible explanation for all these finding is that EAAT4 anion channels are gated by permeant anions from both sites of the membrane. Glutamate and two mutations close to the glutamate binding pocket might alter EAAT anion channel gating via modification of binding and translocation of permeant anions (Melzer et al., 2003). By such a mechanism, EAAT4 anion channel gating, albeit not tightly coupled to transition within the carrier, is affected by conformational changes of the carrier.

Since glutamate is co-transported with multiple sodium ions (Zerangue and Kavanaugh, 1996; Levy et al., 1998), the observed sigmoidicity of the Na^+-dependence of the EAAT4 anion currents (Fig. 8.2) could be explained by an interaction between Na^+ binding steps within a single subunit (Watzke et al., 2001). However, the clear alterations of the sodium-dependence of EAAT4 anion currents by the two tested mutations (Fig. 8.6B), together with the absent changes of coupled glutamate transport in G464S and Q467S EAAT4 transporters (Fig. 8.5C and D) suggest that inter-subunit interactions also play a role in the sodium dependence of anion currents. Such intersubunit interactions also account for the observed modification of sodium and glutamate binding by the concentration of the other substrate (Fig. 8.4).

In conclusion, our data demonstrate that the three subunits of EAAT4 transporters cooperate in activating anion channels, and individually mediate coupled glutamate transport. The results indicate that more than one subunit contribute to the formation of the EAAT-associated anion pore. They illustrate the importance of multimerization of this class of transporters and provide a likely explanation as to how a single protein can perform two mechanically distinct transport processes simultaneously.

Acknowledgements

We would like to thank Dr. J. Rothstein for providing the expression construct for rEAAT4, Dr. Patricia Hidalgo, Nico Melzer and Doreen Nothmann for helpful discussions, and Barbara Poser for excellent technical assistance. These studies were supported by the Deutsche Forschungsgemeinschaft (FOR450) to Ch.F.

8.6 References

Amara SG, Fontana AC (2002) Excitatory amino acid transporters: keeping up with glutamate. Neurochem Int 41: 313-318.

Arriza JL, Eliasof S, Kavanaugh MP, Amara SG (1997) Excitatory amino acid transporter 5, a retinal glutamate transporter coupled to a chloride conductance. Proc Natl Acad Sci USA 94: 4155-4160.

Bendahan A, Armon A, Madani N, Kavanaugh MP, Kanner BI (2000) Arginine 447 plays a pivotal role in substrate interactions in a neuronal glutamate transporter. J Biol Chem 275: 37436-37442.

Bergles DE, Tzingounis AV, Jahr CE (2002) Comparison of coupled and uncoupled currents during glutamate uptake by GLT-1 transporters. J Neurosci 22: 10153-10162.

Billups B, Rossi D, Attwell D (1996) Anion conductance behavior of the glutamate uptake carrier in salamander retinal glial cells. J Neurosci 16: 6722-6731.

Chen TY, Miller C (1996) Nonequilibrium gating and voltage dependence of the ClC-0 Cl^- channel. J Gen Physiol 108: 237-250.

Cooper GJ, fong P. (2003) Relationship between intracellular pH and chloride in Xenopus oocytes expressing the chloride channel ClC-0. Am J Physiol Cell Physiol. 284: C331-C228.

Eskandari S, Kreman M, Kavanaugh MP, Wright EM, Zampighi GA (2000) Pentameric assembly of a neuronal glutamate transporter. Proc Natl Acad Sci USA 97: 8641-8646.

Fairman WA, Vandenberg RJ, Arriza JL, Kavanaugh MP, Amara SG (1995) An excitatory amino-acid transporter with properties of a ligand-gated chloride channel. Nature 375: 599-603.

Gendreau S, Voswinkel S, Torres-Salazar D, Lang N, Heidtmann H, Detro-Dassen S, Schmalzing G, Hidalgo P, Fahlke Ch (2004) A trimeric quaternary structure is conserved in bacterial and human glutamate transporters. J Biol Chem 279: 39505-39512.

Grewer C, Balani P, Weidenfeller C, Bartusel T, Tao Z, Rauen T (2005) Individual subunits of the glutamate transporter EAAC1 homotrimer function independently of each other. Biochemistry 44: 11913 – 11923.

Haugeto O, Ullensvang K, Levy LM, Chaudhry FA, Honore T, Nielsen M, Lehre KP, Danbolt NC (1996) Brain glutamate transporter proteins form homomultimers. J Biol Chem 271: 27715-27722.

Hodgkin AL, Katz B (1949) The effect of sodium ions on the electrical activity of the giant squid axon. J Physiol (Lond) 108: 37-77.

Koch HP, Larsson HP (2005) Small-scale molecular motions accomplish glutamate uptake in human glutamate transporters. J Neurosci 25: 1730-1736.

Larsson HP, Picaud SA, Werblin FS, Lecar H (1996) Noise analysis of the glutamate-activated current in photoreceptors. Biophys J 70: 733-742.

Levy LM, Warr O, Attwell D (1998b) Stoichiometry of the glial glutamate transporter GLT-1 expressed inducibly in a Chinese hamster ovary cell line selected for low endogenous Na^+-dependent glutamate uptake. J Neurosci 18: 9620-9628.

Liman ER, Tytgat J, Hess P (1992) Subunit stoichiometry of a mammalian K^+ channel determined by construction of multimeric cDNAs. Neuron 9: 861-871.

Lin CL, Tzingounis AV, Jin L, Furuta A, Kavanaugh MP, Rothstein JD. (1998) Molecular cloning and expression of the rat EAAT4 glutamate transporter subtype. Brain Res Mol Brain Res 63:174-179.

Marchais D, Marty A (1979) Interaction of permeant ions with channels activated by acetylcholine in Aplysia neurones. J Physiol (London) 297: 9-45.

Melzer N, Biela A, Fahlke Ch (2003) Glutamate modifies ion conduction and voltage-dependent gating of excitatory amino acid transporter-associated anion channels. J Biol Chem 278: 50112-50119.

Melzer N, Torres-Salazar D, Fahlke Ch (2005). A dynamic switch between inhibitory and excitatory currents in a neuronal glutamate transporter. Proc Natl Acad Sci USA 102: 19215 – 19218.

Mitrovic AD, Plesko F, Vandenberg RJ (2001). Zn^{2+} inhibits the anion conductance of the glutamate transporter EAAT4. J Biol Chem 276: 26071-26076.

Neely A, Garcia-Olivares J, Voswinkel S, Horstkott H, Hidalgo P (2004) Folding of active calcium channel ß1b-subunit by size-exclusion chromatography and its role on channel function. J Biol Chem 279: 21689-21694.

Pusch M, Ludewig U, Rehfeldt A, Jentsch TJ (1995) Gating of the voltage-dependent chloride channel ClC-0 by the permeant anion. Nature 373: 527-530.

Ryan RM, Mitrovic AD, Vandenberg RJ (2004) The chloride permeation pathway of a glutamate transporter and its proximity to the glutamate translocation pathway. J Biol Chem 279: 20742-20751.

Shimamoto K, Lebrun B, Yasuda-Kamatani Y, Sakaitani M, Shigeri Y, Yumoto N, Nakajima T (1998) DL-threo-beta-benzyloxyaspartate, a potent blocker of excitatory amino acid transporters. Mol Pharmacol 53(2): 195-201.

Wadiche JI, Amara SG, Kavanaugh MP (1995) Ion fluxes associated with excitatory amino acid transport. Neuron 15: 721-728.

Wadiche JI, Kavanaugh MP (1998) Macroscopic and microscopic properties of a cloned glutamate transporter/chloride channel. J Neurosci 18: 7650-7661.

Watzke N, Bamberg E, Grewer C (2001) Early intermediates in the transport cycle of the neuronal excitatory amino acid carrier EAAC1. J Gen Physiol 117: 547-562.

Yernool D, Boudker O, Jin Y, Gouaux E (2004) Structure of a glutamate transporter homologue from Pyrococcus horikoshii. Nature 431: 811-818.

Zerangue N, Kavanaugh MP (1996) Flux coupling in a neuronal glutamate transporter. Nature 383: 634-637.

Zhang Y, Kanner BI (1999) Two serine residues of the glutamate transporter GLT-1 are crucial for coupling the fluxes of sodium and the neurotransmitter. Proc Natl Acad Sci USA 96: 1710-1715.

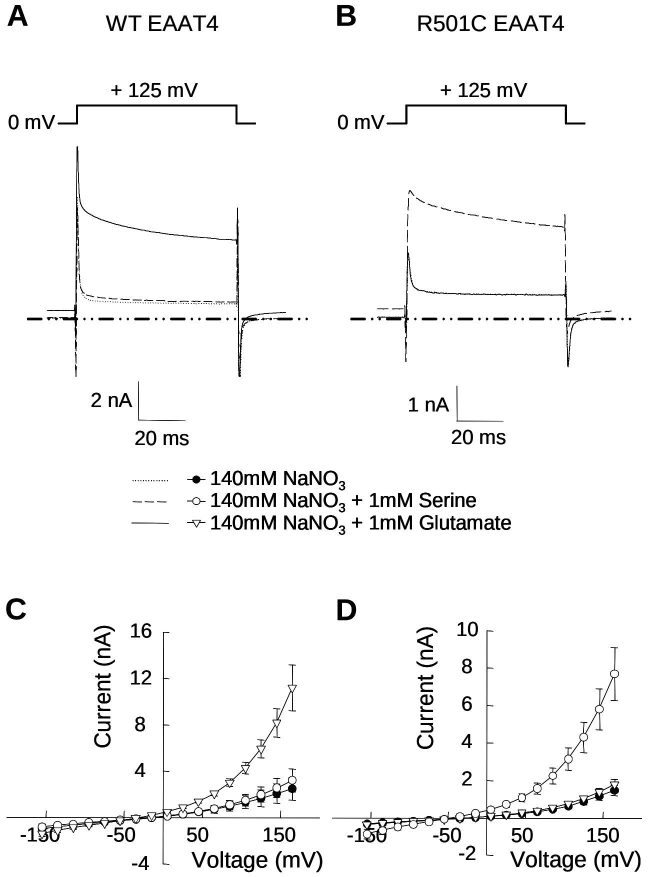

Suplementary Figure 8.9. R501C changes the substrate sensitivity of EAAT4. *A,B*, Representative current responses to a voltage steps to +125 mV from cells transfected with WT (***A***) and R501C (***B***) EAAT4 without application of substrate (dotted line), in the presence of 1 mM serine (dashed line) and 1 mM glutamate (solid line), respectively. ***C**, **D***, Voltage dependence of mean current amplitudes ± SEM (n = 5;***C*** and 6;***D***) upon the application of serine (○), glutamate (▿) and without any of these two substrates (●). WT current amplitudes at 1 mM serine and R501C current amplitudes at 1 mM glutamate were not different from control values without substrate ($p>0.05$ for WT and $p>0.1$ for R501C EAAT4, respectively).

9. Neuronal glutamate transporters vary in substrate transport rate, but not in unitary anion channel conductance

Delany Torres-Salazar[1], Christoph Fahlke[1,2]

[1]Abteilung Neurophysiologie, Medizinische Hochschule Hannover, Germany; [2]Zentrum für Systemische Neurowissenschaften Hannover (ZSN), Germany

Corresponding author: Christoph Fahlke, Abteilung Neurophysiologie, Medizinische Hochschule Hannover, Carl-Neuberg-Str. 1 , D - 30625 Hannover, Tel +49 511 532 2777, Fax +49 511 532 2776, Email: fahlke.christoph@mh-hannover.de

Running title: EAAT3- and EAAT4-associated anion channels

J Biol Chem. **2007 Vol. 282, No 48: 34719-26**

9.1 Abstract

Excitatory amino acid transporters (EAATs) not only sustain a secondary-active glutamate transport, but also function as anion-selective ion channels. The relative proportion of currents generated by glutamate transport or by the chloride conductance varies for each cloned EAAT subtype. For EAAT1, EAAT2, and EAAT3, the anion current is only a small component of the total transporter-associated current amplitude, whereas EAAT4 and EAAT5 transporters mediate predominantly anion currents. We here demonstrate that the distinct current proportions are entirely due to differences in glutamate transport rates. EAAT3 and EAAT4 differ in unitary glutamate transport rates as well as in the voltage- and substrate-dependence of anion channel opening, but ion conduction properties are very similar. Noise analysis revealed identical unitary current amplitudes and similar absolute open probabilities for the two anion channels. The low glutamate transport rate of EAAT4 allows regulation of cellular excitability without interfering with extracellular glutamate homeostasis and makes this EAAT isoform ideally suited to regulate excitability in dendritic spines of Purkinje neurons.

9.2 Introduction

Glutamate is the major excitatory neurotransmitter in the mammalian central nervous system. After the release from glutamatergic nerve terminals, glial and neuronal EAAT glutamate transporters remove glutamate from the synaptic cleft to ensure low resting glutamate levels and to prevent neuronal damage by excessive glutamate receptor activation. EAATs mediate two different transport processes, they are secondary-active glutamate transporters and anion-selective channels (1). Different EAAT isoforms differ in the relative contribution of anion currents to the total transporter-mediated current (2-5). These differences have been interpreted as an indication that some EAATs play a physiological role as glutamate transporters and others as glutamate-gated anion channels involved in the regulation of cellular excitability.

To obtain a better understanding of the functional basis of these differences, we compared the functional properties of two neuronal EAAT isoforms, EAAT3 and EAAT4. EAAT3 displays only modest anion currents in heterologous expression systems (3), while EAAT4 anion currents greatly exceed electrogenic transport currents (2). Here we demonstrate that the unitary current amplitudes and the absolute open probabilities of EAAT3 and EAAT4 are very similar. EAAT3 and EAAT4 anion channels differ in anion channel gating and glutamate dependence of the anion channel activation – two features that might be explained by a variable interaction between individual subunits of the multimeric transporter protein.

9.3 Experimental Procedures

9.3.1 Heterologous expression and functional characterization of EAAT3 and EAAT4

The coding region of hEAAT3 (GenBank^{TM} accession number NP_004161) was excised from pTLN2-hEAAT3 ((6), provided by Dr. Matthias A. Hediger, University of Bern, Switzerland) and subcloned into pcDNA3.1 (Invitrogen, Karlsruhe, Germany). The pcDNA3.1-rEAAT4 construct (GenBank^{TM} accession number NM_114454) was provided by Dr. J. Rothstein, Johns Hopkins University, Baltimore, MD, USA. Point mutations were introduced into the WT hEAAT3 cDNAs using the QuikChange mutagenesis kit (Stratagene). For each construct, two independent recombinants from the same transformation were examined and shown to exhibit indistinguishable functional properties. Transient transfection of tsA201 cells were performed as previously described (5). In some of the experiments, a stable inducible cell line was used (7), generated by selecting Flp-In-T-Rex cells (Invitrogen, Karlsruhe, Germany) after transfection with pcDNA5-FRT-To-rEAAT4.

Capped cRNA was synthesized from MluI-linearized pTLN2-hEAAT3 (6) and from NheI-linearized pGEMHE-rEAAT4 (8) templates through use of MESSAGE machine kits (Ambion, Austin, TX). Injection and handling of oocytes were performed as described elsewhere (9). Oocytes expressing EAAT3 were usually measured 1 day after injection. To account for differences in expression levels, this period was increased to 4 to 5 days for EAAT4.

9.3.2 Electrophysiology

Standard whole-cell patch clamp recordings were performed using an Axopatch 200B (Axon Instruments, Union City, CA, USA) amplifier as described (5;8). Cells were clamped to 0 mV for at least 10 s between test sweeps. In experiments measuring EAAT-associated noise, pipettes were covered with dental wax to reduce their capacitance. Standard solutions contained (in mM): 140 NaSCN (standard NaSCN-based external solution) or NaCl (standard NaCl-based external solution), 4 KCl, 2 $CaCl_2$, 1 $MgCl_2$, 5 HEPES, pH 7.4, intracellular (in mM) 115 NaCl (standard NaCl-based internal solution) or NaSCN (standard NaSCN-based external solution), 2 $MgCl_2$, 5 EGTA, 10 HEPES, pH 7.4. For the concentration dependences of glutamate (Fig. 9.5), a given concentration of L-glutamate was added to the external solution.

In ooctyes, glutamate transporter-associated currents were recorded by two-electrode voltage clamp using a CA1 amplifier (Dagan, Minneapolis, MN, USA). Prior to electrophysiological testing, oocytes were incubated for at least 5 h in a gluconate-based solution containing (in mM): 96 Nagluconate, 4 KCl, 0.3 $CaCl_2$, 1 $MgCl_2$, 5 HEPES, pH 7.4. Voltage-clamp experiments were started in a gluconate-based external solution. Oocytes were held at 0 mV, and currents elicited by 200 ms voltage steps between –120 mV and +60 mV were filtered at 2kHz (-3dB) and digitalized with a sampling rate of 10 kHz using a Digidata AD/DA converter (Axon Instruments, Union City, CA, USA). Glutamate uptake currents were measured by subtracting current amplitudes in a gluconate-based glutamate-free solution from values in an external solution supplemented with 500 µM L-glutamate. Anion currents were determined after exchanging the external solution to (in mM): 96 NaSCN, 4 KCl, 0.3 $CaCl_2$, 1 $MgCl_2$, 5 HEPES, pH 7.4 in the absence or in the presence of 500 µM external glutamate without any current subtraction procedure.

9.3.3 Data analysis

The data was analyzed with a combination of the pClamp9 (Axon Instruments) and SigmaPlot (Jandel Scientific, San Rafael, CA, USA) programs. Current amplitudes were used without applying a subtraction procedure. Current-voltage relationships at various substrate concentrations were constructed by plotting isochronal current amplitudes determined 1 ms after the voltage step versus the membrane potential. Voltage dependences of the relative open probability (Fig. 9.1 and 9.2) were determined by plotting the normalized isochronal current amplitude at +135 mV or –135 mV after 0.2 s prepulses to different voltages versus the preceding potential. Activation curves obtained in this manner were then fit with a single Boltzmann term plus a voltage-independent value ($I(V) = Amp/(1 + e^{(V - V0.5)/kV}) + P_{min}$) (Supplemental Table 9.1). Permeability ratios were calculated from reversal potential measurements using the Goldman-Hodgkin-Katz (GHK) equation (10) as described elsewhere (5) (Supplemental Fig. 9.6). Isochronal anion current amplitudes were measured at various concentrations at a given test potential, in order to obtain the concentration dependence of anion channel activation by glutamate. The substrate dependences thus obtained were normalized to the maximum current amplitude ($I_{max} + I_o$), averaged after normalization and fit with the Hill equation ($I = \frac{I_{max}[substrate]^n}{[substrate]^n + K_D{}^n} + I_o$). The Hill coefficients (n) were determined as a fit parameter. For each membrane potential, apparent dissociation constants (K_Ds) were determined on several cells and averaged. The Student's t-test was used for statistical evaluation. For comparisons between EAAT3 and EAAT4, EAAT3- and EAAT4-expressing cells and oocytes with comparable anion current amplitudes were used.

9.3.4 Noise analysis

The current variance (σ_{ss}^2) and the mean current amplitude (I_{ss}) were determined during the last 50 ms of a 500 ms test step to voltages between -175 mV and +65 mV. Changing the amount of data subjected to analysis (from 10 ms to 70 ms) did not significantly alter the variance. Current traces were sampled at 5 kHz and filtered using a Bessel low pass filter with a cut-off frequency of 1 kHz. For all experiments, the analysis was repeated after digital filtering with a Butterworth filter at 0.5 kHz, yielding similar results. The variance at the current reversal potential was subtracted as background noise.

Lorentzian noise depends on the number of channels (N), the unitary current amplitude (i), and the absolute open probability (p):

$$\sigma^2 = Ni^2 p(1-p) + \sigma_0^2$$

with σ_o^2 being the background noise. Dividing the variance (σ_{ss}^2) by the mean current amplitude (I_{ss}= Npi), after subtraction of the background noise, results in:

$$\frac{\sigma_{ss}^2 - \sigma_0^2}{I_{ss}} = i(1-p)$$

In order to determine the unitary current amplitudes and the absolute open probabilities of EAAT3 and EAAT4, we employed a variation of stationary variance analysis (11;12). EAAT3 and EAAT4 anion channels display a voltage-dependent rectification of the unitary current amplitude (Fig. 9.1). To account for this voltage-dependent conductance, the instantaneous current amplitude was measured by extrapolating the current amplitude back to the moment of the voltage jump; this extrapolation was done by fitting a biexponential function to the time dependence of the current relaxation. The instantaneous current is proportional to the unitary current amplitude (I_{inst} = const*i) so that dividing both sides of the equation by the instantaneous current amplitude results in:

$$\frac{\sigma_{ss}^2 - \sigma_0^2}{I_{ss}} = i(1-p) = i - \frac{I_{ss}}{N}$$

$$\frac{\sigma_{ss}^2 - \sigma_0^2}{I_{ss} I_{inst}} = \frac{i}{I_{inst}} - \frac{I_{ss}}{I_{inst} N} = \frac{1}{const} - \frac{I_{ss}}{I_{inst} N}$$

Plotting the variance divided by the product of the mean and the instantaneous current amplitudes ($\frac{\sigma^2 - \sigma_0^2}{I_{ss} I_{inst}}$) versus the ratio of the mean current amplitude by the instantaneous current amplitude ($\frac{I_{ss}}{I_{inst}}$) results in a linear relationship (Fig. 9.3). Multiplication of the y-axis intercept (1/const) of the fitted straight with instantaneous current amplitudes provides the unitary current amplitudes, whereas the slope, -1/N, gives the number of channels.

This analysis was only possible in the presence of glutamate, as the open probability changed only a little with voltage in the absence of glutamate (Fig. 9.1 and 9.2). We therefore measured first the number of channels in the presence of glutamate and used this value to obtain the unitary current amplitude from the current variance and the mean steady-state current amplitude measured at the same cells without glutamate:

$$i = \frac{\sigma^2 - {\sigma_0}^2}{I_{ststate}} + \frac{I_{ststate}}{N}$$

9.4 Results

9.4.1 Voltage-dependent gating of EAAT3- and EAAT4-associated anion currents

We expressed hEAAT3 and rEAAT4 glutamate transporters heterologously in tsA201 cells and measured currents through whole-cell patch clamp experiments. Electrogenic glutamate uptake was abolished by dialyzing cells with a K^+ free internal solution. Using Cl^- or NO_3^- as main permeant anions, EAAT3-associated anion currents were quite small, and we therefore used SCN^- (3;5) as the main anion on one membrane side and Cl^- on the other. Under these conditions, whole-cell currents in cells expressing EAAT3 and EAAT4 were significantly larger than those in untransfected tsA201 cells, in the absence as well as in the presence of glutamate (Fig. 9.1). Complete substitution of anions with gluconate$^-$ resulted in negligible current amplitudes (at +165 mV: 0.2 ± 0.04 nA (n = 5) after substitution of internal and external anions with gluconate in the presence of 500 µM L-glutamate). Moreover, application of 200 µM L-threo-β-benzyloxyaspartate (L-TBOA) (13), reduced the current amplitudes to values close to background levels (Fig. 9.1). These results demonstrate that, under our experimental conditions, EAAT3 and EAAT4 whole-cell currents predominantly represent transporter-associated anion currents (5;7;8).

Both transporter isoforms conduct anions in the absence of glutamate. Application of glutamate increases the amplitudes and changes the time- and voltage-dependence of anion currents (Fig. 9.1 and 9.2). With SCN^- on the internal membrane side, glutamate augments EAAT3 and EAAT4 anion current amplitudes to a similar extent (Fig. 9.1*B* and *E*). With the anion distribution reversed, increases of glutamate-induced current amplitudes were much smaller for EAAT3 than for EAAT4 (Fig. 9.2*B* and *E*). EAAT anion channels exhibit time- and voltage-dependent current relaxations upon voltage steps. Under all tested conditions, the anion currents of both the EAAT3 and EAAT4 isoforms rise instantaneously upon voltage-

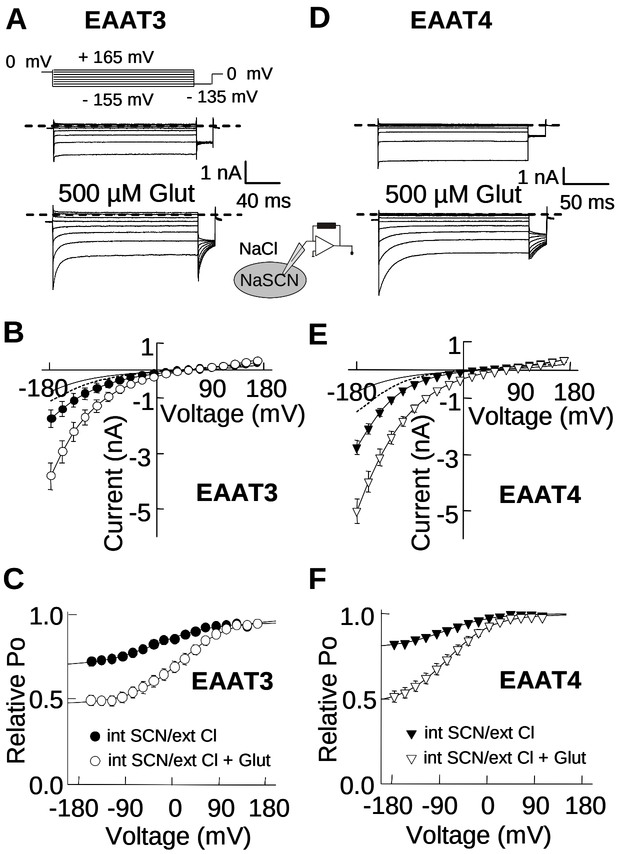
A
EAAT3
0 mV
+ 165 mV
0 mV
- 155 mV
- 135 mV
1 nA
40 ms
500 µM Glut
NaCl
NaSCN
D
EAAT4
1 nA
50 ms
500 µM Glut
B
1
-180
90
180
-1
Voltage (mV)
-3
-5
Current (nA)
EAAT3
E
1
-180
90
180
-1
Voltage (mV)
-3
-5
Current (nA)
EAAT4
C
1.0
0.5
0.0
Relative Po
EAAT3
● int SCN/ext Cl
○ int SCN/ext Cl + Glut
-180 -90 0 90 180
Voltage (mV)
F
1.0
0.5
0.0
Relative Po
EAAT4
▼ int SCN/ext Cl
▽ int SCN/ext Cl + Glut
-180 -90 0 90 180
Voltage (mV)

Figure 9.1. Voltage– and substrate-dependence of EAAT3- and EAAT4-associated anion currents in cells dialyzed with SCN^-- based solutions. (*A,D*) Representative current recordings from cells expressing EAAT3 (*A*) or EAAT4 (*D*). (*B,E*) Mean isochronal current-voltage relationships for EAAT3 (*B*) and EAAT4 *(E*). Experiments were performed in the absence (closed symbols, n = 4 and n = 9, respectively) and the presence (open symbols, n = 4 and n = 9, respectively) of 500 µM L-glutamate. Solid lines represent current-voltage relationships determined with untransfected tsA201 cells in the presence of 500 µM L-glutamate at the same anion distribution (n = 3); dashed lines gives amplitudes from transfected cells after addition of 200 µM TBOA (n =3 for each). (*C,F*) Voltage dependence of the relative open probabilities of EAAT3 or EAAT4 anion channels in the absence (closed symbols (n = 5) and the presence (open symbols n = 7 for EAAT3; n = 8 for EAAT4) of 500 µM L-glutamate.

steps to negative and positive potentials (Fig. 9.1 and 9.2). This instantaneous rise was followed by isoform-specific and anion-dependent current relaxations. With SCN^- being the main internal anion, voltage-dependent gating of EAAT3 and EAAT4 anion channels is very similar. The instantaneous rise at negative voltages was followed by a time- and voltage-dependent current decay, and this time-dependent decay was more pronounced in the presence than in the absence of glutamate (Fig. 9.1*A* and *D*). The gating of EAAT3 and EAAT4 anion channels was completely different when studied with external SCN^- and internal Cl^- (Fig. 9.2*A* and *D*). With this anion distribution, there is a fast time-dependent and voltage-dependent deactivation of EAAT4 currents at positive voltages, while EAAT3 shows a depolarisation-induced activation in the absence or presence of glutamate. The depolarisation-induced relative current increase of EAAT3 was augmented by glutamate, whereas current deactivation of EAAT4 was less pronounced in the presence of glutamate than in its absence. Voltage dependences of relative open probabilities were determined by plotting normalized isochronal current amplitudes at a fixed test step *versus* the preceding potential (Figs. 9.1*C* and *F*, 9.2*C* and *F*). These activation curves can be described well by Boltzmann functions for both isoforms and both ionic conditions (Supplemental Table 9.1). The activation curves of EAAT3 and EAAT4 are similar for SCN_{int}/Cl_{ext}, but there are prominent isoform-specific gating differences at the reverse anion distribution.

9.4.2 Permeation properties of EAAT3 and EAAT4 anion channels

For both isoforms, currents are inwardly rectifying in cells internally dialyzed with the more permeant anion SCN^-, but outwardly rectifying with SCN^- in the external membrane site (Fig. 9.1 and 9.2). Reversal potentials enable a calculation of the relative permeabilities using the Goldman-Hodgkin-Katz equation. In the absence of glutamate, the SCN^- over Cl^- permeability coefficients are identical for EAAT3 and EAAT4. Application of glutamate

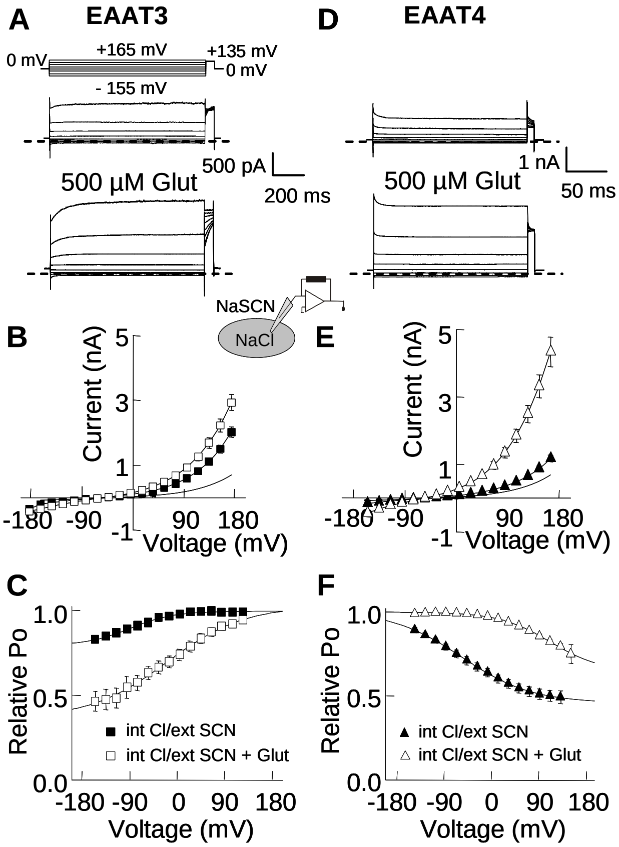
A
EAAT3
0 mV
+165 mV
+135 mV
0 mV
- 155 mV
500 pA
200 ms
500 µM Glut
D
EAAT4
1 nA
50 ms
500 µM Glut
NaSCN
NaCl
B
Current (nA)
5
3
1
-1
-180 -90
90 180
Voltage (mV)
E
Current (nA)
5
3
1
-1
-180 -90
90 180
Voltage (mV)
C
Relative Po
1.0
0.5
0.0
■ int Cl/ext SCN
□ int Cl/ext SCN + Glut
-180 -90 0 90 180
Voltage (mV)
F
Relative Po
1.0
0.5
0.0
▲ int Cl/ext SCN
△ int Cl/ext SCN + Glut
-180 -90 0 90 180
Voltage (mV)

Figure 9.2. Voltage- and substrate-dependence of EAAT3- and EAAT4-associated anion currents in cells dialyzed with Cl$^-$- based solutions. (*A,D*) Representative current recordings from cells expressing EAAT3 (*A*) or EAAT4 (*D*). (*B,E*) Mean isochronal current-voltage relationships for EAAT3 (*B*) and EAAT4 *(E*). Experiments were performed in the absence (closed symbols, n = 12 and n = 6, respectively) and the presence (open symbols, n = 12 and n = 6, respectively) of 500 µM L-glutamate. Solid lines represent current-voltage relationships determined with untransfected tsA201 cells in the presence of 500 µM L-glutamate at the corresponding anion distribution (n=3). (*C,F*) Voltage dependence of the relative open probabilities of EAAT3 and EAAT4 anion channels in the absence (closed symbols, n = 3 for EAAT3; n = 5 for EAAT4) and the presence (open symbols, n = 9 for EAAT3; n = 7 for EAAT4) of 500 µM L-glutamate.

changes the anion selectivity of EAAT anion channels (5). It causes an increased relative permeability of internal SCN^- for EAAT3 and for EAAT4. However, for external SCN^-, glutamate results in a decreased P_{SCN}/P_{Cl} ($p < 0.05$) of EAAT4, but leaves the reversal potential of EAAT3 currents unaffected (Supplemental Fig. 9.6).

In order to study unitary anion channel properties, we performed noise analysis (Fig. 9.3). Variance analysis of whole-cell currents can be used to study EAAT3 and EAAT4 anion channels for the following reasons. Current variances are larger in cells expressing EAAT3 or EAAT4 than in untransfected cells (7). Application of glutamate and changes of the membrane potential changes the current variance, and blocking EAAT-associated anion currents reduce the current variance (data not shown). Glutamate-induced increases of anion current amplitudes are associated with reduced current variances (data not shown), demonstrating that the measured current variance is not thermal noise associated with the recording pipettes, shunt resistances, membrane impedances, or electrical circuits but instead is Lorentzian noise associated with gating of EAAT-associated channels.

Mean current amplitudes (I) and current variances (σ^2) were determined in the last 50 ms of 500 ms test steps to various voltages (Fig. 9.3*A* and *E*). Current variance was analyzed in two ways. First, the ratio of current variance by mean current amplitude was calculated for both anion conditions and in the presence and absence of glutamate. For channel-mediated currents, this ratio is equal to the product of the single channel amplitude (i) and the fraction of time spent in a closed state (1-p, with p being the absolute open probability) ($\sigma^2/I=i(1-p)$). EAAT3 and EAAT4 did not differ in this value (for SCN_{int}/Cl_{ext} at -135 mV: 40.5 ± 16 fA for EAAT3, $n = 3$; and 49.8 ± 11 fA for EAAT4, $n = 4$, $p = 0.6$; for Cl_{int}/SCN_{ext} at + 65 mV: 4.0 ± 0.8 fA for EAAT3, $n = 6$; and 4.6 ± 0.8 fA for EAAT4 $n = 4$, $p = 0.1$). To determine the unitary current amplitude and the absolute open probability separately, we performed a

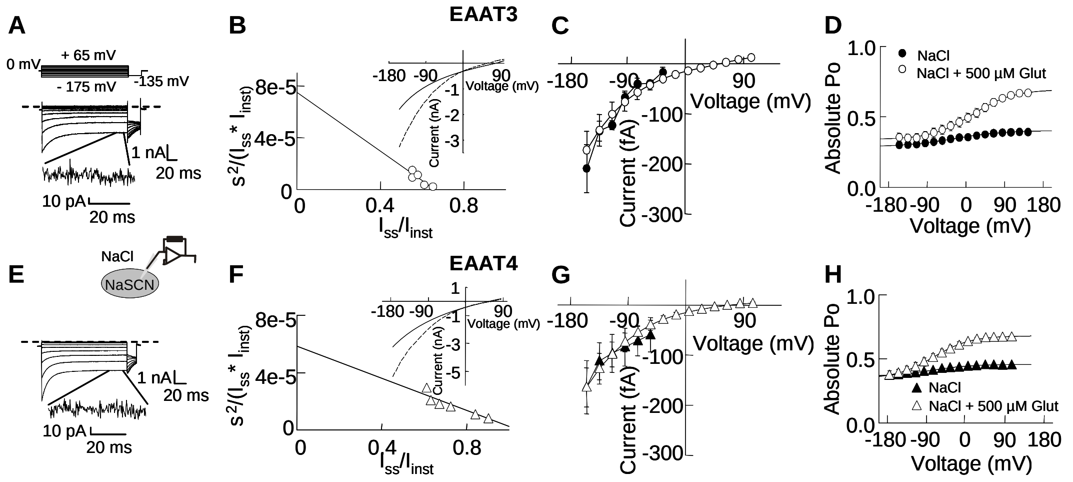

Figure 9.3. Unitary current amplitudes and absolute open probabilities of EAAT3 and EAAT4 anion channels. (*A,E*) Pulse protocols and whole-cell current traces from whole-cell recordings on tsA201 cells expressing EAAT3 (*A*) and EAAT4 (*E*) with SCN$^-$ at the internal, and Cl$^-$ at the external membrane site. Insets give a magnification of the time dependence of the steady-state currents, demonstrating the statistical variation of the current amplitude. (*B,F)* Plot of the current variance, normalized by the product of the instantaneous (I_{inst}) and the late (I_{ss}) current amplitude versus the ratio of I_{ss} to I_{inst}. Voltage dependences of instantaneous (dashed lines) and steady-state (solid lines) currents are given as insets. (*C-H*) Voltage dependence of the mean single-channel current amplitudes (*C,G*) and the absolute open probabilities (*D,H*) of EAAT3 and EAAT4. Open symbols denote measurements in the presence of 500 µM L-glutamate (n = 3 for EAAT3; n = 5 for EAAT4), closed symbols in the absence (n = 3 for EAAT3; n = 5 for EAAT4).

variant of stationary noise analysis (11;12). The variance divided by the product of the mean and the instantaneous current amplitudes was plotted against the ratio of the mean current amplitude by the instantaneous current amplitude. In case of Lorentzian noise, this relationship is expected to be linear, with the slope ($-\frac{1}{N}$) giving the number of channels N and the y-axis intercept providing the ratio between unitary current amplitude and instantaneous current amplitude. We performed such an analysis only at SCN_{int}/Cl_{ext} in the presence of glutamate (Figs. 9.3*B* and *F*), since the open probabilities change only little with voltage at all other tested conditions.

Multiplication of the y-axis intercept and the voltage dependence of the instantaneous current provide the voltage dependence of the single channel current amplitudes (Fig. 9.3*C* and *G*). This value together with the number of channels enables calculation of the absolute open probability (Fig. 9.3*D* and *H*). We obtained comparable results for several cells with varying current amplitudes, indicating that contaminations of the anion current with background currents did not affect the determination of the single channel amplitude.

Noise analysis at the same cells after moving to a glutamate-free external solution provides the unitary current amplitude and absolute open probability also under those conditions (Fig. 9.3*C, D, G* and *H*). For both isoforms, the single channel current amplitudes are identical in the absence as well as in the presence of glutamate. The sole basis for the glutamate-induced increase of macroscopic current amplitudes is a change of the absolute open probability. We conclude that EAAT3 and EAAT4 anion channels differ neither in the unitary current amplitude nor in the absolute open probability in the absence as well as in the presence of glutamate.

9.4.3 EAAT4 glutamate transport rates are significantly smaller than those of EAAT3

The identity of anion transport rates of EAAT3 and EAAT4 indicates that the well established difference in the contribution of anion current to the total transport current of the two isoforms (2;3) must be due to differences in glutamate transport rates. The use of *Xenopus* oocytes provides a simple and direct procedure to determine relative glutamate transport rates (Fig. 9.4). Oocytes were incubated in gluconate-based solution, the removal of permeant anions (14) from the external membrane side results in an almost complete efflux of intracellular Cl^- anions. Under this condition, glutamate-induced currents represent isolated glutamate uptake currents (Fig. 9.4*A*). Consequently, the external solution was switched from a gluconate-based to an SCN^--based solution. Because of the voltage-dependence of the electrogenic glutamate transport (15;16), currents at positive potentials are isolated anion currents. The specificity of anion currents was tightly monitored by testing their TBOA sensitivity (Fig. 9.4*C* and *D*).

EAAT3 expresses much better in *Xenopus* oocytes than EAAT4. We adjusted the length of the time period between injection and experiments so that ooctyes expressing EAAT3 or EAAT4 exhibited comparable absolute current amplitudes. The amplitudes of uptake currents were 234 ± 37 nA for EAAT3 (n = 5) and only 86 ± 17 nA (n = 5) for EAAT4-expressing oocytes at -120 mV (Fig. 9.4*A* and *B*). At +60 mV, anion current amplitudes measured 0.8 ± 0.05 μA in the absence of glutamate and 1.8 ± 0.2 μA in the presence of glutamate for EAAT3 (n=5) and 2.2 ± 0.09 μA in the absence and 4.1 ± 0.1 μA in the presence of glutamate for EAAT4 (n=5) (Fig. 9.4*C* and *D*). These two values were used to calculate the uptake current to anion current ratio (0.13 ± 0.01 (n=9) for EAAT3 and 0.02 ± 0.001 (n=4) for EAAT4; $p<0.001$) (Fig. 9.4*E*). Since mean unitary current amplitude per individual transporter for the two isoforms are identical, these values enable a comparison of glutamate

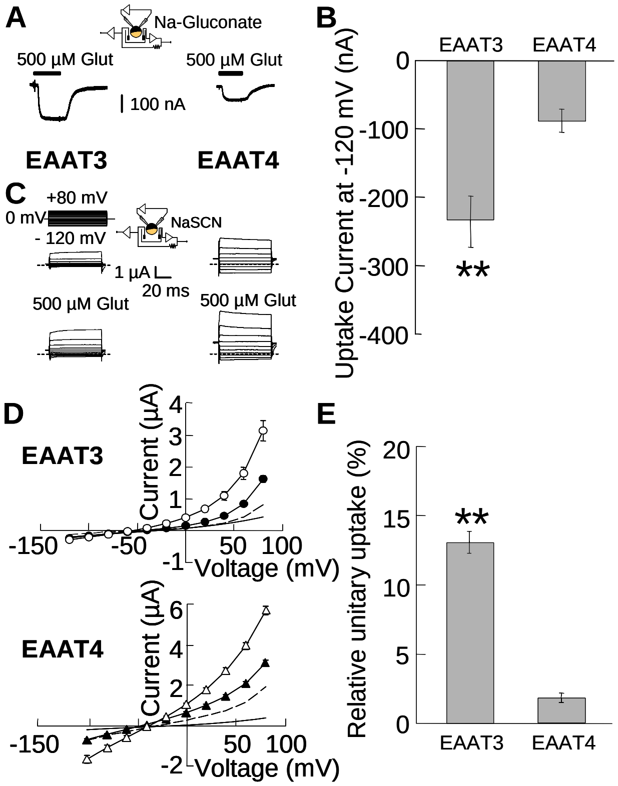
A
Na-Gluconate
500 µM Glut
500 µM Glut
100 nA
EAAT3
EAAT4
B
EAAT3
EAAT4
Uptake Current at -120 mV (nA)
0
-100
-200
-300
-400
**
C
+80 mV
0 mV
- 120 mV
NaSCN
1 µA
20 ms
500 µM Glut
500 µM Glut
D
EAAT3
Current (µA)
4
3
2
1
-1
-150
-50
50
100
Voltage (mV)
EAAT4
Current (µA)
6
4
2
-2
-150
50
100
Voltage (mV)
E
Relative unitary uptake (%)
20
15
10
5
0
**
EAAT3
EAAT4

Figure 9.4. Relative unitary glutamate transport rates of EAAT3 and EAAT4. (*A)* Representative changes of the current amplitude at -120 mV upon application of 500 µM L-glutamate from ooctyes perfused with gluconate-based external solutions. (*B*) Mean glutamate uptake current-amplitudes at -120 mV from oocytes expressing EAAT3 (n=9) or EAAT4 (n=4). (C) Representative current recordings from ooctyes perfused with SCN-based solutions in the absence as well as in the presence of 500 µM L-glutamate. (*D)* Voltage dependence of the EAAT3- and EAAT4-associated current in the absence (closed symbols, n = 9 for EAAT3; n = 6 for EAAT4) as well as in the presence (open symbols, n = 9 for EAAT3; n = 6 for EAAT4) of glutamate. Solid lines represent current-voltage relationships determined with uninjected oocytes in the presence of 500 µM L-glutamate at the same anion distribution (n = 4); dashed lines gives amplitudes from injected oocytes after addition of 200 µM TBOA (n =5 for EAAT3 and n=6 for EAAT4). (*E*) Ratio of uptake current amplitudes at -120 mV to SCN^- current amplitudes at +60 mV from oocytes expressing EAAT3 (n = 9) and EAAT4 (n = 4).

transport rates for the two isoforms. We conclude that EAAT3 glutamate transport rates are at least 7 times larger than for EAAT4.

9.4.4 Glutamate dependence of EAAT3 and EAAT4 anion currents

Glutamate increases EAAT3- and EAAT4-associated anion currents with an isoform-specific concentration-dependence (Fig. 9.5). We recently reported that EAAT4 anion currents exhibit a sigmoidal glutamate dependence (8). Apparent dissociation constants (K_D) and the Hill coefficient (n) depend on the internal and external solutions ($n = 3.7$, $K_D = 35.0 \pm 0.3$ μM ($n = 5$) for Cl_{int}/NO_{3ext}; $n = 5.2$, $K_D = 23.2 \pm 0.4$ μM ($n = 5$) for Cl_{int}/SCN_{ext}; (Fig. 9.5*B*) (8)). For EAAT3, we obtained a perfectly hyperbolic relationship with a Hill coefficient of 1.0 and a K_D of 20.5 ± 8 μM at Cl_{int}/SCN_{ext}. EAAT3 and EAAT4 anion channels thus exhibit similar glutamate affinities, but differ in the steepness of the concentration dependence of anion currents. The two isoforms also differ in the relative amplitudes of the glutamate-independent anion currents under this anion conditions (Cl_{int}/SCN_{ext}). In the absence of glutamate, TBOA-sensitive anion currents could be measured in cells expressing EAAT3 as well as in cells with EAAT4. For EAAT3, the glutamate-independent current amplitude is 67 ± 3% of the maximum anion current amplitude at a saturating glutamate concentration (Fig. 9.2*B* and 9.5*B*). For EAAT4 anion channels, relative anion current amplitudes in the absence of glutamate are considerably lower (20 ± 2%) (Fig. 9.2*E* and 9.5*B*).

Two point mutations, G464S and Q467S, were recently found to increase the cooperativity and affect the apparent glutamate affinity of the glutamate activation of EAAT4 anion channels (8). We constructed the homologous point mutations, G410S and Q413S, in EAAT3. EAAT3 expressed much better in oocytes than in cells, and we therefore used the oocyte expression system to study the effects of these mutations on the glutamate dependence of EAAT3 anion currents. G410S and Q413S change the apparent glutamate affinity, but leave

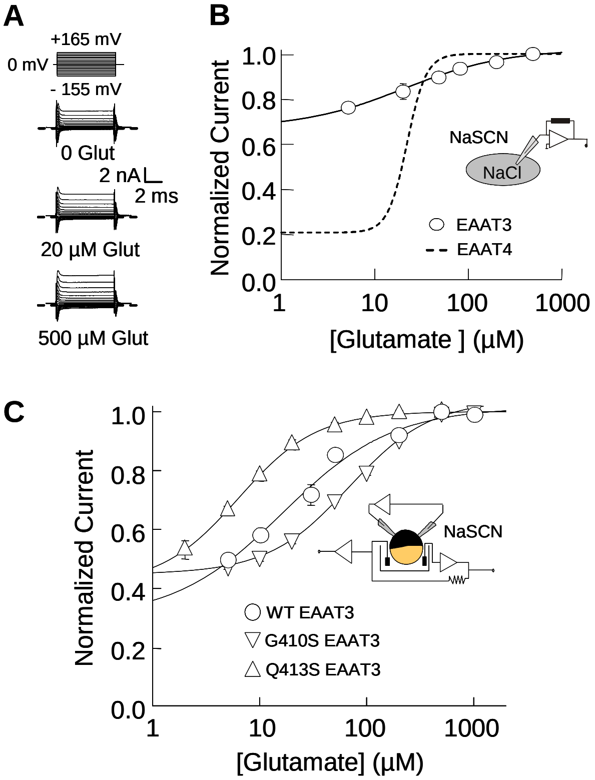
A
+165 mV
0 mV
- 155 mV
0 Glut
2 nA
2 ms
20 µM Glut
500 µM Glut
B
Normalized Current
1.0
0.8
0.6
0.4
0.2
0.0
1
10
100
1000
[Glutamate] (µM)
NaSCN
NaCl
EAAT3
EAAT4
C
Normalized Current
1.0
0.8
0.6
0.4
0.2
0.0
1
10
100
1000
[Glutamate] (µM)
NaSCN
WT EAAT3
G410S EAAT3
Q413S EAAT3

Figure 9.5. EAAT3 and EAAT4 differ in the glutamate dependence of associated anion currents. (*A*) Pulse protocols and representative whole-cell current traces recorded from tsA201 cells expressing EAAT3 transporters at different glutamate concentration. (*B*) Glutamate dependence of anion currents in cells expressing EAAT3 (○, n = 4) and EAAT4 (dashed lines,(8)) with NaCl-based internal and NaSCN-based external solutions. The solid line represent fits with the Hill equation. (*C*) Glutamate dependence of WT (open circle, n = 9), G410S (triangles down, n = 7), and Q413S (triangles up, n = 7) EAAT3 anion currents, obtained from injected oocytes at +60 mV in NaSCN-based external solution.

the steepness of glutamate dependence in EAAT3 basically unaffected (G410S: n = 1.1, K_D = 68.4 ± 4.5 (n=7); Q413S: n = 1.1, K_D = 6.4 ± 0.2 (n=7)) (Fig. 9.5*C*). We conclude that, while EAAT4 subunits interact cooperatively during activation of anion channels, no such interaction occurs in EAAT3.

9.5 Discussion

EAAT3 and EAAT4 represent two extremes of the apparent specialization of EAAT isoforms into glutamate carriers and glutamate-gated anion channels. EAAT3 is characterized by a high glutamate transport rate (17) and only small associated anion current (3). In contrast, EAAT4 exhibits a predominant anion current and has been generally assumed to function as an anion channel rather than as a glutamate transporter (2). We here demonstrate that the anion conduction pathways of EAAT3 and EAAT4 are functionally very similar, whereas the two isoforms differ greatly in glutamate transport rates (Fig. 9.4). Since not only unitary current amplitudes, but also absolute open probabilities are comparable (Fig. 9.3), the anion conductance of EAAT4 does not dominate total transporter currents because of high anion transport rates, but because of low glutamate transport rates (Fig. 9.4). A large difference in glutamate transport rates was recently also reported for rEAAT3 and hEAAT4. Using a kinetic analysis of reaction steps of the glutamate uptake cycle, Mim *et al.* (18) determined glutamate transport rates of $3s^{-1}$ for hEAAT4 as compared to 90 s^{-1} (both at -90 mV) for rEAAT3 (19). A comparison of transport rates (18) and relative anion currents (2;3) of various EAATs suggest that glutamate transport rates are inversely related to relative anion conductances and that unitary anion channel amplitudes are comparable for all EAATs. While glutamate transport rates differ greatly among different EAAT isoforms, the anion conduction pathway is conserved. The functional specialization within the EAAT family thus occurs by adjusting the glutamate transport alone.

Single channel amplitudes of EAAT3 and EAAT4 anion channels are too small to be measured directly. We used stationary noise analysis and determined identical unitary current amplitudes for EAAT3 (at -155 mV: 172 ± 38 fA, n=4) and EAAT4 (at -155 mV: 164 ± 39 fA, n=5) (Fig. 9.3) in cells dialyzed with SCN-based solution. Under these conditions, EAAT3 and EAAT4 anion currents are very similar in the voltage dependence of the open probability, the time dependence of current relaxations and the ratio of current variance and current amplitudes, providing perfect conditions for a comparison of unitary channel properties by noise analysis. The noise analysis presented here provided consistent results, with and without glutamate (Fig. 9.3), and the results agree well with our earlier results on EAAT4, that were obtained by non-stationary noise analysis (5). Earlier publications reported differing single channel amplitudes of EAAT anion channels (5;14;20;21). However, since experiments were performed under dissimilar ionic conditions, these earlier results did not allow a direct comparison of anion conduction properties of different isoforms.

While conduction properties are conserved between EAAT3 and EAAT4 anion channels, there are marked differences in time-, voltage-, and substrate-dependence of anion currents. The isoform-specificity of EAAT anion channel gating most likely arises from differences in intersubunit interactions. EAAT transporters are assembled as trimers (9), with each subunit transporting glutamate independently from the adjacent subunits (22;23). We recently reported a cooperative interaction between the subunits in activating EAAT4 anion channel. No cooperativity was observed in the glutamate dependence of glutamate transport, indicating that intersubunit interaction does not occur in glutamate binding, but rather in gating processes coupling glutamate binding and anion channel opening (8). Mutations affecting intersubunit interactions modify gating transitions of EAAT4 anion channels (8), in full agreement with the idea that voltage-dependent gating involve conformational changes of individual subunits relative to their neighbours. In contrast to these results on EAAT4, we did not observe cooperativity in glutamate activation of WT or mutant EAAT3 anion channels (Fig. 9.5).

EAAT4 glutamate transporters have been studied by several groups in native cells or heterologous expression systems (2;18;24;25). Rat and human EAAT4 were reported to bind glutamate with apparent dissociation constants between 0.6 µM (18) and 30 µM (25). We determined apparent glutamate dissociation constants of 10 µM for the glutamate transport (8) and of about 30 µM for activation of the anion current ((8), Fig. 9.5). In contrast to all other reports, the glutamate concentration dependence of anion currents determined by our group could not be fit with a Michaelis-Menten relationship, but rather with a Hill relationship and a Hill coefficient larger than 3. We determined the glutamate concentration dependence of anion currents by plotting isochronal current amplitudes determined 1 ms after stepping from a holding potential of 0 mV to the test potential. This approach accounts for the voltage-dependent gating of EAAT anion channels that is modified by external substrates (5;7;8). All other groups measured late current amplitudes, thus lumping the glutamate- and the voltage-dependence of anion channel opening together. The differences between our results and those by other groups are likely due to the different methods used to determine apparent dissociation constants. We now compared the glutamate dependences of EAAT3 and EAAT4 anion currents, using exactly the same experimental approach for both transporter isoforms. The different steepness of the glutamate dependences of EAAT3 and EAAT4 indicates an isoform-specific difference, irrespective of the reason for the differences between our results on EAAT4 and those of other groups

EAAT3 is responsible mainly for neuronal glutamate and cysteine uptake (26) and seems to be the major glutamate carrier in tubular glutamate reabsorption (27). The physiological role of EAAT4 is not clear. It does not play a crucial role in cerebellar glutamate homeostasis (28), in good agreement with its low unitary glutamate transport rates. Mim *et al.* (18) recently postulated that human EAAT4 mainly serves to bind glutamate with high affinity to prevent spillover to adjacent synapses. Although rat EAAT4 used in our study has a tenfold larger glutamate dissociation constant than hEAAT4 (8;18), it also represents a high affinity glutamate transporter well suited for such a task.

It has been generally assumed that EAAT4 function as anion channel and regulate neuronal excitability because of a large unitary conductance of the associated anion channel. Our finding that anion conduction pathways of EAAT are conserved does not argue against a specific role of the EAAT4 anion conductance. In contrast, low glutamate transport rates might be necessary to allow EAAT4 functioning as a gated channel involved in the regulation of cellular excitability. We recently reported a voltage-dependent gating step that controls anion-to-cation selectivity of EAAT4 anion channels (7). Trains of phasic depolarizations and long-lasting depolarizations result in an increased cation permeability and in excitatory inward current through EAAT4 channels (7). EAAT4 anion channels can therefore mediate inhibitory currents in resting cells and excitatory currents in electrically active cells. In dendritic spines of Purkinje cells, where EAAT4 is mainly expressed (29), such an excitatory currents might result in substantial depolarizations (7). In spines, glutamate receptor-mediated Na^+ signals can cause substantial increases of internal $[Na^+]$ (30), and dendrites are tightly encased by glial cells facilitating extracellular K^+ accumulation (31). Glutamate transporters in spines are thus prone to an inversion of the glutamate transport direction, resulting in glutamate extrusion into the external medium and activation of ionotropic glutamate receptors. The low transport capacity of EAAT4 minimizes transporter-associated glutamate release and allows regulation of cellular excitability without interfering with extracellular glutamate homeostasis.

Aknowledgments

We would like to thank Dr. J. Rothstein for providing the expression construct for rEAAT4; Dr. Matthias Hediger for hEAAT3; Drs. Alexi Alekov, Jennie Garcia-Olivares, and Patricia Hidalgo for helpful discussions; and Birgit Begemann and Toni Becher for excellent technical assistance. These studies were supported by the Deutsche Forschungsgemeinschaft (FOR450) to Ch.F.

9.6 References

1. Fairman, W. A. and Amara, S. G. (1999) *Am. J. Physiol* **277,** F481-F486
2. Fairman, W. A., Vandenberg, R. J., Arriza, J. L., Kavanaugh, M. P., and Amara, S. G. (1995) *Nature* **375,** 599-603
3. Wadiche, J. I., Amara, S. G., and Kavanaugh, M. P. (1995) *Neuron* **15,** 721-728
4. Watzke, N. and Grewer, C. (2001) *FEBS Lett* **503,** 121-125
5. Melzer, N., Biela, A., and Fahlke, Ch. (2003) *J Biol. Chem.* **278,** 50112-50119
6. Trotti, D., Peng, J. B., Dunlop, J., and Hediger, M. A. (2001) *Brain Res.* **914,** 196-203
7. Melzer, N., Torres-Salazar, D., and Fahlke, C. (2005) *Proc. Natl. Acad. Sci. U. S. A* **102,** 19214-19218
8. Torres-Salazar, D. and Fahlke, C. (2006) *J. Neurosci.* **26,** 7513-7522
9. Gendreau, S., Voswinkel, S., Torres-Salazar, D., Lang, N., Heidtmann, H., Detro-Dassen, S., Schmalzing, G., Hidalgo, P., and Fahlke, Ch. (2004) *J Biol. Chem.* **279,** 39505-39512
10. Hodgkin, A. L. and Katz, B. (1949) *J Physiol (London)* **108,** 37-77
11. Sesti, F. and Goldstein, S. A. N. (1998) *J. Gen. Physiol.* **112,** 651-663
12. Sigworth, F. J. and Zhou, J. (1992) *Methods Enzymol.* **207,** 746-762
13. Shimamoto, K., Lebrun, B., Yasuda-Kamatani, Y., Sakaitani, M., Shigeri, Y., Yumoto, N., and Nakajima, T. (1998) *Mol Pharmacol* **53,** 195-201
14. Wadiche, J. I. and Kavanaugh, M. P. (1998) *J Neurosci* **18,** 7650-7661
15. Zerangue, N. and Kavanaugh, M. P. (1996) *Nature* **383,** 634-637
16. Levy, L. M., Warr, O., and Attwell, D. (1998) *J Neurosci* **18,** 9620-9628
17. Grewer, C., Madani Mobarekeh, S. A., Watzke, N., Rauen, T., and Schaper, K. (2001) *Biochemistry* **40,** 232-240

18. Mim, C., Balani, P., Rauen, T., and Grewer, C. (2005) *J. Gen. Physiol* **126,** 571-589

19. Grewer, C., Watzke, N., Wiessner, M., and Rauen, T. (2000) *Proc. Natl. Acad. Sci. USA* **97,** 9706-9711

20. Larsson, H. P., Picaud, S. A., Werblin, F. S., and Lecar, H. (1996) *Biophys J* **70,** 733-742

21. Palmer, M. J., Taschenberger, H., Hull, C., Tremere, L., and von Gersdorff, H. (2003) *J Neurosci* **23,** 4831-4841

22. Koch, H. P. and Larsson, H. P. (2005) *J Neurosci.* **25,** 1730-1736

23. Grewer, C., Balani, P., Weidenfeller, C., Bartusel, T., Tao, Z., and Rauen, T. (2005) *Biochemistry* **44,** 11913-11923

24. Koch, H. P., Brown, R. L., and Larsson, H. P. (2007) *J. Neurosci.* **27,** 2943-2947

25. Otis, T. S. and Jahr, C. E. (1998) *J Neurosci* **18,** 7099-7110

26. Aoyama, K., Suh, S. W., Hamby, A. M., Liu, J., Chan, W. Y., Chen, Y., and Swanson, R. A. (2006) *Nat. Neurosci.* **9,** 119-126

27. Peghini, P., Janzen, J., and Stoffel, W. (1997) *EMBO J* **16,** 3822-3832

28. Huang, Y. H., Dykes-Hoberg, M., Tanaka, K., Rothstein, J. D., and Bergles, D. E. (2004) *J Neurosci.* **24,** 103-111

29. Dehnes, Y., Chaudhry, F. A., Ullensvang, K., Lehre, K. P., Storm-Mathisen, J., and Danbolt, N. C. (1998) *J Neurosci.* **18,** 3606-3619

30. Callaway, J. C. and Ross, W. N. (1997) *J. Neurophysiol.* **77,** 145-152

31. Harvey, R. J. and Napper, R. M. (1991) *Prog. Neurobiol.* **36,** 437-463

9.7 Suplemental Information

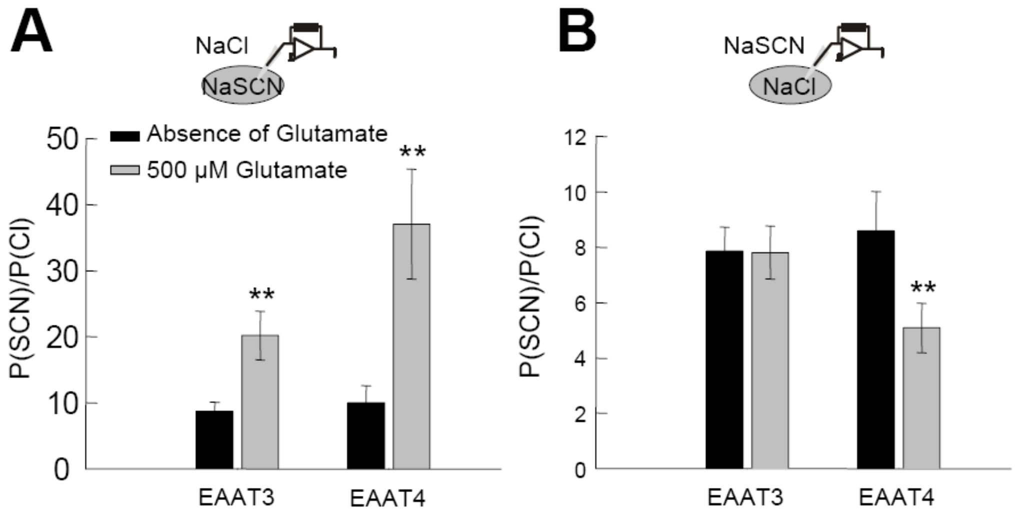

Figure 9.6. Anion permeability ratios of EAAT3- and EAAT4-associated anion channels. (*A,B*) P_{SCN}/P_{Cl} for EAAT3- and EAAT4-associated anion channels from cells dialyzed with SCN^--based solution and perfused with Cl^--based solution (*A*) (n = 6 for EAAT3 and n = 8 for EAAT4) and from cells dialyzed with a Cl^--based solution and perfused with a SCN^--based solution (*B*) (n = 17 for EAAT3 and n = 12 for EAAT4)

Table 9.1. Boltzmann parameters of the activation curves of EAAT3- and EAAT4-associated anion channels in the absence and presence of 500 µM L-glutamate for two different anion distributions

		EAAT3			**EAAT4**		
		$V_{0.5}$ (mV)	**P_o min**	**n**	**$V_{0.5}$ (mV)**	**P_o min**	**n**
int SCN/ext Cl	0 glutamate	-26.9 ± 5.4	0.7 ± 0.01	5	-78.5 ± 5.6**	0.8 ± 0.01	5
	0.5 mM glutamate	+15.6 ± 2.3	0.5 ± 0.01	7	-74.8 ± 2.0**	0.5 ± 0.01	8
int Cl/ext SCN	0 glutamate	-88.9 ± 8.3##	0.8 ± 0.02	3	-55.2 ± 2.2**	0.5 ± 0.01**##	5
	0.5 mM glutamate	-18.3 ± 6.3##	0.4 ± 0.04	9	+115 ± 9.8**##	0.6 ± 0.03**	7

** p < 0.01 indicate a significant difference between isoforms
p < 0.01 indicate a significant difference between anion conditions

Acknowledgments

I would like to thank Prof. Dr. Christoph Fahlke for the experience transmitted, his trust and patience during all these years, for making me feel free to use my creativity, for believe and promote my future as an independent scientist.

I thank our work groups in RWTH-Aachen and MHH Hannover, especially to Dr. Nico Melzer and Dr. Alexi Alekov for intense and helpful discussion and to Barbara Poser, Toni Becher and Birgit Begemann for an excellent technical assistance. Thanks to Christine Kiesel for her big help with the paperwork.

I would like to thank in advance to Dr. Adolfo Cavalie, Dr. Gonzalo Torres, Dr. Symeon Papadopoulos and Dr. Anaclet Ngezahayo for their disposition of being the reviewers of this dissertation.

Thanks to the DFG for financial support.

For helping with English edition I thank my distinguished friend Rene Villalon

Thanks to Hannelore Heidtmann and Ute Scholl for bringing us her hands in the most difficult moments.

Thanks to Doreen Nothmann for her extensive help and friendship.

Thanks to my family, for their support trough the distance.

Especially I would like to thank Jennie for your patience and unconditional support and love. There is not space in this paper to all I would like to thank you.

And finally I thank my little daughter Mariana, for making every moment of my life more “easy” and happy.

Curriculum Vitae

Personal Information

Name: Delany Torres Salazar
Place and Date of birth: Santa Clara, Cuba. December 3rd, 1975.
Personal Address: Carl-Neuberg-Str 2C. 30625. Hannover. Germany.
Work Address: Medizinische Hochschule Hannover (MHH). Carl-Neuberg-Str 1. 30625. Hannover.
Phone: + 49-511-5322876 or 8884
e-mail: torres.delany@mh-hannover.de

Educational Background

Since Sept. 2002 PhD studies. Dr. rer. nat. at Medizinische Hochschule Hannover. Hannover. Germany.

March 2000 to Sept. 2002 Master Degree studies. M.Sc. Mention Neurosciences at Universidad de Valparaiso. Valparaiso. Chile.

Sept. 1994 to July 1999 Universitary studies. Lic. In Microbiology at Universidad de la Habana. Ciudad Habana. Cuba

Professional Background

Since September 2002 I have been performing my research in Germany under the supervision of Prof. Dr. Christoph Fahlke (phone: +49-511-5322777, email: fahlke.christoph@mh-hannover.de). Our main research interest is to study the structure-function relationship of glutamate transporters. Using molecular biology, electrophysiological and radioactive uptake assays, I study the electrical currents mediated by these proteins and trying to understand how they open and close as well as how they are assembled.

From March 2000 to September 2002 I have performed my research work to obtain the Master in Sciences degree with mention in Neurosciences under the supervision of Dr. Alan Neely (phone: +56-32-508054, email: alan@cnv.cl). During this time our research interest was to study the mechanisms that govern the post-transductional trafficking and surface expression of shaker potassium channels, using electrophysiological techniques and *Xenopus laevis* oocytes as a cellular model.

Published Abstract

Torres-Salazar D., Naranjo D. and Neely A. (2003) Incorporation of *Shaker* K^+ channels to the plasma membrane of *Xenopus* oocytes is regulated by Thapsigargin sensitive Ca^{2+} store. *Biophysical Journal* **84** (2): 63A Part 2 Suppl. S.

Torres-Salazar D. and Fahlke Ch. (2004) Na^+ and glutamate-dependent gating of EAAT4 anion channels. *Europ. Journal of Physiology* **447** (1): S142

Torres-Salazar D. and Fahlke Ch. (2005) Substrate and voltage-dependence of EAAT4 anion channels. *Europ. Journal of Physiology* **449** (1): S117

Torres-Salazar D. and Fahlke Ch. (2005) Inter-subunit interaction in EAAT4 glutamate transporters. *15th Neuropharmacology Conference.* (2005) Washington. USA

Torres-Salazar D and Fahlke C (2007) Voltage-dependent gating of anion channels associated with EAAT3 and EAAT4 glutamate transporters. *Biophysical Journal* : 275A-275A Suppl. S JAN

Garcia-Olivares J, **Torres-Salazar D**, Hidalgo P and Fahlke C (2007) Isoform-specific modulation of ClC channels by their carboxy-terminus. *Biophysical Journal*: 273A-273A Suppl. S JAN

List of Publications

Gendreau S, Voswinkel S, **Torres-Salazar D**, Lang N, Heidtmann H, Detro-Dassen S, Schmalzing G, Hidalgo P and Fahlke C (2004) A trimeric quaternary structure is conserved in bacterial and human glutamate transporters. *J. Biol. Chem*. **279**: 39505-512

Melzer N, **Torres-Salazar D**, Fahlke C (2005) A dynamic switch between inhibitory and excitatory currents in a neuronal glutamate transporter. *Proc Natl Acad Sci USA* **102**: 19215 – 19218.

Torres-Salazar D and Fahlke C (2006) Intersubunit Interactions in EAAT4 Glutamate Transporters. *J Neurosci* **26**(28): 7513-7522 (with This Week in the Journal).

Torres-Salazar D and Fahlke Ch (2007) Parawixin1: a spider toxin opening new avenues for glutamate transporter pharmacology. *Mol Pharmacol* **72**(5):1100-2

Torres-Salazar D and Fahlke Ch (2007) Neuronal glutamate transporters vary in substrate transport rate but not in unitary anion channel conductance. *J Biol Chem* **282**(48):34719-26.

Detro-Dassen S, Schanzler M, Lauks H, Martin I, Meyer Zu Berstenhorst S, Nothman D, **Torres-Salazar D**, Hidalgo P, Schmalzing G, Fahlke C (2007) Conserved dimeric subunit stoichiometry of SLC26 multifunctional anion exchangers. *J Biol Chem. Online publication* Dec 11

Grants and Awards.

International travel award from the International Brain Research Organization (IBRO). Institute of Physiology, Universidad Nacional Autónoma de México (UNAM) México. (2001)

International travel Grant from the Biophysical Society. 46th Annual Meeting of the Biophysical Society. San Francisco. California. USA. (2002)

January, 2008